UNIVERSIDAD DE CONCEPCIÓN

FACULTAD DE FARMACIA

DOCTORADO EN CIENCIAS Y TECNOLOGÍA ANALÍTICA

TÍTULO DE LA TESIS

ANÁLISIS METABOLÓMICO EN LA CARACTERIZACIÓN DE MECANISMOS DE RESISTENCIA A AGENTES ANTINEOPLÁSICOS EN EL CÁNCER DE OVARIO Y SU USO PARA LA IDENTIFICACIÓN DE POTENCIALES BLANCOS TERAPÉUTICOS

Tesis presentada a la Facultad de Farmacia de la Universidad de Concepción para optar al grado académico de Doctor en Ciencias y Tecnología Analítica

POR: Pedro Felipe Alarcón Zapata

Profesor Guía: Felipe Andrés Zúñiga Arbalti

Profesor Co-guía: Andy Jorge Pérez de Armas

Concepción, Diciembre 2023

“Y sabemos que a los que aman a Dios, todas las cosas les ayudan a bien”

AGRADECIMIENTOS

Agradezco a mi Dios por estar siempre conmigo, ayudarme y ser mi guía día a día. Dios es fiel.

A mi amada esposa Guissella Camila y mi tierna hija María Jesús, quienes son mi soporte y aliento diario. Las amo.

A mis padres Pedro y Carmen por su apoyo incondicional. A mi hermana Barbara, y hermanos Pablo y Franco por acompañarme siempre. Les amo.

A los doctores y amigos, Felipe Zúñiga y Valeska Ormazábal por apoyarme en cada paso de este trabajo doctoral y confiar en mí. También a todo el grupo de investigación por su importante apoyo.

Al Doctor Andy Pérez, quien me ayudó a enfrentar los desafíos desarrollados en este trabajo.

A mi amigo Héctor Antonio, por ser un apoyo fundamental en esta etapa. También a mis amigos y compañeros de doctorado.

Al programa de doctorado en ciencias y tecnología analítica, y al departamento de bioquímica clínica e inmunología. También a la Facultad de Farmacia de la Universidad de Concepción.

A la agencia nacional de investigación y desarrollo, por financiar este trabajo a través de la beca de doctorado nacional 21201654 y los beneficios complementarios de gastos operacionales.

TABLA DE CONTENIDO

ÍNDICE DE TABLAS

ÍNDICE DE ILUSTRACIONES

RESUMEN

La resistencia a la quimioterapia en el cáncer de ovario es un desafío significativo que complica la efectividad de los tratamientos farmacológicos. Esta tesis se centró en la evaluación de dos modelos celulares de cáncer de ovario con distintas respuestas a fármacos antineoplásicos, utilizando una estrategia analítica metabolómica basada cromatografía líquida acoplada a espectrometría de masas de alta resolución. Las células sensibles mostraron un predominio en el metabolismo glucosídico y aminoacídico, mientras que las células resistentes presentaron una sobrerregulación en el metabolismo lipídico y del glutatión. La inhibición farmacológica del glutatión en las células resistentes generó un cambio significativo en la resistencia a los agentes antineoplásicos, aumentó la eficacia farmacológica. Además, mediante análisis lipídico, observamos un aumento en el metabolismo lipídico exclusivamente en las células resistentes, no en las células sensibles, lo que podría contribuir al fenotipo de resistencia a la quimioresistencia. Aunque esta investigación se centró en modelos celulares, las conclusiones obtenidas ofrecen perspectivas prometedoras para la investigación traslacional y futuras aplicaciones clínicas. Los análisis metabolómicos podrían utilizarse para predecir la resistencia a los fármacos en pacientes, permitiendo un enfoque de tratamiento más personalizado. Además, identificar metabolitos como posibles blancos terapéuticos podría ayudar a contrarrestar la quimiorresistencia manipulando las vías metabólicas clave en el cáncer de ovario.

ABSTRACT

Chemotherapy resistance in ovarian cancer presents a significant challenge that complicates the efficacy of pharmacological treatments. This thesis focused on the evaluation of two cellular models of ovarian cancer with different responses to antineoplastic drugs, using an analytical metabolomic approach based on high-resolution liquid chromatography coupled with mass spectrometry.

Drug-sensitive cells exhibited a predominance in glycosidic and amino acid metabolism, while drug-resistant cells showed an overexpression in lipid and glutathione metabolism. The pharmacological depletion of glutathione in resistant cells generated a significant change in resistance to antineoplastic agents, with an increase in pharmacological efficacy. Additionally, through lipidomic analysis, we observed an increase in lipid metabolism exclusively in resistant cells, not in sensitive cells, which could contribute to the chemotherapy-resistant phenotype.

Although this research focused on cellular models, the conclusions offer promising perspectives for translational research and future clinical applications. Metabolomic analyses could predict patient drug resistance, allowing for a more personalized treatment approach. Furthermore, identifying metabolites as potential therapeutic targets could help counteract chemotherapy resistance by manipulating critical metabolic pathways in ovarian cancer.

CAPÍTULO 1 : INTRODUCCIÓN GENERAL

1.1 Contexto general sobre la problemática del cáncer.

El cáncer es uno de los grandes problemas de salud pública en el mundo, contribuyendo a la primera o segunda causa de muertes a nivel mundial, de esta manera, se transforma en un obstáculo importante para aumentar la esperanza de vida en todos los países del mundo [1]. En el año 2020, según cifras del Observatorio Global del Cáncer (GLOBOCAN), se reportaron 19,3 millones de nuevos casos de cáncer y 9,9 millones de muertes por cáncer en el mundo. En este sentido, el cáncer de pulmón es la principal causa de muerte (18,0%), seguido por el cáncer hepático (8,3%), cáncer gástrico (7,7%), cáncer de mama (6,9%), cáncer de colon (5,8%) y cáncer de próstata (3,8%) [2]. Se proyecta que esta enfermedad continúe en aumento, estimando al 2030 un aumento en el número de muertes por cáncer a 21 millones [3].

En Chile el panorama es similar. Los tumores (malignos o benignos) son la primera causa de muerte después de las enfermedades cardiovasculares. En el año 2019 se produjo un total de 28.492 defunciones por tumores (25,9%) y 28.079 defunciones por enfermedades del sistema circulatorio (25,6%). Según los últimos datos de mortalidad validados del DEIS, durante el año 2019, la tasa

bruta de mortalidad por tumores (malignos y benignos) por 100.000 habitantes fue de 149,1 [4].

Considerando una perspectiva de género en Chile, el cáncer de estómago, próstata y pulmón son la principal causa de fallecimiento por esta enfermedad en los hombres del país. En el caso de las mujeres, los cánceres con mayor mortalidad e incidencia son el cáncer de mama, pulmón, y vesícula y vías biliares [5].

2. El cáncer de ovario.

2.1 La problemática del cáncer de ovario.

Los cánceres ginecológicos son un grupo de tumores malignos originados en el sistema reproductivo femenino, los que incluyen: cáncer vaginal, cáncer de útero, cáncer de vulva y cáncer de ovario [6]. Aunque el cáncer de ovario (CaOv) representa solo un 3,4% de la incidencia de cáncer mundial [7], corresponde a la quinta causa de muerte por cáncer del mundo en mujeres [8] y es considerado uno de los cánceres ginecológicos más letales debido a que es la segunda causa con mayor número de muertes de todas las neoplasias malignas ginecológicas [2]. Lamentablemente, la tasa de supervivencia relativa a los cinco años, oscila solo entre un 30% al 40%, lo cual explica su alta tasa de fatalidad [9, 10]. Otra de las causas importantes que contribuyen a la baja sobrevida, es debido a que su

diagnóstico generalmente se realiza en etapas tardías de la enfermedad ya que presenta síntomas poco específicos [11].

Esta gran letalidad del CaOv se debe en parte a que no existen herramientas de tamizaje o síntomas premonitores que permitan realizar un diagnóstico temprano de la enfermedad [12], siendo considerada como una enfermedad silente. El CaOV permanece asintomático en sus primeras etapas y las pacientes que se encuentran en una etapa avanzada presentan solo distensión abdominal, síntomas gastrointestinales como dispepsia y pérdida de apetito, sin que exista algún síntoma relacionados con la metástasis tumoral [11]. Como consecuencia de esto, alrededor del 60% al 70% de las mujeres con cáncer de ovario se diagnostica en etapas avanzadas o con metástasis abdominal, lo que resulta en una baja tasa de sobrevivencia. Menos del 25% de las mujeres se diagnostica en etapas tempranas, cuando la enfermedad se encuentra localizada en los ovarios, donde la tasa de sobrevivencia a 5 anos es superior al 90% [13].

En relación con la metástasis, el CaOv presenta múltiples modalidades de diseminación. La invasión directa se produce cuando el cáncer se aloja en órganos adyacentes, con mayor frecuencia en el colon sigmoide. También existe diseminación subperitoneal, que incluye la diseminación linfática que afecta a nivel de los ganglios paraórticos, ilíacos e inguinales; la diseminación, que implica la infiltración en el ligamento ancho que afectan a estructuras como el útero, las

trompas de Falopio y el ovario contralateral, que incluso puede extenderse a la pared lateral pélvica y a órganos no contiguos; y la diseminación hematógena que se produce cuando el cáncer penetra en los vasos ováricos o uterinos y posteriormente se desplaza al hígado, la pleura, el pulmón, las glándulas suprarrenales y el bazo, con raras metástasis a los huesos y el cerebro. Por otro lado, se puede producir diseminación intraperitoneal cuando el cáncer se infiltra en la cavidad peritoneal y otras zonas adyacentes que incluso puede ascender a través del diafragma hasta los ganglios linfáticos diafragmáticos, pericárdicos y mediastínicos anteriores [14].

Además de la alta tasa de muerte por el diagnóstico tardío, el CaOv no posee un tratamiento específico. Las pacientes inicialmente responden bien a estos tratamientos, pero luego la mayoría recae dentro de los 18 meses debido a la quimiorresistencia cuyos mecanismos son variados y no han sido totalmente definidos. Se han asociado varios factores asociados con el fracaso de la quimioterapia que incluyen la heterogeneidad de células tumorales, la inestabilidad genética o alteraciones epigenéticas y el microambiente tumoral [15]. Respecto a la respuesta al tratamiento, solo el 10 a 20% de los pacientes responden a los agentes antineoplásicos [16], con una tasa de sobrevivencia a 10 años cercana al 15% [17].

2.2 Clasificación del CaOv.

La Federación Internacional de Ginecología y Obstetricia (FIGO) ha dividido el diagnóstico de cáncer de ovario en cuatro etapas clínicas, que a su vez, presentan subetapas [18, 19]:

- En la etapa I del cáncer de ovario, el tumor se encuentra en los ovarios o las trompas de Falopio. Esta etapa presenta tres subetapas: IA, en donde el tumor está limitado a un solo ovario o una trompa de Falopio, con la cápsula que lo rodea intacta durante la cirugía, sin presencia del tumor en la superficie externa ni células malignas en líquido ascítico o lavados peritoneales; IB, en donde el tumor afecta ambos ovarios o trompas de Falopio, con la cápsula intacta y ausencia de tumor en la superficie y sin presencia de células malignas en el líquido ascítico o lavados peritoneales; y IC, en donde el tumor puede estar en uno o ambos ovarios o trompas de Falopio, con la rotura de la cápsula durante la cirugía (IC1), la rotura previa a la intervención o presencia del tumor en la superficie exterior (IC2), o la presencia de células tumorales malignas en líquido ascítico o lavados peritoneales (IC3).
- En la etapa II del cáncer de ovario, el tumor afecta a uno o ambos ovarios o las trompas de Falopio y se ha extendido a otros órganos con propagación pélvica o desarrollo de cáncer peritoneal primario. Esta etapa presenta dos subetapas: IIA, en donde el tumor ha diseminado o invadido el útero y/o las trompas de Falopio y/o los ovarios; y IIB, donde

el tumor está presente en la superficie externa o ha invadido otros tejidos pélvicos intraperitoneales, como la vejiga, el colon sigmoide o el recto.

- En la etapa III del cáncer de ovario, el tumor afecta a uno o ambos ovarios con metástasis peritoneal fuera de la pelvis o con linfoadenopatía retroperitoneal. Esta etapa presenta tres subetapas: IIIA, en donde el tumor se ha diseminado e invadido ganglios linfáticos retroperitoneales, y se subclasifica en IIIA1 cuando la diseminación e invasión se limita a los ganglios linfáticos retroperitoneales, con metástasis menor o igual a 10 mm (IIIA1(i)) o mayor a 10 mm (IIIA1(ii)) y en la subetapa IIIA2 que implica depósitos tumorales en la zona peritoneal extra-pélvica, con o sin compromiso de los ganglios retroperitoneales; la subetapa IIIB que presenta depósitos tumorales a la observación macroscópica con metástasis peritoneal extra pélvica menor o igual a 2 cm, con o sin compromiso de los ganglios retroperitoneales, y extensión a la cápsula del hígado o bazo; y la subetapa IIIC implica metástasis peritoneal extra-pélvica macroscópica mayor a 2 cm, con o sin compromiso de ganglios linfáticos retroperitoneales, y extensión a la cápsula del hígado o bazo.
- En la etapa IV del cáncer de ovario, se observa la presencia de metástasis tumoral a tejidos distantes, excluyendo la metástasis peritoneal. Esta etapa presenta dos subetapas: IVA, en la cual se

identifica la presencia de células tumorales en el líquido pleural, indicativo de derrame pleural maligno y sin evidencia de propagación del tumor a otras áreas; y por otro lado, la IVB que implica metástasis tumoral al parénquima hepático y/o esplénico, así como a órganos extra abdominales, que incluyen ganglios linfáticos, pulmones y huesos.

En la tabla 1 se resumen cada etapa y subetapas según la clasificación FIGO para CaOv.

Tabla 1.2: Clasificación FIGO del cáncer de ovario.

Etapa	**Subetapas**	**Descripción.**
Etapa I. El tumor está confinado solo en los ovarios o las trompas de Falopio.	IA	Localización tumoral en un ovario y restringido al interior de este; o el tumor está en una trompa de Falopio y se encuentra restringido en su interior. La cápsula, se encuentra intacta en la intervención quirúrgica. Ausencia de tumor en la superficie externa. Ausencia de células malignas en líquido ascítico o en los lavados peritoneales.
	IB	Localización tumoral en ambos ovarios o en las trompas de Falopio. La cápsula, se encuentra intacta en la intervención quirúrgica. Ausencia de tumor en la superficie. Ausencia de células malignas en ascitis o lavados peritoneales.
	IC	Localización tumoral en uno o ambos ovarios o en las trompas de Falopio, y tiene cualquiera de las siguientes características: - IC1: La cápsula, se reventó durante la intervención quirúrgica. - IC2: Rotura de la cápsula, antes de la intervención quirúrgica o localización tumoral en la superficie exterior de al menos un ovario o trompas de Falopio. - IC3: Células tumorales malignas en el líquido ascítico o lavados peritoneales.

Etapa II. El tumor afecta a uno o ambos ovarios o en las trompas de Falopio y se ha propagado a otros órganos con extensión pélvica o cáncer peritoneal primario.	IIA	Diseminación e invasión tumoral al útero y/o trompas de Falopio y/o ovarios.
	IIB	Localización tumoral en la superficie externa o invasión a otros tejidos pélvicos intraperitoneales (vejiga, colon sigmoide o el recto)
Etapa III. El tumor afecta a uno o ambos ovarios con metástasis peritoneal fuera de la pelvis o con linfoadenopatía retroperitoneal.	IIIA	Diseminación tumoral a ganglios linfáticos retroperitoneales y/o metástasis microscópica atrás del borde pélvico. Se subclasifican en: - IIIA1: Diseminación e invasión tumoral solo en ganglios linfáticos retroperitoneales. IIIA(i), con metástasis menor o igual a 10 mm; y IIIA1(ii), con metástasis mayor a 10 mm. - IIIA2: Presencia de depósitos tumorales al análisis microscópico en la zona peritoneal extra-pélvica (por encima del borde pélvico) con o sin compromiso de los ganglios retroperitoneales.
	IIIB	Presencia de depósitos tumorales a la observación macroscópica con metástasis peritoneal extra-pélvica menor o igual a 2 cm, y con o sin compromiso de los ganglios retroperitoneales. Extensión tumoral a la cápsula del hígado o bazo.
	IIIC	Presencia de depósitos tumorales macroscópicos, metástasis peritoneal extra pélvica mayor a 2 cm con o sin compromiso de ganglios linfáticos retroperitoneales. Extensión tumoral a la cápsula del hígado o bazo.
Etapa IV. Metástasis tumoral a tejidos distantes excluyendo la metástasis peritoneal.	IVA	Presencia de células tumorales en el líquido pleural (derrame pleural maligno) sin otra área de propagación del tumor.
	IVB	Metástasis tumoral al parénquima hepático y/o esplénico, metástasis a órganos extra abdominales que incluyen ganglios linfáticos, pulmones y huesos.

Información obtenida y adaptada desde Cummings y col., 2022.

Según las características histológicas, el CaOv se clasifica en tres tipos principales de tumores: epitelial, de células germinales y del estroma del cordón sexual. Dentro de esta clasificación, el cáncer ovario epitelial (COE) es el de mayor malignidad ginecológica y se relaciona con el 90% de todos los tumores

ováricos [20]. Dentro de los tipos de COE un 97% corresponden a no mucinosos y un 3% a mucinosos. Los COE mucinosos, presentan diferentes histotipos, los cuales a su vez, están clasificados en: serosos, endometrioides de alto grado y de bajo grado, células claras de y no diferenciados. [21]. Los tumores serosos se clasifican en dos categorías con perfiles moleculares, presentaciones clínicas y pronóstico distintos: carcinomas serosos de alto grado (HGSC) y carcinomas serosos de bajo grado (LGSC) (Figura 1).

En relación con los carcinomas serosos, los LGSC tienden a originarse en los ovarios y son responsables del 10% de todos los tipos de tumores serosos, sin embargo, tienen un mejor pronóstico y son diagnosticados en etapas tempranas del desarrollo del cáncer [22]. Por otro lado, los HGSC son uno de los cánceres ginecológicos más letales, ya que más de un 85% de las mujeres con este tipo de cáncer se diagnóstica en etapas avanzadas de la enfermedad con una elevada carga tumoral. Se originan desde el epitelio de las trompas de Falopio con diseminación hacia los ovarios y el peritoneo, con un fenotipo altamente indiferenciado. Los HGSC se asocian a un pronóstico más fatal ya que presentan una tasa de supervivencia estimada a los 10 años menor al 15%, que sumado al diagnóstico tardío, y una alta tasa de recurrencia posterior a la terapia, contribuyen a esta tasa.

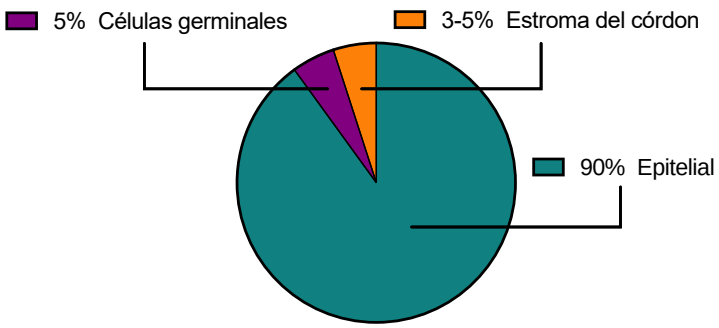

Figura 1.1: Distribución porcentual de los tipos de cáncer de ovario según características histológicas. Elaboración propia.

1.2.3 Factores de riesgo asociados al CaOv.

En general, la mayoría de los CaOv son esporádicos, sólo del 5% al 10% son de origen familiar [23]. Respecto a los factores de riesgo, existen muchos factores que se han asociado con el aumento de la prevalencia del CaOv. Podemos dividir estos factores de riesgo en demográficos (que incluye nivel socioeconómico), reproductivos (factores relacionados con la menstruación, edad de la menarquia y menopausia, paridad, características del embarazo, y mayor edad de parto), ginecológicos (enfermedades inflamatorias de la pelvis y endometriosis), hormonales (métodos anticonceptivos, terapia hormonal de reemplazo y tratamientos para la infertilidad), genéticos (historial familiar, y mutaciones en genes BCRA1/BRCA2 relacionados con el estilo de vida (nutrición, consumo de alcohol, consumo de cafeína, consumo de cigarro, obesidad y actividad física) y otros como la lactancia [24].

Entre los mencionados anteriormente, las características demográficas y nivel socioeconómico, la mayor incidencia de CaOv se encuentra en países con alto nivel de ingreso *per cápita*, sin embargo, la mayor tasa de mortalidad se encuentra en países con un nivel de ingreso menor [25].

En relación con los factores asociados con el estilo de vida, se ha reportado que en mujeres que fuman, existe un 6% mayor de probabilidad de padecer de CaOv en comparación con aquellas que no lo realizan [26]. Por otro lado, el consumo alcohol se asocia con un mayor de desarrollar cáncer de ovario [27]. Las mujeres con el nivel más alto de actividad física tenían un menor riesgo de padecer CaOv, en comparación con las mujeres con el nivel más bajo de actividad física [28]. Además, las mujeres con sobrepeso presentan un 7% de probabilidad mayor de padecer CaOv, y un 28% de probabilidad de aquellas que tienen obesidad [29], Se ha visto que las mujeres con niveles aumentados de ácidos grasos incrementa riesgo de padecer CaOv [30]. También, la presencia de síndrome metabólico también se asocia a un mayor riesgo de padecer CaOv [31].

Los ciclos menstruales juegan un factor muy relevante, se ha observado un aumento del riesgo de padecer CaOv en pacientes con un mayor número de ciclos ovulatorios, como las pacientes con una edad más temprana en la menarquia y una edad tardía en la menopausia [32]. El aumento del número de ciclos ovulatorios incrementa las divisiones celulares predisponiendo al desarrollo

de neoplasias malignas, sin embargo, este cáncer se considera principalmente una enfermedad posmenopáusica. Por otro lado, a una mayor edad aumenta el riesgo de un tipo de tumor más agresivo [33]. Pese a que la edad es un factor importante, en los últimos años existe una tendencia al aumento en la incidencia de mujeres más jóvenes, en comparación las mayores a 40 años. Este aumento es atribuible al alza de la prevalencia de la obesidad, el síndrome metabólico, la exposición a estrógenos, la nuliparidad y al incremento en la presencia de mutaciones en el gen BRCA en este grupo [34].

1.2.4 Diagnóstico del CaOv.

Una causa de la alta tasa de mortalidad del cáncer de ovario se atribuye a su diagnóstico tardío en etapas avanzadas. En todos los tipos de CaOv, el 34% se encuentra en etapa III en el momento del diagnóstico y el 26% en etapa IV. Es relevante destacar que cáncer de ovario epitelial se diagnostica en etapas aún más avanzadas, con un 37% en etapa III y un 28% en etapa IV [35].

La enfermedad en sus etapas iniciales suele ser asintomática, manifestándose posteriormente con síntomas inespecíficos como distensión abdominal, dolor en la región abdominal y pélvica, así como síntomas gastrointestinales que incluyen saciedad precoz y alteraciones en los hábitos intestinales. Además, se pueden experimentar síntomas urinarios, siendo la distensión abdominal por ascitis el síntoma más frecuente [36].

En general las pruebas diagnósticas para el cáncer de ovario son limitadas y poco específicas. El antígeno carcinogénico-125 (CA-125) y las imágenes transvaginales se utilizan habitualmente como pruebas de detección del cáncer de ovario y son las indicadas por la Sociedad Americana del Cáncer [37].

El CA-125 es el principal biomarcador utilizado para el cáncer de ovario, es una glucoproteína ubicada en la superficie de las células epiteliales, implicada en la promoción del crecimiento y la metástasis de las células cancerosas [38]. A pesar de su uso frecuente, el CA-125 presenta baja especificidad y puede aumentar en condiciones ginecológicas no cancerosas como endometriosis y embarazo, pero solo en el 50% de los cánceres epiteliales de ovario en Etapa I limitando su utilidad en el diagnóstico en esta etapa, a pesar de estar elevado en aproximadamente el 80% de los COE en general [39]. Su eficacia diagnóstica depende del riesgo y etapa de la enfermedad. La FDA lo recomienda principalmente para monitorear respuestas al tratamiento en cáncer de ovario epitelial (COE) y para detectar enfermedades residuales o recurrentes durante el seguimiento post-terapia [40].

Respecto al uso de este biomarcador en el monitoreo de pacientes sometidas a terapia, las elevaciones de CA-125 sobre 35 U/mL después de la cirugía y la quimioterapia, indican una probable enfermedad residual (> 95% de precisión). Un aumento persistente del valor de CA-125 después de tres ciclos de quimioterapia sugiere una enfermedad maligna progresiva y una respuesta

terapéutica deficiente. Sin embargo, los niveles de CA-125 por debajo de 35 U/mL no descartan la recurrencia ya que las pacientes con evidencia histopatológica de CaOv pueden tener concentraciones de CA-125 dentro del rango de individuos sanos [37].

En relación con la ecografía transvaginal (TVU), es la modalidad de imagen más comúnmente utilizada para la detección del cáncer de ovario, permitiendo a los profesionales clínicos identificar irregularidades en el tamaño y la forma de los tejidos ováricos. Los radiólogos revisan las imágenes obtenidas por la TVU para evaluar la presencia de características clínicas específicas, siguiendo las reglas simples del Análisis Internacional de Tumores de Ovario (IOTA). Algunas de las características evaluadas incluyen la presencia de proyecciones papilares, ascitis y/o tumores internos, así como el flujo sanguíneo interno [41]. La TVU es útil para obtener imágenes de los ovarios y los órganos circundantes; sin embargo, es difícil distinguir la formación de tumores de los quistes funcionales en ovarios premenopáusicos y debe ser utilizada en combinación con biomarcadores [38].

Como nuevos avances en el diagnóstico, se han propuesto varios algoritmos que incluyen más de un biomarcador sanguíneo, sin embargo, solo dos han sido aprobados por la FDA. En el año 2009, se aprobó la prueba OVA1®. El objetivo clave de esta prueba es identificar el riesgo de cáncer de ovario en mujeres que están planeando cirugía. La prueba considera la medición proteínas

significativas en el suero (CA 125-II, transtiretina, apolipoproteína A1, microglobulina beta 2, y transferrina) y combinados con un algoritmo para producir una puntuación general de OVA1®, el cual difiere dependiendo en el estado menopáusico, estratificando a pacientes en un grupo de bajo o alto riesgo [23]. La prueba OVA1® fue mejorada hacia un modelo de segunda generación denominado Overa®, el cual integra tres de los biomarcadores originales de OVA1® (CA125, ApoA-1, TF) junto con dos marcadores adicionales (HE4 y la hormona estimulante del folículo) para estratificar el riesgo de malignidad sin tener en cuenta el estado menopáusico. [42].

El segundo algoritmo diagnóstico basado en biomarcadores sanguíneos, fue aprobado el 2010 como un algoritmo de riesgo de malignidad ovárica (ROMA ®), el cual incorpora un índice predictivo que combina mediciones en suero de CA-125 y HE4 con el estatus menopáusico para generar una puntuación de riesgo para estratificar mujeres con tumores ováricos para predecir en alto o bajo riesgo de malignidad [43]. En general, las pruebas OVA1®, Overa® y ROMA® no están pensadas para ser utilizadas como pruebas diagnóstico independientes y no deben utilizarse sin pruebas de imagen o evaluaciones clínicas adicionales [44].

1.2.5 Tratamiento del CaOv.

En cuanto al tratamiento del CaOv, la cirugía citorreductiva primaria combinada de quimioterapia basada en agentes antineoplásicos derivados de platino ha sido una pieza fundamental para el tratamiento por más de medio siglo. La cirugía citorreductiva se realiza para establecer un diagnóstico preciso a través de la biopsia, eliminar tejido mal perfundido que pueda albergar la enfermedad y reducir el volumen tumoral para mejorar la eficacia de la quimioterapia adyuvante. La enfermedad residual después de la cirugía está inversamente relacionada con la supervivencia global; las pacientes con una citorreducción óptima (definida como enfermedad residual <1 cm) tienen un pronóstico más favorable en comparación con aquellas con citorreducción subóptima (enfermedad residual >1 cm) [45]. La efectividad del tratamiento está centrada en lograr la ausencia de enfermedad residual tras la cirugía citorreductiva y quimioterapia posterior, sin embargo e, CaOv lamentablemente no siempre se consiguen resecciones de la enfermedad residual [46].

En Chile, de acuerdo a la guía clínica AUGE, el esquema de tratamiento sigue 2 líneas principales: la cirugía primaria que tiene por objetivo la clasificación y estratificación del tumor para considerar un método directo que logre su máxima reducción, y la quimioterapia para aquellos casos confirmados histológicamente en cualquiera de las etapas y como terapia postcirugía [47]. La primera línea de quimioterapia sobre el CaOv en estados avanzados de la enfermedad,

comúnmente involucra fármacos que contengan agentes derivados de platino, la que a menudo se combina con un taxano [48].

Los complejos de platino II como Cisplatino o *cis*-diaminodicloroplatino(II) (CDDP), y Carboplatino o cis-diamina-(1,1-ciclobutanocarboxilato) de platino (II) (CP) son importantes fármacos anticancerígenos y ampliamente utilizadas en el tratamiento de CaOv como terapias de primera línea y son importantes en las decisiones clínicas del tratamiento de pacientes con esta enfermedad [49, 50].

1.2.5.1 Agentes de platino en quimioterapia de CaOv.

El cisplatino estructuralmente consiste en un átomo de platino acomplejado con dos grupos amonio y dos residuos de cloruro (Fig. 2A) [51]. Por otro lado, el carboplatino contiene un ligando bidenato ciclopropil malonato sustituido en lugar de ligandos cloruros que se encuentran en el CDDP (Fig. 2B) [52].

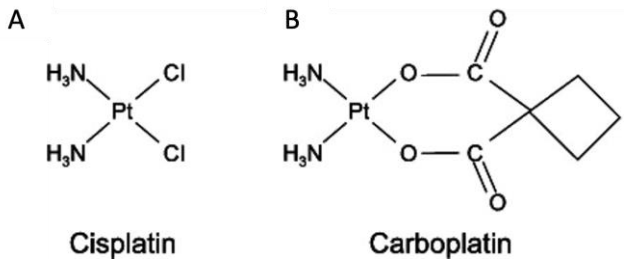

Figura 1.2: Estructura química de los agentes de platino.

La primera línea de defensa contra el cáncer de ovario en estadio avanzado suele consistir en agentes quimioterápicos a base de platino, como el cisplatino y el carboplatino. Estos fármacos

inducen la apoptosis, o muerte celular programada, al interferir con los mecanismos de reparación celular. A) Corresponde a la estructura molecular de Cisplatino y B) corresponde a Carboplatino. Tomado de Hay et al., 2000.

El Cisplatino ingresa a la célula a través de difusión pasiva, mediante el transportador de cobre 1 o 2 (CTR1 o CTR2) o mediante endocitosis. En el citoplasma, los átomos de cloro ligados al platino son desplazados por moléculas de agua debido a que la concentración de Cl^- es menor en el espacio intracelular, dando como resultado una especie electrófila fuerte que puede unirse a sitios nucleofílicos en el ADN, como la posición N7 de la guanina. Esta unión genera daño en el ADN de las células cancerosas y activando procesos de apoptosis [53]. Además, entrecruza las bases de guanina en las hebras de la doble hélice del ADN, impidiendo su desenrollamiento y separación, necesarios para la replicación del ADN, provocando un arresto en el ciclo celular S, G1 o G2-M induciendo apoptosis [54]. Además, CDDP genera daño en el DNA mitocondrial, provocando un cambio en la permeabilidad de las membranas mitocondriales, lo que conduce a la liberación de citocromo C y procaspasa 9. Estas moléculas liberadas se unen a APAF-1 y ATP para formar un apoptosoma, que a su vez activa la vía de las caspasas induciendo apoptosis [55]. Otro mecanismo de la acción citotóxica de CDDP es la inducción de estrés oxidativo en las células mediante el aumento del nivel de producción de especies reactivas del oxígeno, como los radicales hidroxilo y los superóxidos. En la membrana celular, una gran

cantidad de especies reactivas de oxígeno provoca la activación de la esfingomielinasa ácida, que, al hidrolizar los esfingolípidos a ceramidas, conduce a la agrupación de receptores FAS en la membrana plasmática, lo que conduce a la muerte celular. Además, el exceso de ROS, activa la proteína pro-apoptótica BAX, activando también apoptosis [56].

El carboplatino ingresa a la célula por difusión pasiva, por transporte activo utilizando canales iónicos, o mediante CTR1 [57]. En el citoplasma experimenta la hidrólisis del 1,1-ciclobutanedicarboxilato, adquiriendo una carga positiva. Esto permite que el carboplatino interactúe con moléculas nucleófilos dentro de la célula, uniéndose covalentemente a ligandos de tiol como cisteína y glutatión y también directamente con guanosina al sitio N7 de las bases de purina, dando lugar a interacciones ADN-proteína o ADN-ADN formando monoaductos de platino [52]. El CP se une covalentemente. El mecanismo de acción es similar al del CDDP generando lesiones en el ADN, inhibiendo la replicación y la transcripción, y conduciendo a la muerte celular [57].

Al comparar estos agentes de platino, CP presenta una reducción de los efectos secundarios de CDDP, especialmente la eliminación de los efectos nefrotóxicos. No obstante, su principal inconveniente es su efecto mielosupresor. Aunque el carboplatino es menos potente que el cisplatino, su eficacia varía. La norma clínica de dosificación del carboplatino suele ser una relación de 4:1 en

comparación con el cisplatino; es decir, se requiere cuatro veces más carboplatino para lograr la misma eficacia que el cisplatino [58].

En pacientes con cáncer de ovario recurrente, el pronóstico y la eficacia del tratamiento dependen de la sensibilidad al platino influenciando el éxito o la recurrencia del tratamiento del CaOv. Aunque el platino inicialmente muestra en los pacientes una respuesta positiva, la experiencia muestra que la mayoría presenta un relapso de la enfermedad después de 6 a 12 meses de tratamiento, estas pacientes son categorizados como platino-sensibles. Sin embargo, si el relapso ocurre con menos de 6 meses posterior al tratamiento, se considera a estas pacientes como platino-resistentes [59]. Para estas pacientes, la mediana de supervivencia global es de aproximadamente 1 año y las tasas de respuesta esperadas a las terapias disponibles son pobres, oscilando entre el 3 y el 30% [60], la razón puede ser atribuida a múltiples factores aún no comprendidos asociados a mecanismos de quimiorresistencia y se necesitan nuevas terapias basadas en el conocimiento de estos mecanismos para responder a esta necesidad insatisfecha de nuevas terapias y avances en la atención a pacientes con CaOv resistentes al platino.

Las pacientes platino-resistentes, son complejas de tratar mediante quimioterapia, ya que son esencialmente incurables, y el objetivo del tratamiento es la paliación. En ese caso, la quimioterapia con agentes individuales de segunda línea muestra buena actividad y menor toxicidad que el uso de una

quimioterapia combinada. En este contexto, el uso secuencial de agentes quimioterapéuticos individuales es la mejor opción a considerar, ya que ninguna combinación de fármacos ha demostrado ser superior [61].

Cuando las terapias basadas en platino muestran poca efectividad, se debe utilizar una segunda línea de quimioterapéuticos. Se ha propuesto la utilización de inhibidores de la poli(ADP-ribosa) polimerasa (PARPi) ya que ha mostrado buenos resultados en la terapia en pacientes con mutaciones en BRCA1/2 y en cáncer de ovario recurrente sensible al platino [62, 63]. Sin embargo, en casos de cáncer de ovario resistente al platino y recurrente, el tratamiento de segunda línea se centra en el uso de antraciclinas, destacando la utilización de doxorrubicina (DOX) [64].

1.2.5.2 Doxorrubicina en quimioterapia de CaOv.

La doxorrubicina (DOX) es un fármaco antineoplásico ampliamente utilizado en el tratamiento de neoplasias malignas [65]. Es un fármaco perteneciente a la familia de antraciclinas y actúa como un potente agente con actividad citotóxica. Aunque sus mecanismos de acción no están completamente descritos, este fármaco ejerce sus efectos mediante la intercalación en el ADN con los anillos D, C y B, como se muestra en la Figura 1.2.6. También interactúa con un carbohidrato (daunosamina) en el sitio catalítico de la topoisomerasa-II, interrumpiendo los mecanismos de reparación celular mediados por esta enzima.

Además, la oxidación de la quinona (anillo C) promueve la generación de especies reactivas de oxígeno (ROS) que inducen daño en las membranas mediante estrés oxidativo y peroxidación lipídica [66]. La doxorrubicina inhibe la cadena transportadora de electrones a nivel mitocondrial, causando daño por estrés oxidativo generado por los radicales libres [67].

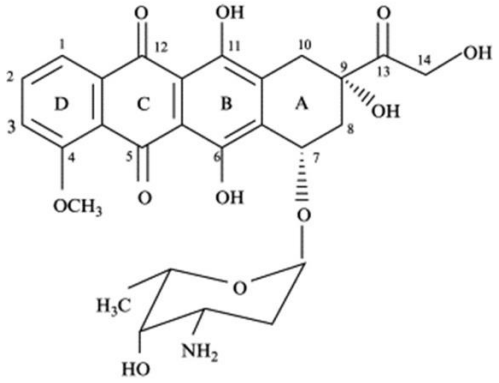

Figura 1.3: Estructura de la doxorrubicina.

La doxorrubicina (DOX) es un fármaco citotóxico de amplio espectro derivado de la familia de las antraciclinas. Se utiliza en la terapia del cáncer y es uno de los agentes quimioterapéuticos más efectivos. Sus anillos D, C y B se unen fuertemente al ADN, bloqueando su reparación mediada por la Topoisomerasa II, mientras que el anillo A y la porción tipo carbohidrato (Daunosamina) se asocian al sitio catalítico de la enzima. La quinona (anillo C) se oxida a semi-quinona, promoviendo la producción de especies reactivas de oxígeno (ROS).

La doxorrubicina liposomal pegilada (PLD), es la forma de administración para el tratamiento de CaOv recurrente o resistente a platino, sugiriendo que la PLD puede mejorar la tasa de supervivencia de las pacientes con CaOv

recurrente y con un perfil de toxicidad diferente en comparación con otros fármacos [68]. En terapias con PLD se ha visto prolonga el intervalo libre de platino hasta al menos 6 meses en el 32,3% de las pacientes con relapso y disminuye los niveles de CA-125 como biomarcador de seguimiento al tratamiento [69]. Sin embargo, es crucial señalar que la respuesta a la DOX puede verse obstaculizada por la quimiorresistencia, limitando su efectividad terapéutica [70-72].

Pese al uso de la quimioterapia en CaOv, estos tratamientos son poco específicos. Se ha visto que los pacientes responden a los quimioterapéuticos, pero la mayoría recae dentro de los 15 meses debido a la quimiorresistencia [73].

1.3. Quimiorresistencia en CaOv.

1.3.1 Generalidades de quimiorresistencia en CaOv.

La mayoría de las pacientes con CaOv que son tratadas, posterior a la cirugía citorreductora y la quimioterapia adyuvante, alcanzan una remisión clínica completa. Sin embargo, el 25% de las pacientes en etapa temprana y el 80% en etapas avanzadas, experimentan la recurrencia del cáncer debido a la quimiorresistencia, limitando la efectividad de la terapia [74].

La quimiorresistencia resistencia a la quimioterapia se clasifica en 2 tipos: resistencia intrínseca a la quimioterapia, donde las células cancerosas son inherentemente resistentes al tratamiento con medicamentos; y resistencia

adquirida a la quimioterapia, que puede adquirirse durante el curso del tratamiento. La resistencia intrínseca a la quimioterapia se debe a que las células cancerosas poseen varias modificaciones biológicas, incluida la inhibición de la captación de fármacos, el aumento del flujo de medicamentos, el aumento de la desintoxicación de los medicamentos quimioterapéuticos, la inhibición de la apoptosis, aumento en la expresión de proteínas de sobrevida, entre otros. Mientras que la resistencia adquirida a la quimioterapia puede surgir debido a alteraciones genéticas y epigenéticas que ayudan a las células cancerosas a adaptarse a los efectos inducidos por la quimioterapia, como el estrés, el daño al ADN y la apoptosis [45]. Estos mecanismos se presentan en la Figura 1.2.4.

En cáncer de ovario, varios mecanismos han sido identificados como contribuyentes a la quimiorresistencia en CaOv, tales como: aumento de la expresión de transportadores de eflujo, como el aumento en a la expresión de la glucoproteína P (P-gp), que les permite expulsar agentes quimioterapéuticos de la célula, reduciendo su efectividad; disminución de la absorción de los fármacos; disminución de la reparación; disminución de la apoptosis; alteraciones en la activación de reparación del ADN, mutaciones en P53 y aumento en la expresión de enzimas detoxificadoras [75]. Estos mecanismos se presentan en la Figura 1.2.4.

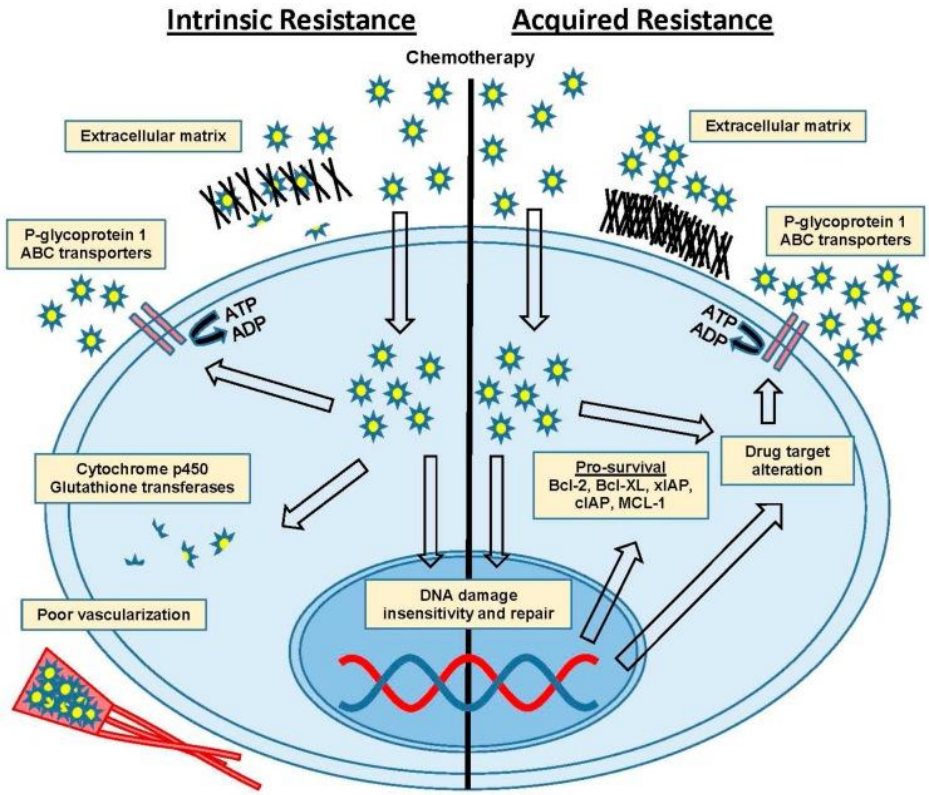

Figura 1.4: Mecanismos de quimiorresistencia intrínsecos y adquiridos en cáncer de ovario.

La quimiorresistencia en cáncer de ovario, incluye proteínas de la matriz extracelular, bombas de eflujo de glucoproteína P (P-gp); aumento en la expresión de enzimas detoxificadoras como citocromo p450 y glutatión transferasas; disminución en la vascularización; insensibilidad al daño del ADN y reparación, alteración de la diana farmacológica; y regulación al alza de proteínas pro-supervivencia y anti-apoptóticas. Abreviaciones: adenosina difosfato (ADP), adenosina trifosfato (ATP), linfoma de células B 2 (BCL-2), linfoma de células B extragrande (BCL-XL), Leucemia de células mieloides 1 (MCL-1), proteína inhibidora de la apoptosis ligada al cromosoma X/inhibidor celular de la apoptosis (xIAP/cIAP). Adaptado desde Cornelisom y col., 2017.

La heterogeneidad intra-tumoral (ITH), también complejiza el tratamiento ya que aumenta la capacidad del tumor para adaptarse al microambiente inhóspito. Durante el tratamiento con quimioterapéuticos, los subclones, en función de los fenotipos o genotipos, tienen ventaja de supervivencia con una mayor expansión y evolución clonal. Por lo tanto, el grado de ITH se correlaciona con la tasa de enfermedad recurrente. [76].

Otro aspecto interesante a considerar, son las adaptaciones metabólicas ejercidas por las células tumorales, tales como: incremento de la captación de glucosa, aumento en la glucólisis, aumento en la fosforilación oxidativa, alteraciones del microambiente tumoral, modificación del metabolismo lipídico, entre otros [77]. Estos cambios metabólicos pavimentan el desarrollo de la quimiorresistencia.

1.3.2 Metabolismo y quimiorresistencia en CaOv.

En cáncer, las células tumorales muestran una alta flexibilidad metabólica, es decir, la capacidad de utilizar diferentes nutrientes. Además, las células tumorales pueden cooperar entre ellas (es decir, simbiosis metabólica) o competir con las poblaciones de células no cancerosas. Estos escenarios participan en la heterogeneidad metabólica intratumoral, proporcionando a las células cancerosas múltiples adaptaciones y opciones de escape cuando son enfrentados a fármacos quimioterapéuticos.

En relación a las adaptaciones metabólicas en células en CaOv, se ha observado un aumento en la actividad de Piruvato deshidrogenasa con un aumento en la glucólisis y producción de lactato, las cuales están relacionadas con resistencia al tratamiento con cisplatino y mal pronóstico en este cáncer [78]. El aumento en la tasas de glucólisis también se ha relacionado con una actividad mitocondrial reducida en células resistentes en comparación con las células sensibles a cisplatino [79]. En relación con la actividad mitocondrial, se ha descrito una mayor dependencia del metabolismo energético mitocondrial, en particular la fosforilación oxidativa como una característica distintiva en quimiorresistencia en varios tipos de cánceres que incluyen el CaOv [80].

Las células tumorales presentan una alta variación en su metabolismo. Es por esto que células quimiorresistentes, frente a una disminución en la disponibilidad de glucosa, son capaces de adaptarse y utilizar otras fuentes de energía para recargar la generación de ATP mediante la fosforilación oxidativa [81].

Frente al daño generado de los agentes de platino en el ADN, que inducen a apoptosis y generación de especies reactivas del oxígeno, las células se protegen activando la biosíntesis de glutatión, molécula que se une a agentes de platino para su depuración dentro de la célula [82]. Además, frente a la exposición con doxorrubicina, se ha observado que aumentan también los niveles intracelulares de glutatión como una respuesta de protección celular [83].

El metabolismo de la glutamina es una de las vías relacionadas con la biosíntesis de glutatión, anaplerosis, síntesis de aminoácidos y nucleótidos. Se ha descubierto que las células resistentes dependen del metabolismo de la glutamina y la privación de glutamina conduce al deterioro de la biosíntesis de nucleótidos, lo que sensibiliza a células resistentes a la muerte celular, mejorando la terapia inducida por cisplatino [84].

Otro aspecto interesante a abordar en el metabolismo es lo relacionado con los lípidos. La fosfolipasa A2 citosólica (cPLA2) asociada a las grandes gotas de lípidos en células de cáncer de ovario resistentes, participa en la resistencia a fármacos con carboplatino. La cPLA2 es fosforilada y activada por la enzima 6-fosfofructo-2-quinasa/fructosa-2,6-bifosfatasa 3 (PFKFB3), una serina/treonina quinasa y reguladora de la glucólisis, que evita la lipofagia de las gotas lipídicas. Este fenotipo está asociado con la resistencia a la quimioterapia. Por el contrario, el inhibidor de PFKFB3, desactiva la cPLA2 y la lipofagia, mejorando la sensibilidad a fármacos y aportando a la importancia del metabolismo lipídico en la quimiorresistencia [85]. Interesantemente, la inhibición de la ácido graso sintasa (FASN), sensibiliza a células resistentes de CaOv quimiorresistentes al tratamiento con cisplatino [86].

Por lo tanto, los adaptaciones metabólicas en tumores de CaOv juegan un rol relevante en el desarrollo de quimiorresistencia, siendo importante estudiar a profundidad las vías metabólicas implicadas en estos fenómenos. Esto implica

un desafío por lo complejo que es el metabolismo, sin embargo, el desarrollo de plataformas analíticas ha aportado a resolver estos retos, tal como lo ha hecho la metabolómica.

1.4 Metabolómica.

La metabolómica se refiere a la identificación y cuantificación sistemática de moléculas pequeñas como productos metabólicos o del metaboloma de un sistema biológico tanto como de una célula, tejido, órgano, fluido biológico u organismo en un momento específico. Los metabolitos son los productos finales de las rutas metabólicas, las cuales son reflejo del fenotipo de la muestra biológica respuesta a cambios genéticos o ambientales [87]. Por lo tanto, el metabo loma proporciona una lectura funcional o “fotografía” de estos cambios corriente arriba. A su vez, metabolitos individuales afectan la actividad de las proteínas y, de esta manera, alteran la transcripción del ARN y la replicación del ADN (Figura 1.2.5). Los perfiles metabólicos son una herramienta prometedora para el análisis del fenotipo maligno, la evaluación de dianas farmacológicas y el diagnóstico de tumores [88].

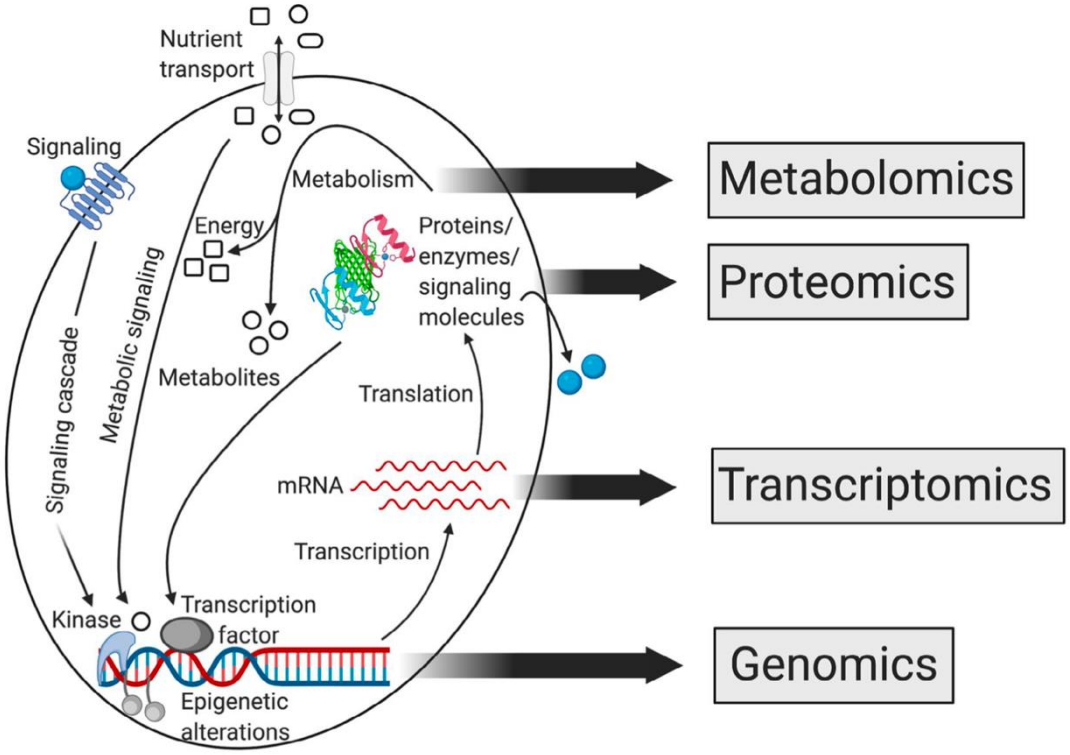

Figura 1.5: La relación entre los enfoques ómicos en los sistemas biológicos.

El cáncer es causado por cambios a nivel genómico que resultan en una transcripción de ARN alterada, expresión de proteínas y función proteica. El metaboloma proporciona una lectura funcional de estos cambios aguas arriba e implica la interacción con el ambiente. A su vez, los metabolitos individuales afectan la actividad de las proteínas y, de esta manera, alteran la transcripción del ARN y la replicación del ADN. Adaptado desde Schmidt y col., 2021.

En la práctica, la metabolómica se define como el análisis de metabolitos de moléculas pequeñas (≤1500 Daltons y no péptidos) en una muestra biológica. Implica la identificación simultánea de cientos a miles de sustancias químicas, en parte, basándose en las propiedades químicas y/o el peso de los átomos dentro de una molécula. Esto contrasta con la medición clínica estándar de metabolitos,

como la glucosa y la urea, que se basa en la identificación de sustancias químicas mediante reacciones enzimáticas y requiere una prueba separada para cada metabolito [89].

En general, la metabolómica no dirigida se utiliza para la generación de hipótesis y se emplea ampliamente en el descubrimiento de biomarcadores. En genómica, transcriptómica y proteómica, el objetivo es identificar la estructura de macromoléculas a partir de una secuencia de constituyentes químicos (nucleótidos, aminoácidos) que están bien definidos y son relativamente limitados en diversidad. En contraste, la metabolómica trata con un conjunto químicamente diverso y complejo de moléculas. Dado que los lípidos, carbohidratos, ácidos orgánicos y otras moléculas polares tienen una amplia gama de características físicas, se requieren múltiples métodos para la preparación de muestras y la adquisición de datos para su análisis. Además, los metabolitos que son anotados en experimentos no dirigidos requieren una validación posterior. Por lo tanto, la utilidad de la metabolómica no dirigida para ayudar a la comprensión e interpretación biológica está limitada por la capacidad para identificar metabolitos desconocidos [90].

Las técnicas que se utilizan con mayor frecuencia para la elaboración de perfiles de metabolomas, son la espectrometría de masas (MS) acopladas a sistemas cromatográficos y la resonancia magnética nuclear (RMN) [13]. La espectrometría de masas (MS) es la técnica analítica más ampliamente utilizada

en metabolómica. Se basa en determinar la relación de masa a carga (m/z) de una molécula y/o sus fragmentos característicos. Una muestra en fase líquida o gaseosa se inyecta en el espectrómetro de masas, donde los metabolitos se ionizan y luego se separan según su m/z. La MS suele estar acoplada con una etapa cromatográfica inicial, lo que aumenta la resolución de compuestos isobáricos (misma masa) y mejora la detección de especies menos abundantes al reducir la supresión de la señal por especies más abundantes. La cromatografía líquida (LC) implica el paso de una solución líquida de metabolitos sobre una columna de fase sólida, durante la cual se separan según su afinidad química con la fase estacionaria. Para la LC-MS es necesario utilizar diferentes columnas de fase sólida y composiciones de fase móvil para la separación óptima de compuestos de diferentes clases químicas. Por ejemplo, la lipidómica, que se centra en el subconjunto lipídico del metaboloma, implica técnicas cromatográficas fundamentalmente diferentes de las técnicas utilizadas para analizar metabolitos polares como carbohidratos o ácidos orgánicos. Sin embargo, dada la combinación de facilidad de uso con biofluídos, alta sensibilidad y amplio rango de metabolitos que se pueden medir, la LC-MS es el método analítico más integral y ampliamente utilizado asociado con la metabolómica.

La clasificación de metabolitos está basada en los grupos funcionales de las moléculas, los cuales son de bajo peso molecular (< 900 Da), estos incluyen

alcoholes, aminoácidos, ácidos carboxílicos y carbohidratos [91]. Otro grupo de metabolitos son los lípidos y sus derivados [92].

En metabolómica, es importante establecer un claro flujo de trabajo. Por ejemplo para LC-MS implica varios pasos clave para analizar la composición de metabolitos de muestras biológicas, los cuales se resumen en los siguientes pasos [93] y en la Figura 1.6:

- Preparación de la muestra: Este paso implica la extracción de la muestra según la cobertura de la naturaleza química de los metabolitos a estudiar (desde altamente polares a no polares).
- Separación y adquisición de datos. El sistema LC separa los metabolitos en la muestra según sus propiedades químicas, mientras que el espectrómetro de masas ioniza las muestras (según las fuentes de ionización disponibles) detecta y analiza la relación masa-carga (m/z) de los metabolitos.
- Procesamiento de datos: Los datos crudos se procesan para eliminar ruido y artefactos, así como para alinear y normalizar. En este paso se obtiene el Bucket Table, que corresponden a la matriz de *features* (señal tridimensional constituida por la relación m/z, tiempo de retención e intensidad de la señal).

- Análisis estadísticos: Se utilizan para comparar los perfiles de señales. Por ejemplo, en el contexto de CaOv, aquellos con diferentes subtipos histológicos o respuestas al tratamiento con fármacos.
- Anotación e identificación de compuestos: Se realiza comparando los valores m/z y los tiempos de retención de los picos detectados con una base de datos espectrales de metabolitos conocidos o utilizando estándares para garantizar la exactitud de la identificación. Acá se anotan los biomarcadores potenciales o vías asociadas con una condición o tratamiento específico, con el fin de entregar la interpretación biológica.

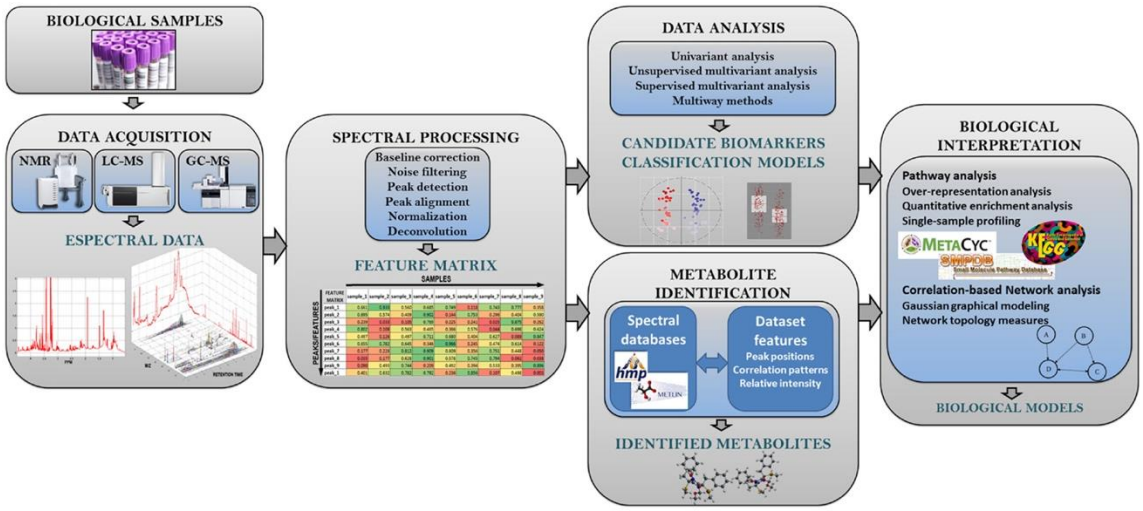

Figura 1.6: Flujo de trabajo para un análisis en metabolómica.

Adaptado desde Alonso y col., 2015.

1.5 Modelos biológicos para el estudio del impacto del metabolismo en quimiorresistencia del CaOv.

El principal problema en CaOv, radica en que la identificación de pacientes predispuestas a la quimiorresistencia, ya que actualmente no existen pruebas para guiar a los médicos a tomar decisiones informadas para alterar el curso del tratamiento antes de la quimioterapia. Por lo tanto, es importante elucidar los mecanismos moleculares implicados en el rol del metabolismo sobre la quimiorresistencia, dentro de los modelos biológicos se encuentran los modelos celulares.

Se han establecido diferentes modelos de líneas celulares con características histológicas y genéticas únicas para estudiar el cáncer de ovario, incluyendo subtipos de alto grado seroso y no seroso clasificados según sus perfiles genómicos [94]. Las células SK-OV-3, son una línea celular de cáncer de ovario humano derivada de carcinoma de ovario no seroso, muestra una morfología similar a la epitelial. Proviene de líquido ascítico en lugar de un tumor primario, asociado con enfermedad en etapa avanzada, y por lo tanto, SK-OV-3 presenta un comportamiento invasivo típico del cáncer de ovario avanzado [95]. Por otro lado, las células OVCAR-3 son una línea celular de cáncer de ovario humano derivada de carcinoma seroso de alto grado y muestra una morfología similar a la epitelial [96]. Se ha demostrado que las líneas celulares SK-OV-3 y OVCAR-3 muestran comportamientos diferentes, las células SK-OV-3 son más rápidas en migración, significativamente más invasivas [97-99], y generan

metástasis más sustanciales en modelos *in vivo* [100]. Ambas líneas celulares desarrollan resistencia a fármacos de quimioterapia de primera línea como el CDDP, siendo SK-OV-3 la que muestra una mayor tasa de supervivencia después del tratamiento [101]. Adicionalmente, las dos líneas celulares han mostrado comportamientos de respuesta diferentes al tratamiento con DOX [102, 103]. Estas diferencias en el comportamiento celular relacionadas con la sensibilidad a fármacos quimioterapéuticos, destacan características distintivas de cada modelo celular en el contexto del CaOv, con el fin de estudiar las diferencias metabólicas a través de metabolómica que contribuyan a la quimiorresistencia.

CAPÍTULO 2 : HIPÓTESIS Y OBJETIVOS

2.1 Hipótesis.

El cáncer de ovario representa un desafío clínico importante, la resistencia a los medicamentos sigue siendo una barrera crítica que limita la eficacia del tratamiento. La metabolómica ha surgido como una herramienta prometedora para descubrir biomarcadores y analizar las vías metabólicas involucradas en la resistencia a los fármacos. Sin embargo, hay una falta de comprensión integral sobre cómo los cambios en los metabolitos específicos y como las vías metabólicas contribuyen a este fenómeno. En particular, no está claro cómo los perfiles metabólicos y lipídicos se modifican en las células de cáncer de ovario resistentes en comparación con las sensibles, y cómo estas alteraciones pueden influir en la eficacia de los agentes antineoplásicos. Por lo tanto, es esencial investigar y caracterizar los cambios metabólicos específicos asociados con la resistencia a estos medicamentos para mejorar las estrategias de tratamiento y superar la resistencia a los fármacos en el cáncer de ovario.

Nuestra Hipótesis de trabajo es:

La aplicación de la metabolómica utilizando UHPLC-HR-QTOF-MS en células sensibles y resistentes de cáncer de ovario nos permite identificar metabolitos importantes involucrados en los mecanismos de resistencia a los

agentes antineoplásicos. Las alteraciones en las vías metabólicas pueden influir significativamente en estos mecanismos de resistencia, modificando así la respuesta de las células a estos fármacos reduciendo su eficacia.

2.2 Objetivo general.

Investigar el papel de los metabolitos en los mecanismos de resistencia a agentes antineoplásicos en células de cáncer de ovario mediante una estrategia analítica basada en metabolómica utilizando UHPLC-HR-QTOF-MS, con el fin de comprender mejor las vías metabólicas alteradas y su impacto en los parámetros farmacológicos.

2.3 Objetivos específicos.

1. Analizar el fenotipo de sensibilidad y respuesta frente a agentes antineoplásicos en líneas celulares SK-OV-3 y OVCAR-3.
2. Caracterizar los perfiles metabólicos en las líneas celulares SK-OV-3 y OVCAR-3 mediante el uso de análisis metabolómico utilizando UHPLC-HR-QTOF-MS.
3. Evaluar como las alteraciones en las vías metabólicas específicas afectan la respuesta de las células de cáncer de ovario a los agentes antineoplásicos.

CAPÍTULO 3 : ESTRATEGIA ANALÍTICA

La presente tesis doctoral tiene como objetivo identificar las diferencias metabólicas mediadas entre células de cáncer de ovario con distintas sensibilidades a fármacos antineoplásicas a través de una estrategia analítica basada en metabolómica utilizando UHPLC-HR-QTOF-MS, y evaluar su contribución en los mecanismos de quimiorresistencia.

Para lograr a cabo este objetivo se estableció una línea de trabajo comenzando con la caracterización del fenotipo de respuesta a tres fármacos antineoplásicos de primera línea (cisplatino y carboplatino) y una de segunda línea de terapia (doxorrubicina) sobre células de cáncer de ovario OVCAR-3 y SK-OV-3, mediante el análisis de la inhibición del crecimiento celular *Growth Rate metrics*. Este análisis permite medir si la respuesta a fármacos es citostática, totalmente citostática o citotóxica, potencia y eficacia de los fármacos, sobre el crecimiento de las células neoplásicas.

Como segunda etapa se estableció un análisis de metabolitos presentes en las células OVCAR-3 y SK-OV-3 a través de un estudio metabolómico basado en una estrategia analítica de cromatografía líquida acoplada a espectrometría de masas de alta resolución UHPLC-HR-QTOF-MS (Bruker). Se estandarizaron la cantidad de material biológico, las condiciones cromatográficas y de espectrometría de masas. Para el análisis se utilizaron dos columnas de

cromatografía, una de fase normal HILIC Acquity UPLC BEH Amide HILIC (2,1 × 100 mm; 1,7 µm) y otra de fase reversa Acquity BEH C18 (2,1 × 100 mm; 17 µm). Ambas condiciones fueron analizadas en modos de ionización por electrospray (ESI) positivo y negativo, con el fin de lograr una mayor cobertura del metaboloma. La data cruda obtenida fue procesada utilizando el programa *MetaboScape 3.0* de Bruker mediante el algoritmo *Time aligned Region complete eXtraction (T-ReX 3D)*, el cual sigue un flujo de trabajo que involucra la recalibración de masas, alineamiento de los tiempos de retención y extracción de las características *(features)*. Los *features* están conformados por la masa/carga (m/z), el tiempo de retención y la intensidad normalizada de cada señal analítica contenida en una matriz de datos llamado *Bucket Table*.

Los *Bucket Tables* de cada análisis obtenido fue exportado al programa de acceso libre *Metaboanalyst 5.0* para la confección de los modelos estadísticos de Análisis de Componentes Principales (PCA) y Análisis Discriminante por Regresión de Mínimos Cuadrados Parciales Ortogonal (OPLS-DA), con el fin de identificar las diferencias entre células OVCAR-3 y SK-OV-3 caracterizadas por los *features*. Luego, los *features* fueron anotados y luego identificados mediante la *Metaboscape 3.0* que integra una herramienta de trabajo que contempla el análisis espectral según error de masa, error isotópico y búsqueda en distintas bases de datos. Además, la identificación fue acompañada por el programa de acceso libre *Sirius 4.0* que integra análisis de patrones isotópicos de alta resolución y árboles de fragmentación para la elucidación estructural.

Posteriormente, para esta etapa, los metabolitos identificados fueron integrados a la herramienta *Metabolite Set Enrichment Analysis (MSEA)* del programa de acceso libre *Metaboanalyst* para el análisis de las rutas metabólicas enriquecidas en células OVCAR-3 y SK-OV-3.

Como tercera etapa, se intervino una ruta metabólica aumentada en células SK-OV-3, las cuales presentaron un comportamiento de respuesta resistente al tratamiento con antineoplásicos. Para esto, se observó que glutatión estaba aumentado en células SK-OV-3, por lo tanto las células fueron depletadas farmacológicamente de este metabolito y luego se analizó la respuesta al tratamiento con fármacos antineoplásicos mediante análisis de la inhibición del crecimiento celular *Growth Rate metrics*.

Finalmente, como cuarta etapa y para una mayor comprensión del metabolismo. Se analizó la dependencia del metabolismo glucolítico mediante su inhibición sobre células OVCAR-3 y SK-OV-3 y luego se realizó un análisis del metabolismo con una estrategia lipidómica. Para el estudio se utilizaron una columna de cromatografía de fase reversa Phenomenex Kinetex® C18 (4,6 $\times$ 100 mm; 2,6 µm) y analizadas en los modos de ionización por electrospray (ESI) positivo y negativo. Se realizó un flujo de trabajo, en este programa, que incluyó la recalibración de masas, alineamiento de los tiempos de retención, extracción de los features, administración de aductos, normalización por controles de calidad, filtrado de la data por los blancos y generación de los *Bucket Tables*. Los

Bucket Tables de cada análisis fueron exportados al programa de acceso libre *Metaboanalyst 5.0* para la confección de los modelos estadísticos de Análisis de Componentes Principales (PCA) y Análisis Discriminante por Regresión de Mínimos Cuadrados Parciales Ortogonal (OPLS-DA) y los *features* que caracterizaron las diferencias entre células OVCAR-3 y SK-OV-3. La identificación de los lípidos fue realizada por comparación de los espectros obtenidos con la base de datos de LipidBlast, solo con aquellos que se obtuvo los espectros de MS/MS.

La estrategia analítica general de esta tesis doctoral se puede visualizar en la Figura 3.1A y B.

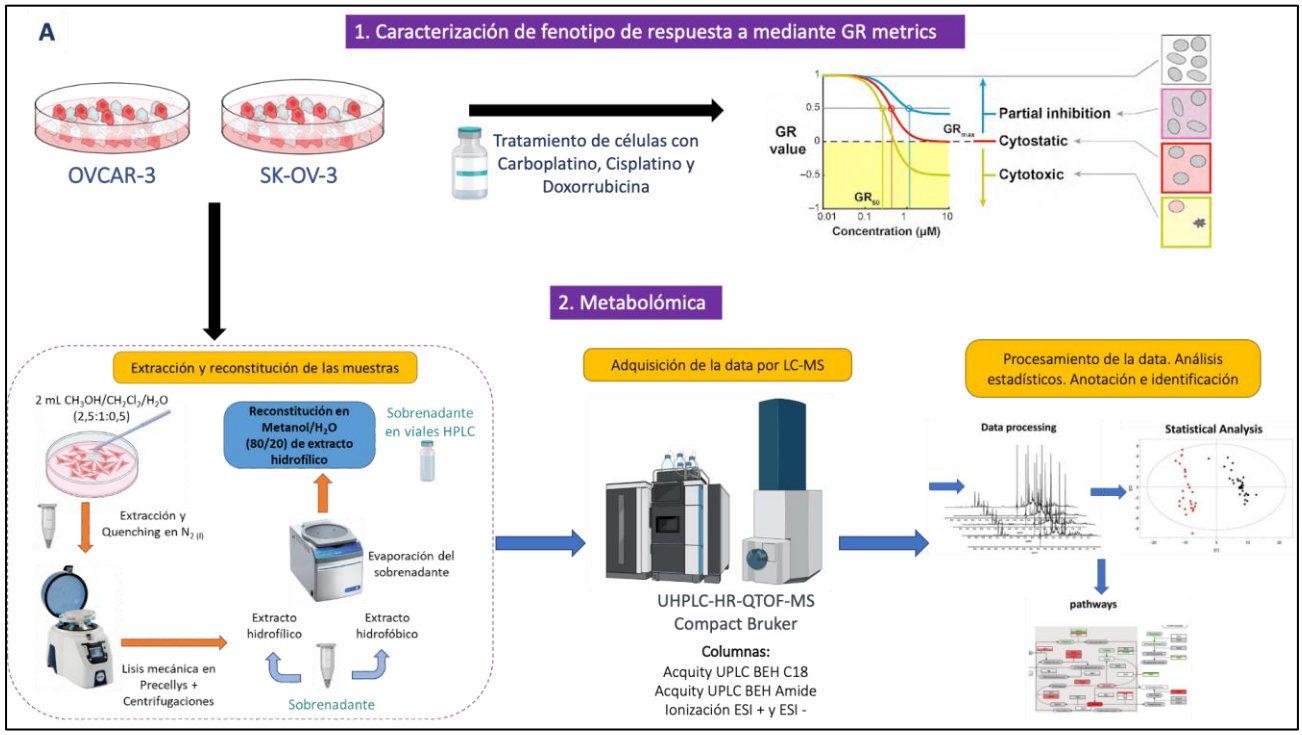

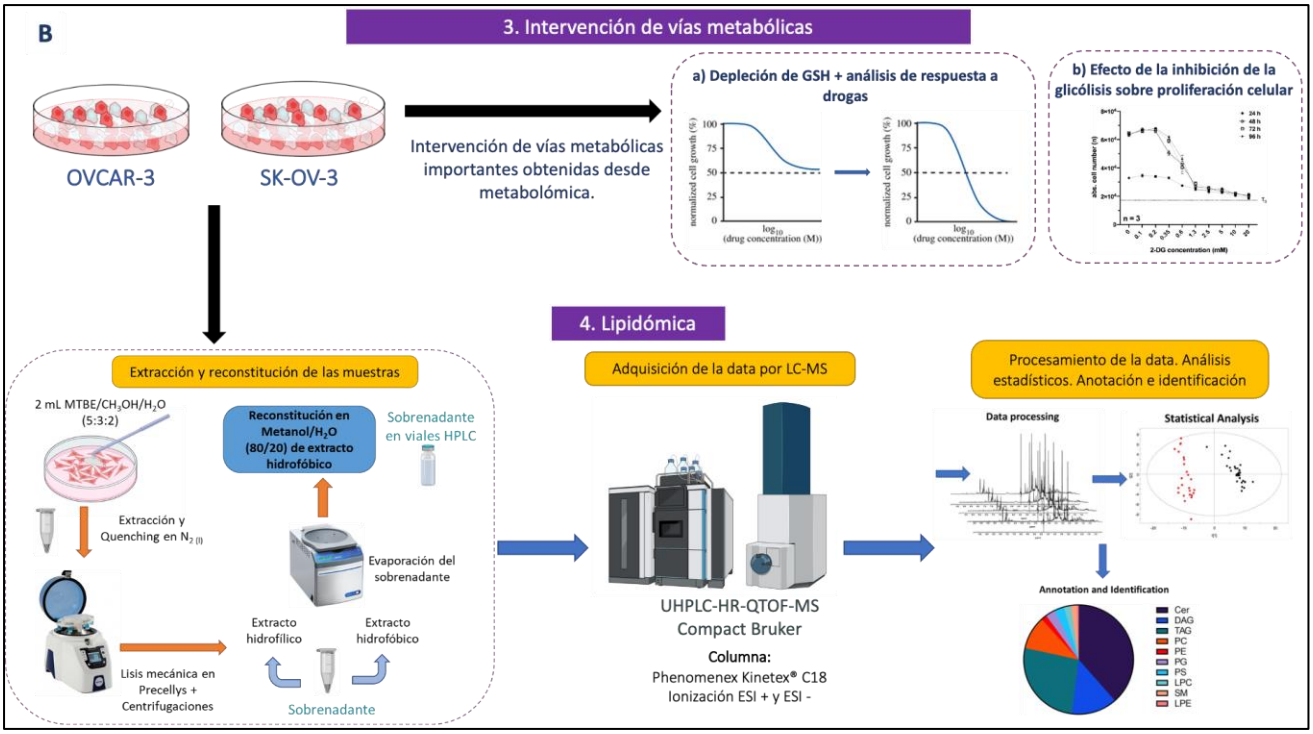

Figura 3.1: Estrategia analítica utilizada para el estudio de las diferencias metabólicas relacionadas con quimiorresistencia en células de cáncer de ovario.

La estrategia analítica para el desarrollo de los objetivos planteados involucra: A) la caracterización del fenotipo de respuesta a agentes antineoplásicos, y el análisis metabolómico de las células OVCAR-3 y SK-OV-3; además, B) la intervención de vías metabólicas relevantes obtenidas por metabolómica, y el análisis lipidómico de las células OVCAR-3 y SK-OV-3.

Referencias

[1] Bray F, Laversanne M, Weiderpass E, Soerjomataram I. The ever-increasing importance of cancer as a leading cause of premature death worldwide. Cancer. 2021;127:3029-30. https://doi.org/10.1002/cncr.33587

[2] Sung H, Ferlay J, Siegel RL, Laversanne M, Soerjomataram I, Jemal A, et al. Global Cancer Statistics 2020: GLOBOCAN Estimates of Incidence and Mortality Worldwide for 36 Cancers in 185 Countries. CA Cancer J Clin. 2021;71:209-49. https://doi.org/10.3322/caac.21660

[3] Organización_Mundial_de_la_Salud. El diagnóstico temprano del cáncer salva vidas y reduce los costos de tratamiento.

[4] Ministerio_de_Salud. Marco general del Plan Nacional de Cáncer 2022-2027. 2022.

[5] Carrasco-Garcia MA, Neira-Mellado C, Klett B, Carcamo-Ulloa L. [Portrayal of cancer prevalence and mortality in Chilean digital media]. Rev Med Chil. 2021;149:716-23. https://doi.org/10.4067/s0034-98872021000500716

[6] Zhao S, Chen L, Zang Y, Liu W, Liu S, Teng F, et al. Endometrial cancer in Lynch syndrome. Int J Cancer. 2022;150:7-17. https://doi.org/10.1002/ijc.33763

[7] Torre LA, Trabert B, DeSantis CE, Miller KD, Samimi G, Runowicz CD, et al. Ovarian cancer statistics, 2018. CA Cancer J Clin. 2018;68:284-96. https://doi.org/10.3322/caac.21456

[8] Luvero D, Plotti F, Aloisia A, Montera R, Terranova C, Carlo De Cicco N, et al. Ovarian cancer relapse: From the latest scientific evidence to the best practice. Crit Rev Oncol Hematol. 2019;140:28-38. https://doi.org/10.1016/j.critrevonc.2019.05.014

[9] Kumar N. SAK. Advances in Tumour Biomarkers for Screening, Diagnosis and Management of Ovarian Malignancies. Journal of Clinical and Diagnostic Research. 2018;12:QE01 - QE7. https://doi.org/10.7860/JCDR/2018/34896.11453

[10] Berek JS, Renz M, Kehoe S, Kumar L, Friedlander M. Cancer of the ovary, fallopian tube, and peritoneum: 2021 update. Int J Gynaecol Obstet. 2021;155 Suppl 1:61-85. https://doi.org/10.1002/ijgo.13878

[11] Dong X, Men X, Zhang W, Lei P. Advances in tumor markers of ovarian cancer for early diagnosis. Indian J Cancer. 2014;51 Suppl 3:e72-6. https://doi.org/10.4103/0019-509X.154049

[12] Berek JS, Kehoe ST, Kumar L, Friedlander M. Cancer of the ovary, fallopian tube, and peritoneum. Int J Gynaecol Obstet. 2018;143 Suppl 2:59-78. https://doi.org/10.1002/ijgo.12614

[13] Yanisa Rattanapan TC. Integrative omics of ovarian cancer. Genetics and Molecular Research. 2019;18:gmr16039946. https://doi.org/10.4238/gmr16039946

[14] Olsen K, Oliphant M. Spread of Ovarian Cancer. Contemporary Diagnostic Radiology. 2008;31:1-5. https://doi.org/10.1097/01.Cdr.0000336964.29776.91

[15] Castells M, Thibault B, Delord JP, Couderc B. Implication of tumor microenvironment in chemoresistance: tumor-associated stromal cells protect tumor cells from cell death. Int J Mol Sci. 2012;13:9545-71. https://doi.org/10.3390/ijms13089545

[16] Liu MX CD, Ngan HYS. Mechanisms of Chemoresistance in Human Ovarian Cancer at a Glance. Gynecology & Obstetrics. 2012;2:e104. https://doi.org/10.4172/2161-0932.1000e104

[17] Meinhold-Heerlein I, Hauptmann S. The heterogeneity of ovarian cancer. Arch Gynecol Obstet. 2014;289:237-9. https://doi.org/10.1007/s00404-013-3114-3

[18] Prat J, Oncology FCoG. FIGO's staging classification for cancer of the ovary, fallopian tube, and peritoneum: abridged republication. J Gynecol Oncol. 2015;26:87-9. https://doi.org/10.3802/jgo.2015.26.2.87

[19] Cummings M, Nicolais O, Shahin M. Surgery in Advanced Ovary Cancer: Primary versus Interval Cytoreduction. Diagnostics (Basel). 2022;12. https://doi.org/10.3390/diagnostics12040988

[20] Rossing MA, Daling JR, Weiss NS, Moore DE, Self SG. Ovarian tumors in a cohort of infertile women. N Engl J Med. 1994;331:771-6. https://doi.org/10.1056/NEJM199409223311204

[21] Meinhold-Heerlein I, Fotopoulou C, Harter P, Kurzeder C, Mustea A, Wimberger P, et al. The new WHO classification of ovarian, fallopian tube, and primary peritoneal cancer and its clinical implications. Arch Gynecol Obstet. 2016;293:695-700. https://doi.org/10.1007/s00404-016-4035-8

[22] Stewart C, Ralyea C, Lockwood S. Ovarian Cancer: An Integrated Review. Semin Oncol Nurs. 2019;35:151-6. https://doi.org/10.1016/j.soncn.2019.02.001

[23] Rein BJ, Gupta S, Dada R, Safi J, Michener C, Agarwal A. Potential markers for detection and monitoring of ovarian cancer. J Oncol. 2011;2011:475983. https://doi.org/10.1155/2011/475983

[24] Gaona-Luviano P, Medina-Gaona LA, Magana-Perez K. Epidemiology of ovarian cancer. Chin Clin Oncol. 2020;9:47. https://doi.org/10.21037/cco-20-34

[25] Haier J, Sleeman J, Schafers J. Editorial series: cancer care in low- and middle-income countries. Clin Exp Metastasis. 2019;36:477-80. https://doi.org/10.1007/s10585-019-10003-4

[26] Collaborative Group on Epidemiological Studies of Ovarian C, Beral V, Gaitskell K, Hermon C, Moser K, Reeves G, et al. Ovarian cancer and smoking: individual participant meta-analysis including 28,114 women with ovarian cancer from 51 epidemiological studies. Lancet Oncol. 2012;13:946-56. https://doi.org/10.1016/S1470-2045(12)70322-4

[27] Chang ET, Canchola AJ, Lee VS, Clarke CA, Purdie DM, Reynolds P, et al. Wine and other alcohol consumption and risk of ovarian cancer in the California Teachers Study cohort. Cancer Causes Control. 2007;18:91-103. https://doi.org/10.1007/s10552-006-0083-x

[28] Cottreau CM, Ness RB, Kriska AM. Physical activity and reduced risk of ovarian cancer. Obstet Gynecol. 2000;96:609-14. https://doi.org/10.1016/s0029-7844(00)00972-8

[29] Liu Z, Zhang TT, Zhao JJ, Qi SF, Du P, Liu DW, et al. The association between overweight, obesity and ovarian cancer: a meta-analysis. Jpn J Clin Oncol. 2015;45:1107-15. https://doi.org/10.1093/jjco/hyv150

[30] Hada M, Edin ML, Hartge P, Lih FB, Wentzensen N, Zeldin DC, et al. Prediagnostic Serum Levels of Fatty Acid Metabolites and Risk of Ovarian Cancer

in the Prostate, Lung, Colorectal, and Ovarian (PLCO) Cancer Screening Trial. Cancer Epidemiol Biomarkers Prev. 2019;28:189-97. https://doi.org/10.1158/1055-9965.EPI-18-0392

[31] Huang J, Huang JLW, Wang J, Chung VCH, Wong MCS. Metabolic syndrome and risk of cancer in Chinese populations: a systematic review and meta-analysis in 57 260 individuals. The Lancet. 2018;392:S15. https://doi.org/https://doi.org/10.1016/S0140-6736(18)32644-8

[32] Gong TT, Wu QJ, Vogtmann E, Lin B, Wang YL. Age at menarche and risk of ovarian cancer: a meta-analysis of epidemiological studies. Int J Cancer. 2013;132:2894-900. https://doi.org/10.1002/ijc.27952

[33] Singla A. Epidemiology and Risk Factors for Ovarian Cancer. In: Mehta S, Singla A, editors. Preventive Oncology for the Gynecologist. Singapore: Springer Singapore; 2019. p. 223-31. 978-981-13-3438-2. https://doi.org/10.1007/978-981-13-3438-2_17

[34] Huang J, Chan WC, Ngai CH, Lok V, Zhang L, Lucero-Prisno DE, 3rd, et al. Worldwide Burden, Risk Factors, and Temporal Trends of Ovarian Cancer: A Global Study. Cancers (Basel). 2022;14. https://doi.org/10.3390/cancers14092230

[35] Paik ES, Lee YY, Lee EJ, Choi CH, Kim TJ, Lee JW, et al. Survival analysis of revised 2013 FIGO staging classification of epithelial ovarian cancer and

comparison with previous FIGO staging classification. Obstet Gynecol Sci. 2015;58:124-34. https://doi.org/10.5468/ogs.2015.58.2.124

[36] Doubeni CA, Doubeni AR, Myers AE. Diagnosis and Management of Ovarian Cancer. Am Fam Physician. 2016;93:937-44.

[37] Moss EL, Hollingworth J, Reynolds TM. The role of CA125 in clinical practice. J Clin Pathol. 2005;58:308-12. https://doi.org/10.1136/jcp.2004.018077

[38] Scholler N, Urban N. CA125 in ovarian cancer. Biomark Med. 2007;1:513-23. https://doi.org/10.2217/17520363.1.4.513

[39] Cannistra SA. Cancer of the ovary. N Engl J Med. 2004;351:2519-29. https://doi.org/10.1056/NEJMra041842

[40] Su Z, Graybill WS, Zhu Y. Detection and monitoring of ovarian cancer. Clin Chim Acta. 2013;415:341-5. https://doi.org/10.1016/j.cca.2012.10.058

[41] Kaijser J, Bourne T, Valentin L, Sayasneh A, Van Holsbeke C, Vergote I, et al. Improving strategies for diagnosing ovarian cancer: a summary of the International Ovarian Tumor Analysis (IOTA) studies. Ultrasound Obstet Gynecol. 2013;41:9-20. https://doi.org/10.1002/uog.12323

[42] Coleman RL, Herzog TJ, Chan DW, Munroe DG, Pappas TC, Smith A, et al. Validation of a second-generation multivariate index assay for malignancy risk of

adnexal masses. Am J Obstet Gynecol. 2016;215:82 e1- e11. https://doi.org/10.1016/j.ajog.2016.03.003

[43] Moore RG, Miller MC, Disilvestro P, Landrum LM, Gajewski W, Ball JJ, et al. Evaluation of the diagnostic accuracy of the risk of ovarian malignancy algorithm in women with a pelvic mass. Obstet Gynecol. 2011;118:280-8. https://doi.org/10.1097/AOG.0b013e318224fce2

[44] Liberto JM, Chen SY, Shih IM, Wang TH, Wang TL, Pisanic TR, 2nd. Current and Emerging Methods for Ovarian Cancer Screening and Diagnostics: A Comprehensive Review. Cancers (Basel). 2022;14. https://doi.org/10.3390/cancers14122885

[45] Pokhriyal R, Hariprasad R, Kumar L, Hariprasad G. Chemotherapy Resistance in Advanced Ovarian Cancer Patients. Biomark Cancer. 2019;11:1179299X19860815. https://doi.org/10.1177/1179299X19860815

[46] de Jong D, Thangavelu A, Broadhead T, Chen I, Burke D, Hutson R, et al. Prerequisites to improve surgical cytoreduction in FIGO stage III/IV epithelial ovarian cancer and subsequent clinical ramifications. J Ovarian Res. 2023;16:214. https://doi.org/10.1186/s13048-023-01303-1

[47] MINSAL. Estrategia Nacional de Cáncer. Chile 2016. 2016.

[48] Vasey PA. Resistance to chemotherapy in advanced ovarian cancer: mechanisms and current strategies. Br J Cancer. 2003;89 Suppl 3:S23-8. https://doi.org/10.1038/sj.bjc.6601497

[49] Ozols RF. Role of carboplatin in ovarian cancer. Current results and thoughts for the future. Acta Obstet Gynecol Scand Suppl. 1992;155:75-7.

[50] Smith ER, Wang JQ, Yang DH, Xu XX. Paclitaxel resistance related to nuclear envelope structural sturdiness. Drug Resist Updat. 2022;65:100881. https://doi.org/10.1016/j.drup.2022.100881

[51] Han SJ, Ahn TK, Choi HS, Shin JN, Piya S, Kim TH. TRAIL-induced cell death and caspase-8 activation are inhibited by cisplatin but not carboplatin. J Gynecol Oncol. 2009;20:113-6. https://doi.org/10.3802/jgo.2009.20.2.113

[52] Hay RW. 4 - Substitution Reactions in Four- and Five-Coordinate Complexes. In: Hay RW, editor. Reaction Mechanisms of Metal Complexes: Woodhead Publishing; 2000. p. 85-116. 978-1-898563-41-9. https://doi.org/https://doi.org/10.1533/9781782420637.85

[53] Jain A, Jahagirdar D, Nilendu P, Sharma NK. Molecular approaches to potentiate cisplatin responsiveness in carcinoma therapeutics. Expert Rev Anticancer Ther. 2017;17:815-25. https://doi.org/10.1080/14737140.2017.1356231

[54] Hashimoto S, Anai H, Hanada K. Mechanisms of interstrand DNA crosslink repair and human disorders. Genes Environ. 2016;38:9. https://doi.org/10.1186/s41021-016-0037-9

[55] Fuertes MA, Alonso C, Perez JM. Biochemical modulation of Cisplatin mechanisms of action: enhancement of antitumor activity and circumvention of drug resistance. Chem Rev. 2003;103:645-62. https://doi.org/10.1021/cr020010d

[56] Brozovic A, Ambriovic-Ristov A, Osmak M. The relationship between cisplatin-induced reactive oxygen species, glutathione, and BCL-2 and resistance to cisplatin. Crit Rev Toxicol. 2010;40:347-59. https://doi.org/10.3109/10408441003601836

[57] Sousa GFd, Wlodarczyk, Samarina Rodrigues, & Monteiro, Gisele. Carboplatin: molecular mechanisms of action associated with chemoresistance. Brazilian Journal of Pharmaceutical Sciences. 2014;50:693-701. https://doi.org/10.1590/S1984-82502014000400004

[58] Dasari S, Tchounwou PB. Cisplatin in cancer therapy: molecular mechanisms of action. Eur J Pharmacol. 2014;740:364-78. https://doi.org/10.1016/j.ejphar.2014.07.025

[59] Bayram E, Khatib G, Kucukgoz-Gulec U, Guzel AB, Vardar MA, Paydas S. Comparison of the effectiveness of liposomal doxorubicin and gemcitabine in patients with platinum-sensitive recurrent ovarian cancer receiving third-line

chemotherapy. Eur Rev Med Pharmacol Sci. 2023;27:6618-26. https://doi.org/10.26355/eurrev_202307_33132

[60] Morton M, Yao M, Chalif J, Lampert EJ, Chau D, Rose PG, et al. Association of Clinical Trial Participation With Improved Overall Survival for Recurrent, Platinum-Resistant Ovarian Cancer. Obstet Gynecol. 2023;142:459-66. https://doi.org/10.1097/AOG.0000000000005298

[61] Pignata S, Pisano C, Di Napoli M, Cecere SC, Tambaro R, Attademo L. Treatment of recurrent epithelial ovarian cancer. Cancer. 2019;125 Suppl 24:4609-15. https://doi.org/10.1002/cncr.32500

[62] Buklaho PA, Kisluk J, Niklinski J. Diagnostics and treatment of ovarian cancer in the era of precision medicine - opportunities and challenges. Front Oncol. 2023;13:1227657. https://doi.org/10.3389/fonc.2023.1227657

[63] Kim YN, Park B, Kim JW, Kim BG, Kim SW, Kim HS, et al. Triplet maintenance therapy of olaparib, pembrolizumab and bevacizumab in women with BRCA wild-type, platinum-sensitive recurrent ovarian cancer: the multicenter, single-arm phase II study OPEB-01/APGOT-OV4. Nat Commun. 2023;14:5476. https://doi.org/10.1038/s41467-023-40829-2

[64] Gordon AN, Tonda M, Sun S, Rackoff W, Doxil Study I. Long-term survival advantage for women treated with pegylated liposomal doxorubicin compared with topotecan in a phase 3 randomized study of recurrent and refractory epithelial

ovarian cancer. Gynecol Oncol. 2004;95:1-8. https://doi.org/10.1016/j.ygyno.2004.07.011

[65] Licata S, Saponiero A, Mordente A, Minotti G. Doxorubicin metabolism and toxicity in human myocardium: role of cytoplasmic deglycosidation and carbonyl reduction. Chem Res Toxicol. 2000;13:414-20. https://doi.org/10.1021/tx000013q

[66] Thorn CF, Oshiro C, Marsh S, Hernandez-Boussard T, McLeod H, Klein TE, et al. Doxorubicin pathways: pharmacodynamics and adverse effects. Pharmacogenet Genomics. 2011;21:440-6. https://doi.org/10.1097/FPC.0b013e32833ffb56

[67] Bhardwaj JK, Bikal P, Sachdeva SN. Chemotherapeutic drugs induced female reproductive toxicity and treatment strategies. J Biochem Mol Toxicol. 2023;37:e23371. https://doi.org/10.1002/jbt.23371

[68] Li XR, Zhu Y, Zhang GN, Huang JM, Pei LX. The impact of Pegylated liposomal doxorubicin in recurrent ovarian cancer: an updated meta-analysis of randomized clinical trials. J Ovarian Res. 2021;14:42. https://doi.org/10.1186/s13048-021-00790-4

[69] Yuan Z, Zhang Y, Cao D, Shen K, Li Q, Zhang G, et al. Pegylated liposomal doxorubicin in patients with epithelial ovarian cancer. Journal of Ovarian Research. 2021;14:12. https://doi.org/10.1186/s13048-020-00736-2

[70] Ghosh S, Chitgupi U, Sunar U, Lovell JF. Chemophototherapeutic Ablation of Doxorubicin-Resistant Human Ovarian Tumor Cells. Photochem Photobiol. 2023;99:844-9. https://doi.org/10.1111/php.13677

[71] Lorusso D, Sabatucci I, Maltese G, Lepori S, Tripodi E, Bogani G, et al. Treatment of recurrent ovarian cancer with pegylated liposomal doxorubicin: a reappraisal and critical analysis. Tumori. 2019;105:282-7. https://doi.org/10.1177/0300891619839308

[72] Alatise KL, Gardner S, Alexander-Bryant A. Mechanisms of Drug Resistance in Ovarian Cancer and Associated Gene Targets. Cancers (Basel). 2022;14. https://doi.org/10.3390/cancers14246246

[73] Han CY, Patten DA, Richardson RB, Harper ME, Tsang BK. Tumor metabolism regulating chemosensitivity in ovarian cancer. Genes Cancer. 2018;9:155-75. https://doi.org/10.18632/genesandcancer.176

[74] Kim S, Han Y, Kim SI, Kim H-S, Kim SJ, Song YS. Tumor evolution and chemoresistance in ovarian cancer. npj Precision Oncology. 2018;2:20. https://doi.org/10.1038/s41698-018-0063-0

[75] Foster R, Buckanovich RJ, Rueda BR. Ovarian cancer stem cells: working towards the root of stemness. Cancer Lett. 2013;338:147-57. https://doi.org/10.1016/j.canlet.2012.10.023

[76] Alonso C. Mecanismos de quimiorresistencia en terapia de primera línea de cáncer de ovario epitelial. Medwave. 2009;9.

[77] Tondo-Steele K, McLean K. The "Sweet Spot" of Targeting Tumor Metabolism in Ovarian Cancers. Cancers (Basel). 2022;14. https://doi.org/10.3390/cancers14194696

[78] Chakraborty PK, Mustafi SB, Xiong X, Dwivedi SKD, Nesin V, Saha S, et al. MICU1 drives glycolysis and chemoresistance in ovarian cancer. Nat Commun. 2017;8:14634. https://doi.org/10.1038/ncomms14634

[79] Catanzaro D, Gaude E, Orso G, Giordano C, Guzzo G, Rasola A, et al. Inhibition of glucose-6-phosphate dehydrogenase sensitizes cisplatin-resistant cells to death. Oncotarget. 2015;6:30102-14. https://doi.org/10.18632/oncotarget.4945

[80] Gentric G, Kieffer Y, Mieulet V, Goundiam O, Bonneau C, Nemati F, et al. PML-Regulated Mitochondrial Metabolism Enhances Chemosensitivity in Human Ovarian Cancers. Cell Metab. 2019;29:156-73 e10. https://doi.org/10.1016/j.cmet.2018.09.002

[81] Sullivan EJ, Kurtoglu M, Brenneman R, Liu H, Lampidis TJ. Targeting cisplatin-resistant human tumor cells with metabolic inhibitors. Cancer Chemother Pharmacol. 2014;73:417-27. https://doi.org/10.1007/s00280-013-2366-8

[82] Cruz-Bermudez A, Laza-Briviesca R, Vicente-Blanco RJ, Garcia-Grande A, Coronado MJ, Laine-Menendez S, et al. Cisplatin resistance involves a metabolic reprogramming through ROS and PGC-1alpha in NSCLC which can be overcome by OXPHOS inhibition. Free Radic Biol Med. 2019;135:167-81. https://doi.org/10.1016/j.freeradbiomed.2019.03.009

[83] Kim SJ, Kim HS, Seo YR. Understanding of ROS-Inducing Strategy in Anticancer Therapy. Oxid Med Cell Longev. 2019;2019:5381692. https://doi.org/10.1155/2019/5381692

[84] Obrist F, Michels J, Durand S, Chery A, Pol J, Levesque S, et al. Metabolic vulnerability of cisplatin-resistant cancers. EMBO J. 2018;37. https://doi.org/10.15252/embj.201798597

[85] Mondal S, Roy D, Sarkar Bhattacharya S, Jin L, Jung D, Zhang S, et al. Therapeutic targeting of PFKFB3 with a novel glycolytic inhibitor PFK158 promotes lipophagy and chemosensitivity in gynecologic cancers. Int J Cancer. 2019;144:178-89. https://doi.org/10.1002/ijc.31868

[86] Papaevangelou E, Almeida GS, Box C, deSouza NM, Chung YL. The effect of FASN inhibition on the growth and metabolism of a cisplatin-resistant ovarian carcinoma model. Int J Cancer. 2018;143:992-1002. https://doi.org/10.1002/ijc.31392

[87] Ramautar R, Berger R, van der Greef J, Hankemeier T. Human metabolomics: strategies to understand biology. Curr Opin Chem Biol. 2013;17:841-6. https://doi.org/10.1016/j.cbpa.2013.06.015

[88] Denkert C, Budczies J, Kind T, Weichert W, Tablack P, Sehouli J, et al. Mass spectrometry-based metabolic profiling reveals different metabolite patterns in invasive ovarian carcinomas and ovarian borderline tumors. Cancer Res. 2006;66:10795-804. https://doi.org/10.1158/0008-5472.CAN-06-0755

[89] Schmidt DR, Patel R, Kirsch DG, Lewis CA, Vander Heiden MG, Locasale JW. Metabolomics in cancer research and emerging applications in clinical oncology. CA Cancer J Clin. 2021;71:333-58. https://doi.org/10.3322/caac.21670

[90] Schrimpe-Rutledge AC, Codreanu SG, Sherrod SD, McLean JA. Untargeted Metabolomics Strategies-Challenges and Emerging Directions. J Am Soc Mass Spectrom. 2016;27:1897-905. https://doi.org/10.1007/s13361-016-1469-y

[91] Hadacek F, Bachmann G. Low-molecular-weight metabolite systems chemistry. Frontiers in Environmental Science. 2015;3. https://doi.org/10.3389/fenvs.2015.00012

[92] Fahy E, Cotter D, Sud M, Subramaniam S. Lipid classification, structures and tools. Biochim Biophys Acta. 2011;1811:637-47. https://doi.org/10.1016/j.bbalip.2011.06.009

[93] Saorin A, Di Gregorio E, Miolo G, Steffan A, Corona G. Emerging Role of Metabolomics in Ovarian Cancer Diagnosis. Metabolites. 2020;10. https://doi.org/10.3390/metabo10100419

[94] Domcke S, Sinha R, Levine DA, Sander C, Schultz N. Evaluating cell lines as tumour models by comparison of genomic profiles. Nat Commun. 2013;4:2126. https://doi.org/10.1038/ncomms3126

[95] Ahmed N, Stenvers KL. Getting to know ovarian cancer ascites: opportunities for targeted therapy-based translational research. Front Oncol. 2013;3:256. https://doi.org/10.3389/fonc.2013.00256

[96] Hamilton TC, Young RC, McKoy WM, Grotzinger KR, Green JA, Chu EW, et al. Characterization of a human ovarian carcinoma cell line (NIH:OVCAR-3) with androgen and estrogen receptors. Cancer Res. 1983;43:5379-89.

[97] Kobayashi M, Salomon C, Tapia J, Illanes SE, Mitchell MD, Rice GE. Ovarian cancer cell invasiveness is associated with discordant exosomal sequestration of Let-7 miRNA and miR-200. J Transl Med. 2014;12:4. https://doi.org/10.1186/1479-5876-12-4

[98] Hallas-Potts A, Dawson JC, Herrington CS. Ovarian cancer cell lines derived from non-serous carcinomas migrate and invade more aggressively than those derived from high-grade serous carcinomas. Sci Rep. 2019;9:5515. https://doi.org/10.1038/s41598-019-41941-4

[99] Sharma S, Alharbi M, Kobayashi M, Lai A, Guanzon D, Zuniga F, et al. Proteomic analysis of exosomes reveals an association between cell invasiveness and exosomal bioactivity on endothelial and mesenchymal cell migration in vitro. Clin Sci (Lond). 2018;132:2029-44. https://doi.org/10.1042/CS20180425

[100] Rezniczek GA, Buggisch J, Sobilo J, Launay A, Lerondel S, Le Pape A, et al. Establishment of a Mouse Ovarian Cancer and Peritoneal Metastasis Model to Study Intraperitoneal Chemotherapy. Cancers (Basel). 2020;12. https://doi.org/10.3390/cancers12123818

[101] Kim MG, Pak JH, Choi WH, Park JY, Nam JH, Kim JH. The relationship between cisplatin resistance and histone deacetylase isoform overexpression in epithelial ovarian cancer cell lines. J Gynecol Oncol. 2012;23:182-9. https://doi.org/10.3802/jgo.2012.23.3.182

[102] Wang CW, Chen CL, Wang CK, Chang YJ, Jian JY, Lin CS, et al. Cisplatin-, Doxorubicin-, and Docetaxel-Induced Cell Death Promoted by the Aqueous Extract of Solanum nigrum in Human Ovarian Carcinoma Cells. Integr Cancer Ther. 2015;14:546-55. https://doi.org/10.1177/1534735415588826

[103] Patankar NA, Pritchard J, van Grinsven M, Osooly M, Bally MB. Topotecan and doxorubicin combination to treat recurrent ovarian cancer: the influence of drug exposure time and delivery systems to achieve optimum therapeutic activity.

Clin Cancer Res. 2013;19:865-77. https://doi.org/10.1158/1078-0432.CCR-12-2459

CAPÍTULO 4 : RESULTADOS Y DISCUSIÓN

4.1 Metabolomics Profiling and Chemoresistance Mechanisms in Ovarian Cancer Cells: Implications for Targeting Glutathione Pathway.

En esta sección se presentan y discuten los resultados que dieron origen al artículo “Metabolomics Profiling and Chemoresistance Mechanisms in Ovarian Cancer Cells: Implications for Targeting Glutathione Pathway”, publicado en la revista Life Sciences (https://doi.org/10.1016/j.lfs.2023.122166).

Metabolomics Profiling and Chemoresistance Mechanisms in Ovarian Cancer Cell Lines: Implications for Targeting Glutathione Pathway

Pedro Alarcon-Zapata [a,b], Andy J. Perez [c], Karin Toledo-Oñate [a], Hector Contreras [a], Valeska Ormazabal [d], Estefania Nova-Lamperti [a], Claudio A. Aguayo [a], Carlos Salomon [e], Felipe A. Zuniga [a,*]

[a] Department of Clinical Biochemistry and Immunology, Faculty of Pharmacy, University of Concepcion. [b] Departamento de Ciencias Básicas, Facultad de Ciencias, Universidad Santo Tomás, Concepción, Chile. [c] Department of Instrumental Analysis, Faculty of Pharmacy, University of Concepcion. [d] Department of Pharmacology, Faculty of Biological Sciences, University of Concepcion. [e] Translational Extracellular Vesicles in Obstetrics and Gynae-Oncology Group, Faculty of Medicine, University of Queensland Centre for Clinical Research, Royal Brisbane and Women's Hospital, The University of Queensland, Brisbane QLD 4029, Australia.

[*] Corresponding author.

E-mail address: fzuniga@udec.cl (F.A. Zuniga).

Highlights

- Metabolomics provides a robust method to distinguish drug responses in OC cells.
- Glycolytic and amino acid metabolism are associated with chemosensitive cells.
- Lipid metabolism and glutathione biosynthesis are related to chemoresistant cells.
- Glutathione depletion notably shifts drug sensitivity to a cytotoxic response.

Abstract

Ovarian cancer presents a significant challenge due to its high rate of chemoresistance, which complicates the effectiveness of drug-response therapy. This study provides a comprehensive metabolomic analysis of ovarian cancer cell lines OVCAR-3 and SK-OV-3, characterizing their distinct metabolic landscapes. Metabolomics coupled with chemometric analysis enabled us to discriminate between the metabolic profiles of these two cell lines. The OVCAR-3 cells, which are sensitive to doxorubicin (DOX), exhibited a preference for biosynthetic pathways associated with cell proliferation. Conversely, DOX-resistant SK-OV-3 cells favored fatty acid oxidation for energy maintenance. Notably, a marked difference in glutathione (GSH) metabolism was observed between these cell lines. Our investigations further revealed that GSH depletion led to a profound change in drug sensitivity, inducing a shift from a cytostatic to a cytotoxic response. The results derived from this comprehensive metabolomic analysis offer potential targets for novel therapeutic strategies to overcome drug resistance. Our study suggests that targeting the GSH pathway could potentially enhance chemotherapy's efficacy in treating ovarian cancer.

Keywords: Ovarian cancer, metabolomics, chemoresistance, glutathione, SK-OV-3 cells.

1. Introduction

Ovarian cancer (OC) is the fifth leading cause of cancer-related death among women worldwide [1], representing the second most lethal gynecological malignancy [2]. Unfortunately, the five-year relative survival rate for OC fluctuates between 30 % and 40 %, underscoring its high fatality [3, 4]. As most OC cases are diagnosed at advanced stages increases the lethality and reducing survival rates.

Despite the high mortality rate resulting from late diagnosis, no specific treatment is available for OC. Chemotherapy drugs such as Carboplatin (CP), Cisplatin (CDDP), and Doxorubicin (DOX) are commonly utilized for ovarian cancer treatment [5, 6]. CP, a platinum-containing compound and a CDDP analog presents lower toxicity and is frequently chosen as a first-line therapy [7, 8]. Platinum therapy is pivotal for ovarian cancer treatment, influencing the treatment's success and recurrence. Although patients initially exhibit a positive response, the majority experience a relapse within 6–12 months and are categorized as platinum-sensitive. A relapse within six months post-treatment is deemed platinum-resistant, attributed to multiple, yet inadequately understood, chemoresistance mechanisms [9]. It is now universally acknowledged, with approval from numerous health regulatory bodies worldwide, that the utilization of poly (ADP-ribose) polymerase inhibitors (PARPi) enhances therapy outcomes for patients harboring mutated BRCA1/2 and recurrent, platinum-sensitive ovarian cancer [10, 11]. However, in platinum-resistant and recurrent ovarian cancer

cases a second-line treatment centered on DOX is usually employed [12]. Only 10_% to 20_% of patients respond favorably to chemotherapeutic agents, resulting in a 10-year survival rate of approximately 15 % [13, 14]. The significant mortality rate and lack of targeted treatment options for OC underline the urgent need for improved diagnostic and therapeutic strategies to enhance patient outcomes.

Different cell line models with unique histological and genetic characteristics have been established for studying OC, including high-grade serous and non-serous subtypes classified based on their genomic profiles [15]. SK-OV-3, a human ovarian cancer cell line derived from non-serous ovarian carcinoma, exhibits an epithelial-like morphology. It is derived from ascitic fluid rather than a primary tumor, associated with advanced-stage disease, and hence, SK-OV-3 displays an invasive behavior typical of advanced ovarian cancer [16]. On the other hand, OVCAR-3 is a human ovarian cancer cell line derived from high-grade serous ovarian carcinoma (HGSOC) and exhibits an epithelial-like morphology [17]. SK-OV-3 and OVCAR-3 cell lines have been shown to display different behaviors: SK-OV-3 cells are faster in migration, significantly more invasive [18–20], and generate more substantial metastasis *in vivo* models [21]. Both cell lines develop resistance to first-line chemotherapy drugs such as CDDP, with SK-OV-3 showing a higher survival rate upon treatment [22]. Interestingly, the two cell lines have observed different response behaviors to DOX treatment [23, 24]. These disparities in cellular behavior underscore the distinctive characteristics of each cell line in the context of ovarian cancer.

The field of omics sciences, which encompasses large-scale biological data analysis, has been critical in understanding the molecular changes associated with chemoresistance [25, 26]. Metabolomics, which provides insights into numerous biochemical events underlying cellular phenotypes [27], has shed light on several metabolic pathways implicated in OC chemoresistance. Studies indicate that pathways related to redox balance, the Pentose Phosphate Pathway, choline metabolism, and fatty acid metabolism play significant roles in chemoresistance in OC [28, 29]. These findings suggest that drug-resistant cells elevate energy production and utilize alternative metabolic pathways to maintain cellular homeostasis.

Using metabolomics, our study aims to elucidate the metabolic landscape of OVCAR-3 and SK-OV-3 ovarian cancer cell lines and determine these metabolic pathways' role in drug sensitivity and resistance. The cellular metabolome can offer insight into the metabolic demands of cancer cells, which are altered to support rapid proliferation, resist cell death, and adapt to the tumor microenvironment. In this context, we pay special attention to the role of glutathione (GSH) - a critical antioxidant in cancer cells known to contribute to chemoresistance [30]. By exploring the differential metabolic profiles and investigating the role of GSH in these cell lines, we aim to enhance our understanding of ovarian cancer metabolism, potentially revealing novel therapeutic targets and strategies for overcoming drug resistance.

2. Material and methods

2.1. Chemical and reagents

Trichloroacetic acid (TCA) and acetic acid were acquired from Winkler, Chile. Sulforhodamine B (SRB), Tris Base, L-Buthionine-Sulfoximine (BSO), and Diethyl Maleate (DEM) were procured from Sigma-Aldrich. Fetal bovine serum was purchased from Hyclone, Cytiva. Solutions of trypsin TrypLE™ and Roswell Park Memorial Institute 1640 (RPMI-1640) were procured from Gibco. Carboplatin (CP), Cisplatin (CDDP), Doxorubicin (DOX), water, formic acid, methanol, dichloromethane, acetonitrile, and ammonium formate of LC/MS grade were obtained from Sigma-Aldrich.

2.2. Cell culture

2.2.1. Cells lines

Human epithelial ovarian adenocarcinoma cell lines OVCAR-3 (HTB-161) and SK-OV-3 (HTB-77) were acquired from the American Type Culture Collection. The cells were cultured in an RPMI-1640 with Glutamine and Sodium Pyruvate medium containing 10 % fetal bovine serum and 100 units/mL penicillin-streptomycin antibiotic mixture in a 95 % relative humidity atmosphere containing 5 % CO_2 at 37°C and harvested at confluence using TrypLE™.

2.2.2. Cell viability assay

Cells of each group were evenly seeded in a 96-well plate, with a concentration of 3×10^4 cells per well in 100 µL of cell suspension. Cell viability was determined using the Sulforhodamine B (SRB) method [31]. To investigate the cytotoxicity of Carboplatin (CP), Cisplatin (CDDP), and Doxorubicin (DOX), serial dilutions of the drugs were administrated to both SK-OV-3 and OVCAR-3 cells for 24 h. Subsequently, cells were fixed with 10 % (w/v) Trichloroacetic acid (TCA) and stained with 0.057 % (w/v) SRB in 1 % (v/v) acetic acid. We established the assay by considering 24 h of culture as time 0. After the stipulated incubation period, the bound dye was dissolved in a 10 mM Tris base, and absorbance was measured at 510 nm using a multiplate reader (Synergy 2, BioTek Instruments).

2.3. Drug sensitivity analysis

We used the GR (Growth Rate inhibition) metrics for drug sensitivity analysis. This approach was preferred over traditional methods such as IC_{50} or E_{MAX} values, which suffer from variations as they do not consider that the cells are growing [32]. Calculations can be performed online using the following website: http://www.grcalculator.org/. The GR_{50}, a measure of potency, signifies the concentration of a drug that reduces cell proliferation rate by half. The GR_{MAX}, an efficacy indicator, is the maximum achievable effect of the drug at the highest concentration analyzed, with values ranging between –1 and 1. A value

approximating 0 implies a fully cytostatic response, whereas a negative value indicates a cytotoxic response. The GR Area Over Curve (GR_{AOC}), an integral value over the curve, is a representative measure of potency and efficacy simultaneously [32, 33]. The raw data was uploaded to the web platform for performance according to the GR metrics. The GR_{MAX} and GR_{AOC} parameters were determined from the online platform. The GR value data was obtained and plotted in GraphPad Prism 9 to visualize the drug dose-response and determine the GR_{50} value using nonlinear regression.

2.4. Metabolomics analysis

2.4.1. Sample preparation and metabolome extraction

The sample preparation and metabolome extraction followed a previously established solvent-scrapping protocol with some modifications [34]. The SK-OV-3 and OVCAR-3 cells were seeded into 100 mm plates, each consisting of three replicate wells and two counting wells. The counting wells were trypsinized and counted, and 8×10^6 cells were obtained for each replicate. The media was removed from the wells and washed twice with water before removal.

For metabolome extraction, a 2 mL methanol/dichloromethane/water mixture solution (2.5,1,0.5) was added to each plate, and the cells were scraped off. The samples were placed in liquid nitrogen for 1 min. Triplicate blanks consisting solely of the extraction solvent were processed similarly. The cells were

subsequently disrupted using a Precellys Evolution Homogenizer (Bertin Instrument) with two 90-second cycles at 6000 rpm. After homogenization, the samples were centrifuged at 13,000 ×g at 4°C for 15 min, after which the supernatants were transferred to new tubes. Liquid-liquid extraction was performed by adding 400 µL of water and an equivalent volume of dichloromethane to each sample. The samples were mixed with a Cell Grinder Retsch at 30 Hz for 3 min.

After centrifugation at 13,000 ×g at 4 °C for 15 min, the two resulting phases were clearly defined with a distinct interface. The hydrophilic fractions (top layer) were carefully transferred to new tubes and dried using a vacuum centrifuge. Simultaneously, the lipophilic fractions (bottom layer) were collected into separate microcentrifuge tubes and dried overnight using a Refrigerated Centrivap Concentrator (LABCONCO) at 4 °C. Following this, the dried extracts were stored at −80 °C until they were required for further analysis.

2.4.2. LC-MS metabolomics

Before analysis, the hydrophilic extracts and blanks were reconstituted with 100 µL of cold 80 % methanol. These were homogenized using a Cell Grinder Retsch at 30 Hz for 1 min and centrifuged at 13000 rpm at 4 °C for 5 min. The resulting supernatant was transferred to 150 µL inserts in 1.5 mL amber vials and placed in a liquid chromatography autosampler maintained at 4 °C, following a

pre-determined random sequence starting with three blank samples. Due to the limited number of injections (two cell lines, three replicates), this study did not include the injection of quality controls (QCs).

Metabolomics analyses were performed using a UHPLC-DAD Bruker Elute LC system coupled to a Q-TOF spectrometer Compact (Bruker, Bremen, Germany). The control system was Compass HyStar (Bruker), and the acquisition software used was otofControl 4.1.402.322-7977-vc110 6.3.3.11 (Bruker). Data analysis was done using Compass DataAnalysis 4.4.200 (Bruker) software and MetaboScape 3.0 (Bruker Daltonics, Bremen, Germany). Positive and negative ion models were employed for data collection to increase the number of differential metabolites. The chromatographic columns used were an Acquity BEH C18 (2.1 × 100 mm, 1.7 μm) and an Acquity UPLC BEH Amide HILIC (2.1 × 100 mm, 1.7 μm) maintained at a column temperature of 45°C. The injection volume was 2 μL, the flow rate was 0.4 mL/min, and the mobile phase for the C18 column comprised solvents A (water containing 0.1 % formic acid) and B (acetonitrile containing 0.1 % formic acid). The mobile phase for the HILIC column included solvents A (water containing 10 mM ammonium formate) and B (acetonitrile 90% including 10 mM ammonium formate). For the C18 column, a gradient elution process of 3 % to 95 % B linear over 15 min was used, and for the HILIC column, a gradient elution process of 5 % to 30 % B linear over 15 min was employed. The DAD was operated in the 194–600 nm wavelength range at a data acquisition rate of 10.0 Hz. Mass spectrometry was performed using positive ionization ESI

+4500 V and negative ionization ESI –3500V with a dry gas flow rate of 9 L/min, nebulizer pressure of 2 Bar, and a temperature of 200 °C. In stepping mode, the end capillary voltage was set at 500 V, and the collision energy was set at 10–25 eV. Auto MS/MS mode (2 precursor/cycle) was used with a scan range of 50–1500 m/z and a scan time of 0.2 s in centroid mode. Internal calibration was performed using a sodium formate solution (10 mM in iso-PrOH/H2O, 1,1) with a mass accuracy of less than three ppm.

2.4.3. Data processing and statistics

The data obtained from LC-MS analysis was processed using MetaboScape 3.0 software, and the Time aligned Region complete eXtraction (T-ReX 3D) algorithm was selected for this purpose. The software transformed the raw data into a matrix containing the features such as m/z, retention time (Rt) pairs, and normalized peak intensity, which were saved in a .csv file. The workflow involved several steps such as a mass recalibration, Rt alignment, feature extraction (m/z - RT pairs), adducts and neutral losses administration, import of MS/MS spectra, and generation of the Bucket Table. The parameters used for the bucket table generation through the T-ReX 3D algorithm were as follows: intensity threshold (1000 counts), minimum spectrum peak length (5), minimum recursive peak length (4), a minimum number of recursive features to be extracted, feature

in a minimum number of analyses, mass range (50-1500 m/z), retention time range (0.5-15.0 min), and MS/MS import (average).

The bucket tables were processed in Metaboscape and then exported to the MetaboAnalyst 5.0 online software for an analysis metabolomics pipeline [35 ,36]. After uploading, the data was filtered based on standard deviation, and Pareto scaling was applied again. Then, an unsupervised model was used, applying principal component analysis (PCA) to reduce data dimensionality and uncover inherent cluster patterns in the data [37]. The results showed a natural separation of the data with PCA reliability, followed by a supervised method to enforce class separation [38]. The supervised modeling method, Orthogonal Projection to Latent Structures Discriminant Analysis (OPLS-DA), was then applied to the dataset to discover correlated features and select significant characteristic features of the group using an S-plot. The regression method used LC-MS data as the X, and the binary vector Y was formed with 0 for the OVCAR-3 class and 1 for the SK-OV-3 class.

2.4.4. Metabolite annotation

The chemical nature of the significant metabolite was determined using an integrated workflow in MetaboScape for manual annotation. The first step involved the SmartFormula task, which picked molecular formulas based on accurate mass and isotopic pattern information for a given extracted feature. The

calculations considered elements such as C, H, N, O, P, and S, with a tolerance of 5 ppm. Additionally, SmartFormula 3D calculation was applied to all features with available MS/MS spectra, which improved the quality of the calculated molecular formula. This intelligent interface annotated all monoisotopic peaks in the MS/MS spectrum. Therefore, for each possible explanation of the *m*/*z* of a feature precursor and isotopic pattern, SmartFormula 3D identified the ion formulas that best explained the monoisotopic peak and isotopic pattern of the MS/MS fragment spectrum and ranked them according to the MS/MS fragment explained and intensity coverage. In the next step, the Compound Crawler tool searched for possible structures that fit the first rated formula. The tool sent queries for a given molecular formula to databases such as ChEBI, ChemSpider, and PubChem and returned results that could be used to annotate compounds. As multiple structure candidates were typically found in Compound Crawler for a given elemental composition, the correct structure was selected using the MetFrag algorithm. Using the MS/MS fragment spectrum, MetFrag searched for ions that matched the in-silico fragmentation of possible candidates provided by Compound Crawler and ranked them according to explained fragment peaks and intensity coverage [39]. To improve annotation, we also used SIRIUS 4.0, a freely available web service that integrates high-resolution isotopic pattern analysis and fragmentation trees for structural elucidation [40, 41].

Heatmaps of the identified metabolites were generated using the ClustVis web tool [42] and further analyzed using agglomerative Hierarchical Cluster

Analysis (HCA) based on Euclidean correlation with the Ward clustering method. Finally, Metabolite Set Enrichment Analysis (MSEA) was conducted using MetaboAnalyst to assess the enrichment of metabolic pathways associated with the identified metabolites [43]. The data were processed by calculating the -log(*p*-value) to determine the contribution of metabolic pathways in terms of their percentage of importance.

2.5. Glutathione analysis

2.5.1. Glutathione determination

The GSH levels in OVCAR-3 and SK-OV-3 cells were determined by seeding 300,000 cells in 12-well plates and using the Glutathione Colorimetric Detection Kit (Invitrogen) to measure glutathione at 48 h of cell culture. The results were normalized by cell number and presented as fold change.

2.5.2. Glutathione depletion and drug response

GSH depletion was achieved using a previously established protocol with slight modifications [44]. In brief, 200,000 SK-OV-3 cells were seeded in 24-well plates and then incubated with 1 mM Buthionine Sulfoximine (BSO) for 24 h. This treatment was followed by a 1-hour incubation with 1 mM Diethyl Maleate (DEM). The cells were washed twice with PBS 1× and cultured for 24 h before measuring GSH levels. For the drug sensitivity analysis, 20,000 SK-OV-3 cells were seeded

in a 96-well plate, depleted of glutathione using the above protocol, and then treated with CDDP and DOX for 24 h. Cell viability was assessed using the SRB method, and drug sensitivity was analyzed using GR metrics.

2.6. Statistical Analysis

Graphs and statistical analysis of the data were performed using GraphPad Prism 8. Results are expressed as either mean ± standard error of the mean (SEM). Statistical differences between the two groups were analyzed using the Mann-Whitney test, with a *p*-value of <0.05 considered statistically significant.

3. Results

3.1. Drug sensitivity analysis of OVCAR-3 and SK-OV-3 cell lines reveals distinct response behavior

The GR metric was employed to conduct drug sensitivity analyses on OVCAR-3 and SK-OV-3 cells subjected to varying CP, CDDP, and DOX concentrations. GR metrics operate on the principle of a drug's presence relative to untreated control, utilizing either endpoint or time-course assays. The time-course assay method provides a direct way to determine the drug's effect on the cells.

The dose-response curves for CP indicate that the drug has a similar effect on both cell lines (Figure 1A). However, SK-OV-3 cells display a slightly lower sensitivity to the drug, reflected in a 1.8 ± 0.9-fold increase in the GR_{50} value. When assessing drug efficacy via $GR_{MAX,}$ OVCAR-3 cells exhibit a cytostatic response (GR_{MAX} –0.18 ± 0.04 units), while the response for SK-OV-3 cells is fully cytostatic (GR_{MAX} 0.03 ± 0.02 units).

In response to CDDP treatment and upon analysis of the drug response curves, OVCAR-3 cells exhibit significantly higher sensitivity than SK-OV-3 cells at tested concentrations (Figure 1B). This is evidenced by a 1.7 ± 0.6-fold increase in the GR_{50} value for SK-OV-3 cells. In terms of drug efficacy, as indicated by the GR_{MAX} values, OVCAR-3 cells respond in a cytotoxic manner (GR_{MAX} –0.28 ± 0.07 units), whereas SK-OV-3 cells show a cytostatic response (GR_{MAX} 0.12 ± 0.03 units).

For DOX, dose-response curve analysis demonstrates higher sensitivity in OVCAR-3 cells compared to SK-OV-3 cells (Figure 1C). This is validated by a 2.5 ± 1.1-fold higher drug potency as indicated by the GR_{50} value. Evaluating efficacy through GR_{MAX} values, OVCAR-3 cells exhibit a cytotoxic response (GR_{MAX} –0.83 ± 0.05 units), while SK-OV-3 cells display a fully cytostatic response (GR_{MAX} – 0.07 ± 0.05 units). Table 1 summarizes the GR metric values for drug treatment in both cell lines and their interpretation.

The GR_{AOC} analysis for CP does not reveal significant differences (Figure 1D). Nonetheless, there are substantial differences in CDDP treatment, with the drug displaying higher potency and effectiveness on OVCAR-3 cells than SK-OV-3 cells (Figure 1E). Lastly, the GR_{AOC} analysis for DOX shows statistically significant differences between OVCAR-3 and SK-OV-3 cells, with the former being 2.5-fold more responsive. This signifies that DOX shows greater potency and efficacy against OVCAR-3 cells (Figure 1F). These results suggest that OVCAR-3 cells exhibit a cytotoxic response to CDDP and DOX, indicating their chemosensitivity, while SK-OV-3 cells display a cytostatic response, suggesting chemoresistance.

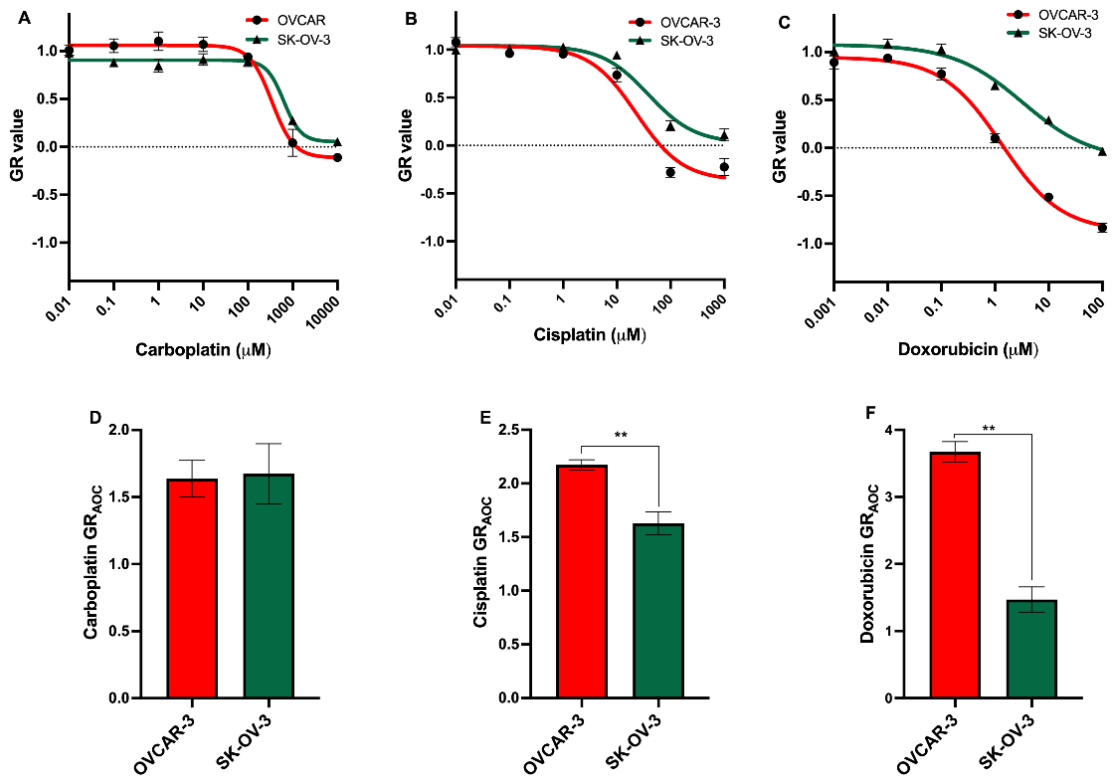

Figure 4.1.1: Drug treatment on OVCAR-3 and SK-OV-3 cells response.

(A) Dose-response curve to Carboplatin, (B) Dose-response curve to Cisplatin, (C) Dose-response curve to Doxorubicin, (D) GRAOC of Carboplatin, (E) GRAOC of Cisplatin, and (F) GRAOC of Doxorubicin on OVCAR-3 and SK-OV-3. OVCAR-3 cells are represented with a red color and SK-OV-3 with a green color. All the values are expressed as mean ± SEM, n = 6, (**) $p < 0.01$.

Table 4.1.1: GR metric values and drug effect analysis from OVCAR-3 and SK-OV-3 exposed drugs.

All the values are expressed as mean ± SEM, n = 6.

Drug	Cell	GR_{50} (μM)	GR_{MAX} units	Response
Carboplatin	OVCAR-3	343.6 ± 135.9	–0.18 ± 0.04	Cytostatic
	SK-OV-3	630.7 ± 168.8	0.03 ± 0.02	Fully Cytostatic
Cisplatin	OVCAR-3	23.1 ± 6.2	–0.28 ± 0.07	Cytotoxic
	SK-OV-3	38.7 ± 9.7	0.12 ± 0.06	Cytostatic
Doxorubicin	OVCAR-3	1.3 ± 0.2	–0.83 ± 0.05	Cytotoxic
	SK-OV-3	3.3 ± 1.3	–0.07 ± 0.05	Fully Cytostatic

3.2. Metabolomic differences between OVCAR-3 and SK-OV-3 cells

3.2.1 Statistical models reveal a differentiation between OVCAR-3 and SK-OV-3 cells associated with metabolomics

We sought to identify potential differences in cellular metabolism between the two cell lines. For this investigation, we employed an LC-MS metabolomics platform featuring polar and apolar columns, facilitating broader metabolite coverage. After LC-MS analysis of the extracts from both cell lines, the raw data was processed through MetaboScape software. This resulted in the creation of bucket tables, serving as the principal matrices for subsequent statistical analyses.

Initially, we examined clustering patterns in the datasets obtained from both cell lines and acquisition modes using unsupervised multivariate Principal Component Analyses (PCA) (Fig. 2). The score plots representing the distribution

of cells across the first two Principal Components (PCs), revealed a distinct separation between OVCAR-3 and SK-OV-3 cells along PC1. This accounted for 85.4 % of the total data variance in the –ESI and 88.1 % in the +ESI for the C18 column (Fig. 2A and B).

Similarly, for the HILIC column, a clear separation was also observed between OVCAR-3 and SK-OV-3 cells along PC1, explaining 83.2% of the variance in –ESI and 52.4 % in the +ESI (Fig. 2C and D). These observations suggest significant metabolic differences between the two cell lines.

The chemical nature of features relevant to discriminate between OVCAR-3 and SK-OV-3 were identified using the OPLS-DA model (Fig. 2). As predicted from the PCA analysis, the scores plotted in the OPLS-DA model demonstrated a complete separation between the two classes in both columns and acquisition modes (Fig. 2E–H).

The S-plots derived from the OPLS-DA models spotlight the most relevant features, or metabolites, that distinguish OVCAR-3 from SK-OV-3 cells. Figures 2I and J illustrate the S-plots of the OPLS-DA models generated from cell datasets acquired in both ionization modes for the C18 column. Likewise, Figures 2K and L depict the S-plots of OPLS-DA models derived from cell datasets acquired in both ionization modes for the HILIC column.

Each point on the S-plot represents a specific feature (m/z; Rt pair) situated at either end of the "S", contributing significantly to class differentiation.

Accordingly, features at the right end correlate with SK-OV-3 cells, indicating that the metabolites they represent are upregulated in these cells. Conversely, features at the left end are associated with OVCAR-3 cells and their correspondingly upregulated metabolites.

For the C18 column, 8 features in –ESI and 7 in +ESI (represented as m/z – Rt pairs) were detected in the OVCAR-3 cells dataset. Meanwhile, 23 features in –ESI and 18 in +ESI were detected in the SK-OV-3 cells dataset. Conversely, for the HILIC column, a total of 9 features in –ESI and 14 features in +ESI were detected in the OVCAR-3 cells dataset, while 24 features in –ESI and 18 features in +ESI were detected in the SK-OV-3 cells dataset (Fig. 2M).

The comprehensive chemical data for each significant metabolite can be found in Supplementary Tables S1 and S2. These findings suggest a significant difference in metabolite profiles between the OVCAR-3 and SK-OV-3 cell lines.

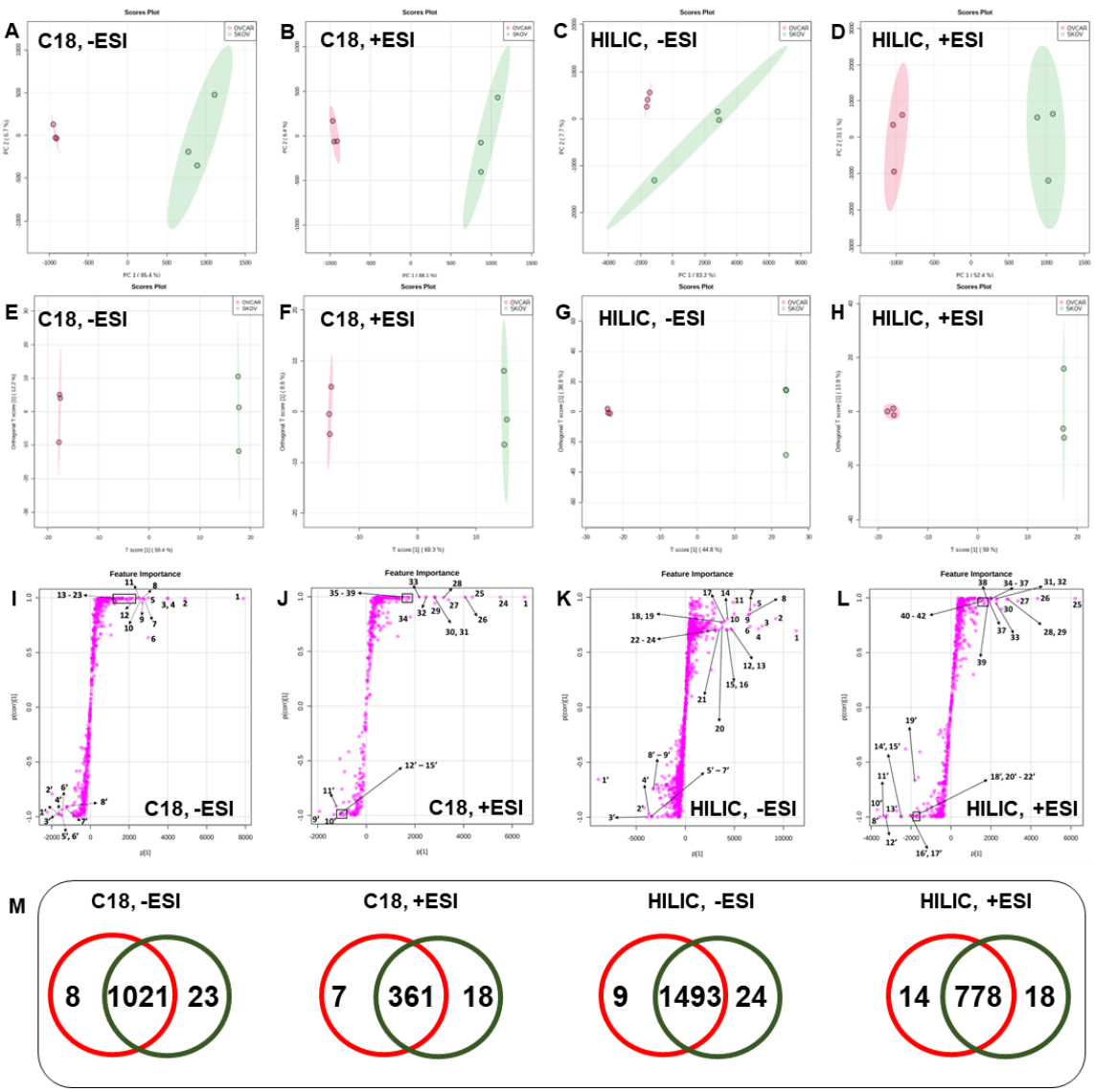

Figure 4.1.2: Statistical analysis results of the LC-MS dataset acquired in C18 and HILIC –ESI and +ESI acquisition modes for the metabolome comparison between OVCAR-3 and SK-OV-3 cells.

PCA score plots based on the LC-MS dataset showing cluster patterns between the first two principal components (PC1 and PC2), red circles represent OVCAR-3 and green circles SK-OV-3 cells samples with their 95 % confidence interval (shadowed regions) for (A) C18, –ESI, (B) C18, +ESI, (C) HILIC, –ESI and (D) HILIC, +ESI. Scores plots of OLPS-DA models showing separation

of OVCAR-3 (red circles) and SK-OV-3 (green circles) cells with their 95% confidence intervals (shadowed regions) for (E) C18, – ESI, (F) C18, +ESI, (G) HILIC, -ESI and (H) HILIC, +ESI. The Y-predictive component (T score [1]) shown on the x-axis represents the variation in the dataset correlated to class separation. In contrast, the orthogonal component shown on the y-axis refers to the uncorrelated variation for class distinction. S-plots showing significant features with their numbers assigned according to Supplementary Table for (I) C18, –ESI, (J) C18, +ESI, (K) HILIC, –ESI, and (L) HILIC, +ESI. The S-plots visualize the features' influence in the predictive component of the model, combining the covariance (p[1]) and correlation (p(corr)[1]) loading profiles. Covariance plotted on the x-axis visualizes the contribution to the predictive component. At the same time, a correlation on the y-axis spans between ± 1 as the reliability has a theoretical minimum of –1 and a maximum of +1 to predict the class 1 (SK-OV-3, indicated in materials and methods); in this way, variables/features visualized toward the right-hand side contribute to class separation by high correlation with SK-OV-3 [Y = 1] and the opposite with OVCAR-3. Thus, significant metabolites were selected based on the combined high covariance (>|2000|, >|1500| or >|1000|) and high correlation (>|0.5|). The number of features related to OVCAR-3 is represented with a red circle, and SK-OV-3, illustrated with a green circle, is shown in (M).

3.2.2 Metabolomic pathway analysis unveils distinct differences between OVCAR-3 and SK-OV-3 cells.

We performed a Hierarchical Cluster (HCA) Heatmap and Metabolite Set Enrichment Analysis (MSEA) using Metaboanalyst, which allowed for the examination of metabolic pathways characterizing both OVCAR-3 and SK-OV-3 cells based on the obtained chemical data and identification from the statistical models.

The HCA analysis results are displayed in Figure 3A. These findings reveal specific clustering of metabolites in OVCAR-3 and SK-OV-3 cells, indicating a clear distinction between these two cell types. This analysis also shows up-regulated and down-regulated metabolites, confirming their unique associations with each cell line. Interestingly, the short distances between clusters of metabolites underscore the strong relationship between both cells.

Within the identified metabolites, those related to lipid metabolism, such as carnitine, propionyl-carnitine, and isovalerylcarnitine, were found to be increased in SK-OV-3 cells. Furthermore, our findings indicate an up-regulation of phenylalanine, tryptophan, and phenylpyruvate in SK-OV-3 cells. By contrast, specific metabolites, namely L-aspartic acid, N-acetyl-L-aspartic acid (NAA), N-acetyl-L-aspartate, and N-acetyl aspartyl glutamic acid (NAAG), were explicitly up-regulated in OVCAR-3 cells, indicating their involvement in aspartate biosynthesis.

Interestingly, glutathione metabolism-related metabolites, such as glutamic acid (glutamate), glutamine, cysteinglicine, and NAAG, were found to be increased in OVCAR-3 cells. In contrast, glutathione (GSH) was up-regulated in SK-OV-3 cells. These findings suggest a differential metabolic profile and potential functional differences between the two cell types.

The Metabolite Set Enrichment Analysis (MSEA) compares enrichment ratios and *p*-values, revealing metabolic pathway distinctions between OVCAR-3

and SK-OV-3 cells. This analysis emphasizes the percentage of importance assigned to each pathway in each cell type.

In OVCAR-3 cells, the top 15 metabolic pathways include aspartate metabolism (16.3 %), GSH metabolism (11.3 %), urea cycle (9.82 %), ammonia recycling (9.4 %), Malate-Aspartate Shuttle (8.7 %), and glutamate metabolism (7.6 %), as shown in Figure 3B.

On the contrary, in SK-OV-3 cells, the top 15 metabolic pathways are characterized by the oxidation of branched-chain fatty acids (14.0 %), phenylalanine and tyrosine metabolism (13.4 %), beta-oxidation of saturated fatty acids (10.9 %), pyruvaldehyde degradation (8.8 %), beta-oxidation of very long-chain fatty acids, and glutathione (GSH) biosynthesis (6.3 %) as illustrated in Figure 3C.

These results suggest that the metabolic priorities of these two cell lines are different: OVCAR-3 cells seem to focus on amino acid and glycolytic metabolism, whereas SK-OV-3 cells prioritize fatty acid metabolism, specifically the oxidation of fatty acids and glutathione biosynthesis. These metabolic preferences may reflect different survival strategies and provide valuable insights for targeted therapies.

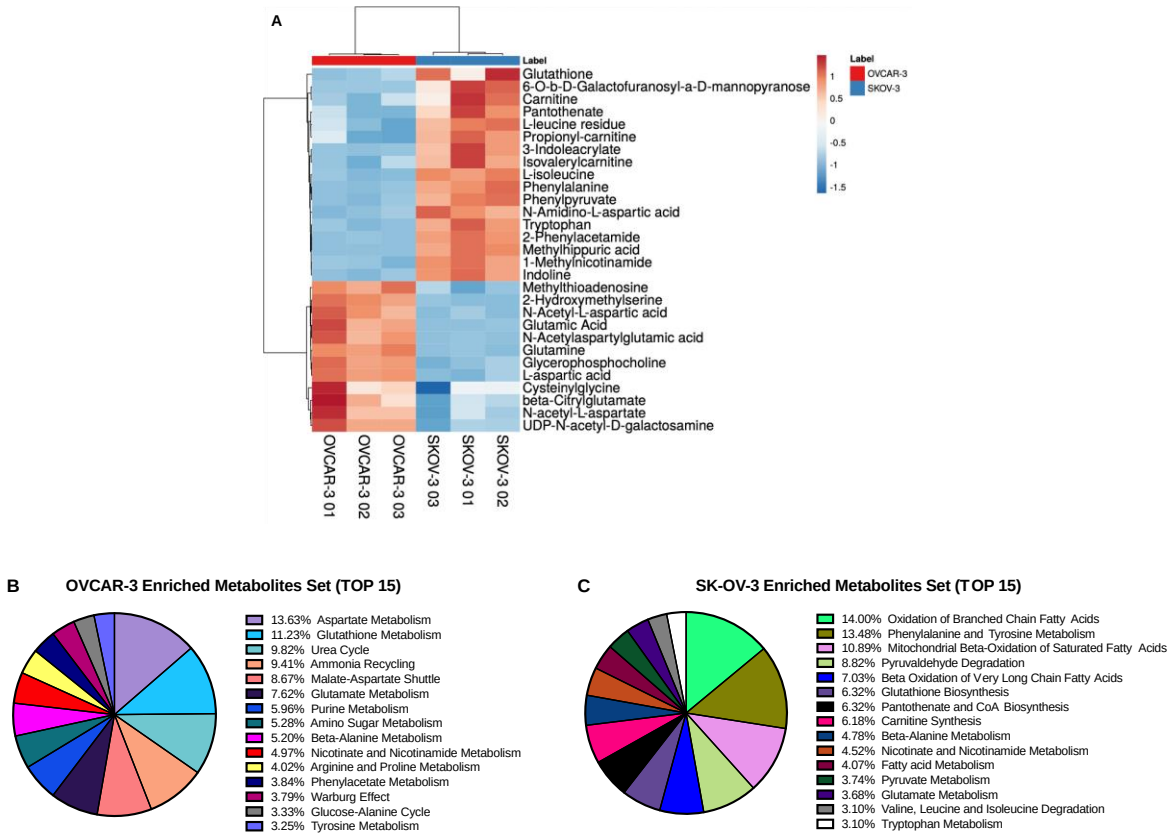

Figure 4.1.3: Metabolite set enrichment overview of OVCAR-3 and SK-OV-3 cells.

(A) Heatmap of the identified metabolites. Each colored square on the map corresponds to a relative concentration value in the data table, with samples in columns and identified metabolites in rows; the classes correspond to OVCAR-3 (red color) and SK-OV-3 cells (green color). (B) Metabolic pathway enrichment in OVCAR-3 cells in percentages based on the -log(*p*-value). (C) Metabolic pathway enrichment in SK-OV-3 cells in rate found in the -log(*p*-value). The most important metabolic pathways (Top 15) are expressed in percentage of the total.

3.3. Depleting glutathione in SK-OV-3 cells shifts the resistance levels of drug treatment.

The metabolomics results establish a fascinating connection between metabolites related to GSH metabolism in OVCAR-3 cells but not to its biosynthesis, whereas GSH biosynthesis is associated with SK-OV-3 cells. In light of these findings, we investigated the potential relationship between GSH and the response to DOX and CDDP treatment in SK-OV-3 cells.

Initially, we measured GSH levels in both cell lines to corroborate the upregulation indicated by the metabolomic analysis, which had identified elevated GSH levels in OVCAR-3 cells in the C18 column (Table S1). We subsequently quantified GSH to validate our findings further. As inferred from the metabolomics data, GSH intensity was threefold higher in SK-OV-3 cells than in OVCAR-3 cells (Fig. 4A). We then utilized a commercial kit to quantify GSH, normalizing the results by cell number. This demonstrated a significant up-regulation of GSH in SK-OV-3 cells, with levels reaching twice those observed in OVCAR-3 cells (Fig. 4B). These results confirmed the conclusions drawn from our metabolomics analysis.

Next, we determine whether the response to cytostatic drugs in SK-OV-3 cells is associated with GSH biosynthesis by depleting GSH in these cells. Following the application of the depletion protocol, we confirmed a decrease in GSH levels in SK-OV-3 cells. Treatment with BSO-DEM alone did not affect cell

viability (data not shown). Furthermore, we quantified GSH in cells exposed to 1 µM DOX for 24h, both with and without GSH depletion, and observed a significant decrease in GSH levels post-depletion in both cases (Fig. 4C).

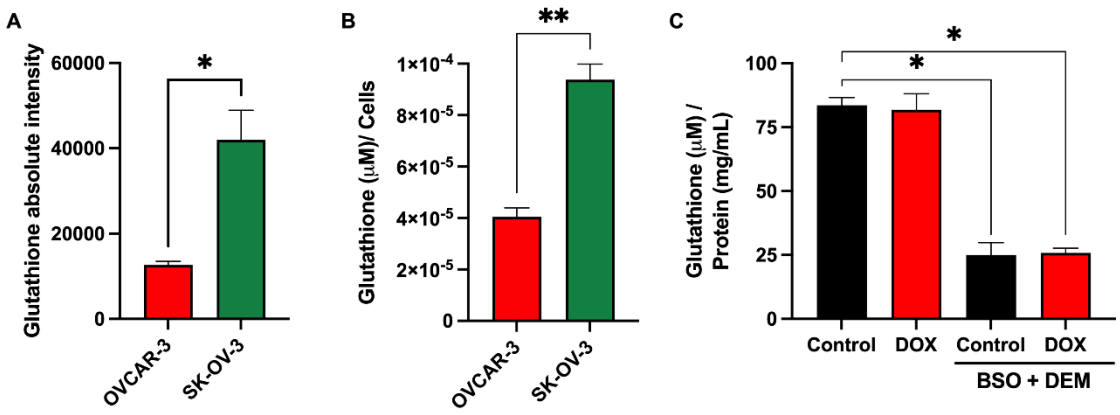

Figure 4.1.4: Glutathione determination in OVCAR-3 and SK-OV-3 cells.

(A) Absolute intensity of GSH in OVCAR-3 (red color) and SK-OV-3 (green color) obtained by metabolomics analysis; (B) Concentration of GSH normalized by cell number between OVCAR-3 (red color) and SK-OV-3 (green color). The values are expressed as mean ± SEM, n = 3, p <0.05; and (C) Concentration of GSH normalized by protein concentration in SK-OV-3 cells before and after application of depletion with BSO + DEM. The values are expressed as mean ± SEM, n = 3, (*) p <0.05.

Finally, we evaluated DOX and CDDP sensibility in GSH-depleted SK-OV-3 cells using GR metrics analysis. GSH-depleted SK-OV-3 cells were exposed to

various dilutions of DOX and CDDP. Drug sensitivity analyses were conducted utilizing the GR metric (Fig. 5A).

The dose-response curves for CDDP treatment demonstrated a higher drug sensitivity in GSH-depleted SK-OV-3 cells (Fig. 5B), displaying an increased drug potency and resulting in a GR_{50} value of 29.3 ± 11.6 μM. A similar effect was observed following DOX treatment on GSH-depleted cells, with a shift in GR_{50} to a value of 2.3 ± 0.9 μM (Fig. 5C).

The GR_{AOC} analysis for DOX and CDDP against GSH-depleted SK-OV-3 cells indicated a trend toward increased drug potency and efficacy (Fig. 5D). Interestingly, the efficacy demonstrated by the $GR_{MAX,}$ which is related to the dose-response curve, suggested that GSH depletion in SK-OV-3 cells shifted the response phenotype from being exclusively cytostatic to also being cytotoxic. This shift was statistically significant, with a decrease in the GR_{MAX} value in both DOX- and CDDP-treated cells, and it was particularly pronounced in the DOX treatment (Fig. 5E).

Table 2 presents a summary of the GR metric values for drug treatment in GSH-depleted SK-OV-3 cells and provides an interpretation of these results. The depletion of GSH in SK-OV-3 cells significantly impacts the efficacy of DOX and CDDP. Notably, this treatment transitions the cellular response from predominantly cytostatic to cytotoxic. This change significantly alters the

resistance levels, resulting in a profound shift during drug treatment, suggesting a phenotypic transformation in the cells.

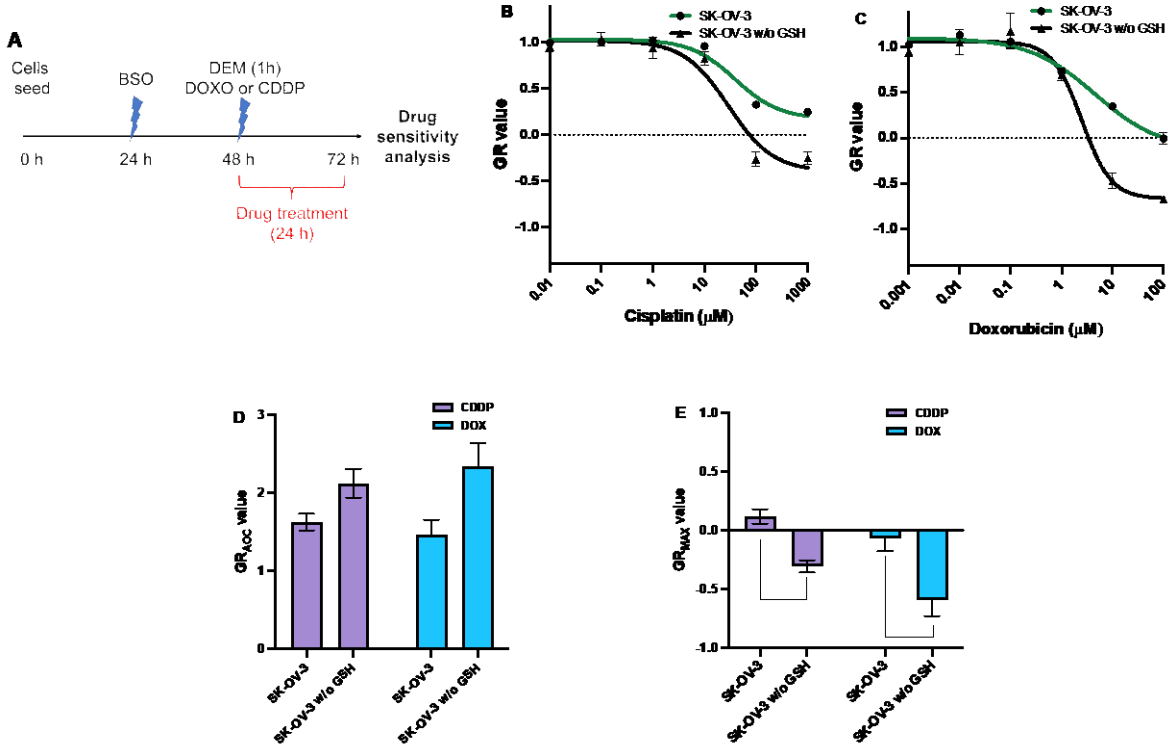

Figure 4.1.5: Drug sensitivity analysis of DOX and CDDP treatment on glutathione-depleted SK-OV-3 cells.

(A) Schematic of drug sensitivity assay on glutathione-depleted SK-OV-3 cells; (B) Dose-response curve to DOX. The green line represented SK-OV-3 cells without depletion, and the black line represented SK-OV-3 cells glutathione depleted; (C) Dose-response curve to CDDP. The green bar represented SK-OV-3 cells without depletion, and the black line represented SK-OV-3 cells glutathione depleted; (D) GR_{AOC} analysis of Cisplatin (purple bars) and Doxorubicin (blue bars) against SK-OV-3 cells glutathione depleted; and (E) GR_{MAX} analysis of Cisplatin (purple bars) and

Doxorubicin (blue bars) against SK-OV-3 cells glutathione depleted. All the values are expressed as mean ± SEM, n = 3, (*) p <0.05.

Table 4.2.1: GR metric values and drug effect analysis in SK-OV-3 cells with GSH depletion. All the values are expressed as mean ± SEM, n=3, (*) p <0.05.

Drug	Cell	GR_{50} (μM)	GR_{MAX} units	Response
Cisplatin	SK-OV-3	39.4 ± 9.7	0.17 ± 0.04	Cytostatic
	SK-OV-3 w/o GSH	29.3 ± 11.6	-0.31 ± 0.05*	Cytotoxic
Doxorubicin	SK-OV-3	4.5 ± 2.2	-0.13 ± 0.15	Fully Cytostatic
	SK-OV-3 w/o GSH	2.3 ± 0.9	-0.59 ± 0.08*	Cytotoxic

4. Discussion

Ovarian cancer remains one of the deadliest gynecological malignancies, primarily due to late-stage diagnosis in over 75% of patients, resulting in a disappointingly low 5-year survival rate [45]. Low survival is often associated with non-specific symptoms in the early stages, leading to a major percentage is diagnosticated in advanced stages. Additionally, this cancer is prone to high relapse after treatment due to chemoresistance development, which results in treatment failure [46]. The first line of defense against advanced-stage ovarian cancer commonly involves platinum-based chemotherapy agents, such as cisplatin and carboplatin. This drug induces apoptosis, or programmed cell death, by interfering with cellular repair mechanisms [47]. When platinum-based

therapies prove ineffective, second-line treatments often involve non-platinum compounds, such as anthracyclines, notably doxorubicin (DOX) [48]. DOX inhibits mitochondrial electron transport, thereby causing oxidative damage by generating free radicals [49]. However, it is crucial to note that the response to DOX can also be hampered by chemoresistance, limiting its therapeutic effectiveness [50-52].

To understand the chemotherapy response in OC, we investigated the responses of two human epithelial ovarian adenocarcinoma cell lines, OVCAR-3 and SK-OV-3, to two platinum-based chemotherapy drugs, cisplatin (CP) and carboplatin (CDDP), as well as to the anthracycline drug doxorubicin (DOX). Then we used Liquid Chromatography-Mass Spectrometry (LC-MS) for a metabolomic analysis, which revealed unique metabolic profiles for these cell lines.

Our study revealed that OVCAR-3 and SK-OV-3 cell lines exhibited a cytostatic response phenotype to CP, suggesting similar drug response behaviors. However, we observed notable differences in drug potency, as evidenced by their GR_{50} value. Interestingly, a comparative analysis using the GR_{AOC} method did not reveal significant differences in drug potency and efficacy between the two cell lines. Previous literature has reported the SK-OV-3 cell line as resistant to CP treatment [53]. Our findings suggest that both cell lines may share similar drug response mechanisms or pathways in response to CP treatment. Notably, similar disparities have been observed in organoids derived from OVCAR-3 and SK-OV-3 cell lines, wherein SK-OV-3 demonstrated higher

IC_{50} values compared to OVCAR-3 [54]. However, it is critical to consider that the IC_{50} or GR_{50} value alone may not be sufficient to determine drug resistance definitively. It is crucial to underscore that integrating the growth rate inhibition metric with the pharmacokinetics of antineoplastic agents can facilitate the development of predictive models for tumor inhibition in vivo, thereby contributing significantly to advancements in translational research. [55].

In response to CDDP treatment, OVCAR-3 cells exhibited a cytotoxic response, while SK-OV-3 cells demonstrated a cytostatic response phenotype. These observations suggest notable differences in drug susceptibility between the two cell lines, consistent in both drug potency and efficacy. Earlier research has established that OVCAR-3 and SK-OV-3 respond differently to CP and CDDP, with OVCAR-3 proving more sensitive than SK-OV-3 [56, 57]. Previous studies have reported IC_{50} values of 8.9 μM for OVCAR-3 cells and 37.1 μM for SK-OV-3 cells [23]. Interestingly these reported IC_{50} values for SK-OV-3 closely align with the GR_{50} values determined in our current study. Furthermore, OVCAR-3 has been categorized as sensitive to CDDP treatment, a sensitivity linked to its high mitochondrial content and oxygen consumption rate [58].

Concerning doxorubicin (DOX) treatment, we observed stark differences in drug susceptibility between the two cell lines. In response to DOX treatment, OVCAR-3 cells exhibited a fully cytotoxic response, indicating a higher sensitivity to DOX. Conversely, SK-OV-3 cells demonstrated a cytostatic response, implying

resistance to DOX. These observations underline the significant disparities in their responses to DOX, highlighting the variations in drug potency and efficacy [57]. Importantly, our findings are consistent with those from the “GR metrics” web platform, indicating a cytostatic response phenotype for SK-OV-3 cells upon DOX treatment [33, 59].

To understand the metabolic differences that could account for the varying sensitivity to chemotherapy agents exhibited by these two cellular models, we employed a metabolomics analytical platform based on Liquid Chromatography-Mass Spectrometry (LC-MS). Our methodology incorporated both apolar and polar columns, ensuring comprehensive metabolite coverage. A natural separation in the data was observed upon application of PCA, suggesting inherent metabolic differences between the two cell lines. To further build on this initial data separation and accentuate the metabolic differences, we subsequently utilized OPLS-DA. The application of OPLS-DA resulted in the definitive segregation of the data. These analyses allowed us to pinpoint and identify the analytical signals associated with the biomarker metabolite analysis.

In OVCAR-3 cells, our metabolomics analysis revealed an upregulation of metabolites implicated in aspartate and glutamate biosynthesis pathways. Aspartate serves a pivotal role in cancer cell metabolism. This amino acid is essential for purine and pyrimidine synthesis, which are needed for DNA replication and RNA transcription, making it critical for rapidly proliferating cells

[60]. Additionally, glutamate is known to play an active role in the Malate-Aspartate Shuttle. This biochemical system facilitates reducing equivalents, NADH, from the cytosol into the mitochondria, which can be used in oxidative phosphorylation for energy production [61]. This shuttle system is crucial for maintaining cellular energy homeostasis, especially in cancer cells with high energy demands [62]. Thus, the observed upregulation of these metabolites and associated pathways suggests a potential metabolic adaptation in OVCAR-3 cells to support their proliferation and survival under chemotherapy stress.

In SK-OV-3 cells, we observed up-regulation of metabolites linked to lipid metabolism, specifically those related to carnitine, which is involved in the transport of fatty acids for beta-oxidation processes. Previous studies conducted on ovarian cancer cells have reported an association between heightened beta-oxidation activity and the overexpression of Carnitine Palmitoyltransferase I (CPT1), a key enzyme involved in the conversion of long-chain fatty acids into acylcarnitines for transport into the mitochondria [63]. Furthermore, this overexpression has been linked to poorer survival outcomes in ovarian cancer patients [64]. Interestingly, increased reliance on fatty acid metabolism and beta-oxidation has been associated with chemoresistance in numerous clinical screenings [65]. These findings suggest that the observed metabolic adaptations in SK-OV-3 cells might contribute to their resistance to chemotherapeutic agents.

It is worth noting that metabolites such as glutamate, glutamine, and aspartate have been reported to be downregulated in patients with chemotherapy resistance and poor prognosis [66]. These findings align with our observations in SK-OV-3 cells, where we also noticed a decrease in these metabolites. Interestingly, we also found a significant up-regulation of phenylalanine and tryptophan in SK-OV-3 cells; these amino acids have been reported to be elevated in patients with relapsed ovarian cancer [67].

As a result, our study uncovered unique metabolic preferences in OVCAR-3 and SK-OV-3 cells, reflecting their divergent responses to drug treatment. OVCAR-3 cells, sensitive to DOX, preferred biosynthetic pathways related to cell proliferation, signifying their active growth and division. In contrast, DOX-resistant SK-OV-3 cells exhibited a metabolic shift toward prioritizing fatty acid oxidation as their primary energy maintenance mechanism. Intriguingly, we also discerned notable differences in glutathione metabolism between the two cell lines. OVCAR-3 cells favored the utilization of glutathione in glutamate biosynthesis, while SK-OV-3 cells prioritized glutathione (GSH) biosynthesis. This difference in glutathione utilization raises questions about its potential role in conferring drug resistance in SK-OV-3 cells.

Glutathione (GSH) is a potent antioxidant that protects cells against oxidative damage by acting as a scavenger of free radicals and detoxifying agent. Upon exposure to oxidative stress, GSH interacts with Reactive Oxygen Species

(ROS), undergoing conversion into its oxidized form, glutathione disulfide (GSSG), with the help of GSH-dependent peroxidases [68].

Significantly, GSH also functions as an active detoxifier, with specialized export pumps that remove glutathione-xenobiotic conjugates from the cytoplasm. Intriguingly, platinum-based drugs display a high affinity for peptides and proteins featuring sulfur residues, particularly those associated with GSH [69, 70]. As such, GSH may interact with these drugs, effectively neutralizing their cytotoxic effects. Therefore, it can be understood that increased GSH levels function as a defense mechanism against tumor agents, as reported in new drugs such as Auranofin and treatment in A2780 cells, reporting a significant increase in GSH biosynthesis [71, 72]. This biochemical interaction could potentially contribute to the resistance of specific cells to platinum-based chemotherapy agents.

To delve deeper into this matter, we utilized a combination of Buthionine sulfoximine (BSO) and Diethyl maleate (DEM) to inhibit the synthesis of GSH and deplete intracellular GSH levels [73, 74]. Remarkably, the depletion of GSH in SK-OV-3 cells markedly influenced the effectiveness of both Cisplatin (CDDP) and Doxorubicin (DOX), even with just a 24-hour treatment duration. This treatment induced a transition from a cytostatic to a cytotoxic response, leading to a significant shift in resistance levels during the drug treatment. These compelling observations suggest a phenotype transformation in the cells, with substantial implications for their drug response behavior.

The data suggest that the lack of efficient glutathione-mediated detoxification and antioxidant defense could facilitate a cytotoxic response to drug treatment. Given the observed changes in CDDP resistance, it is plausible to hypothesize that SK-OV-3 cells may rely on this detoxification mechanism for CDDP, potentially elucidating the altered response phenotype.

Conversely, the impact on the response to DOX in GSH-depleted SK-OV-3 cells was more substantial. As a result, within the context of drug resistance, the antioxidant function of GSH might hold greater significance than its detoxifying role. This compelling finding warrants further exploration and could potentially guide the development of more effective therapeutic strategies for combating chemoresistance.

Our findings suggest that sensitive OVCAR-3 cells leverage GSH metabolism to fuel cellular maintenance and proliferation, while the resistant SK-OV-3 cells prioritize GSH biosynthesis as a protective mechanism. This differential use of GSH between the cell lines underscores the metabolic adaptability of cancer cells and suggests a potential route to target chemoresistance. Figure 6 illustrates the proposed metabolic divergence in both cell lines concerning drug sensitivity, offering a visually simplified summary of our observations. These findings pave the way for future research to explore this unique metabolic interplay and exploit it for improved cancer treatment strategies.

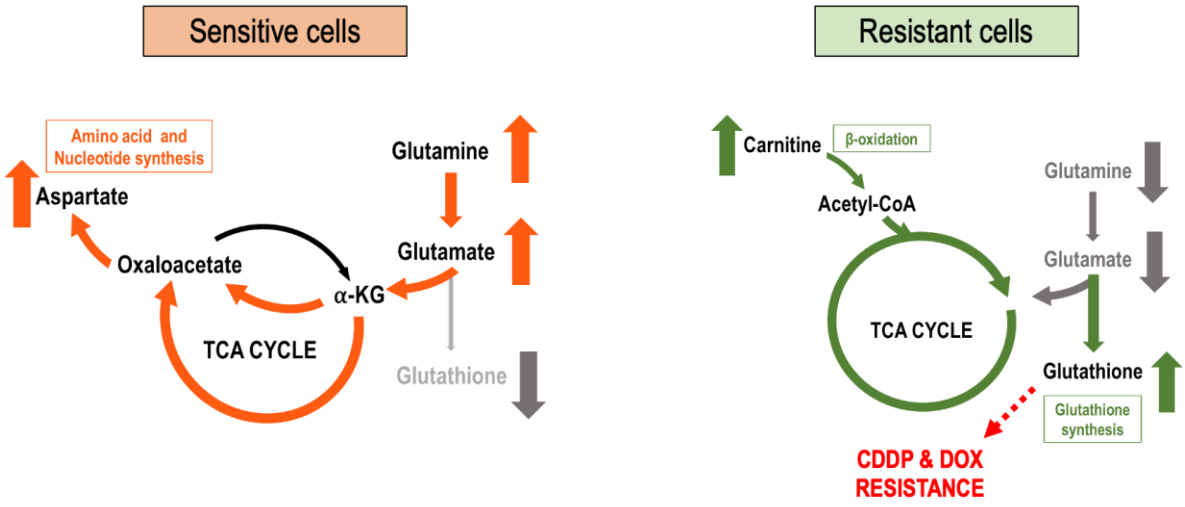

Figure 4.1.6: Proposed schematic metabolism related to drug sensitivity in OVCAR-3 and SK-OV-3 cells.

The orange and green arrows represent upregulated metabolism, and the gray arrows represent downregulated metabolism.

5. Conclusions

In conclusion, our comprehensive metabolomics study using well-established ovarian cancer cellular models has yielded pivotal insights into their distinct drug response behaviors and metabolic profiles. Our results have elucidated pivotal metabolic pathways that segregate drug-sensitive and drug-resistant cells. This knowledge paves the way for identifying potential targets for innovative therapeutic strategies to surmount drug resistance and augment chemotherapy efficacy.

A notable observation in our study was the significant alteration in drug sensitivity following GSH depletion, underscoring the profound role of GSH in modulating the chemotherapy response in drug-resistant cells. These findings bolster our understanding of chemoresistance mechanisms in ovarian cancer at the metabolic level. Metabolomics has proven to be a powerful tool in identifying key metabolites and pathways contributing to chemoresistance, with glutathione playing a starring role in this metabolic narrative.

The elimination of glutathione introduced a striking shift in drug resistance and significantly amplified drug potency, transforming the cellular response from cytostatic to cytotoxic. This compelling evidence opens the door to exploring strategies that target glutathione metabolism, potentially revolutionizing our current approach to managing chemotherapy-resistant ovarian cancer.

While our current study focused on cellular models, the insights garnered are promising for translational research and future clinical application. The lessons learned from these cellular models could be applied to more complex systems such as organoids, further bridging the gap between *in vitro* research and *in vivo* application.

CRediT author statement

PA-Z: Conceptualization, Methodology, Software. PA-Z, FZ: Data curation, Writing - Original draft preparation. PA-Z., HC, KT-O: Visualization,

Investigation. FZ, AP, VO: Supervision. PA-Z, HC, KT-O: Software, Validation. FZ, CA, EN-L, CS: Writing - Reviewing and Editing,

Declaration of competing interests

The authors declare that they have no known competing financial interests or personal relationships that could have appeared to influence the work reported in this paper.

Ethics approval.

This article contains no studies with human participants or animals performed by authors.

Funding

This work was supported by the ANID Doctorado Nacional [21201654], (PA-Z); Fondequip EQM [170023], AP; FONDECYT Regular [1170809], CS; FONDECYT Iniciacion [11190522], VO; and VRID-UDEC [220.072.043-M], FZ.

Appendix A: Supplementary material.

Table S1. Annotation of significant metabolites in OVCAR-3 and SK-OV-3 obtained by C18 column. Table S2. Annotation of significant metabolites in OVCAR-3 and SK-OV-3 obtained by HILIC column.

References

[1] D. Luvero, F. Plotti, A. Aloisia, R. Montera, C. Terranova, N. Carlo De Cicco, G. Scaletta, S. Lopez, A. Miranda, S. Capriglione, A. Gatti, P. Pierluigi Benedetti, R. Angioli, Ovarian cancer relapse: From the latest scientific evidence to the best practice, Crit Rev Oncol Hematol, 140 (2019) 28-38. https://doi.org/10.1016/j.critrevonc.2019.05.014

[2] H. Sung, J. Ferlay, R.L. Siegel, M. Laversanne, I. Soerjomataram, A. Jemal, F. Bray, Global Cancer Statistics 2020: GLOBOCAN Estimates of Incidence and Mortality Worldwide for 36 Cancers in 185 Countries, CA Cancer J Clin, 71 (2021) 209-249. https://doi.org/10.3322/caac.21660

[3] S.A.K. Kumar N., Advances in Tumour Biomarkers for Screening, Diagnosis and Management of Ovarian Malignancies, Journal of Clinical and Diagnostic Research, 12 (2018) QE01 - QE07. https://doi.org/10.7860/JCDR/2018/34896.11453

[4] J.S. Berek, M. Renz, S. Kehoe, L. Kumar, M. Friedlander, Cancer of the ovary, fallopian tube, and peritoneum: 2021 update, Int J Gynaecol Obstet, 155 Suppl 1 (2021) 61-85. https://doi.org/10.1002/ijgo.13878

[5] G. International Collaborative Ovarian Neoplasm, Paclitaxel plus carboplatin versus standard chemotherapy with either single-agent carboplatin or cyclophosphamide, doxorubicin, and cisplatin in women with ovarian cancer: the ICON3 randomised trial, Lancet, 360 (2002) 505-515. https://doi.org/10.1016/S0140-6736(02)09738-6

[6] J. Nguyen, D.A. Solimando, Jr., J.A. Waddell, Carboplatin and Liposomal Doxorubicin for Ovarian Cancer, Hosp Pharm, 51 (2016) 442-449. https://doi.org/10.1310/hpj5106-442

[7] R.F. Ozols, Role of carboplatin in ovarian cancer. Current results and thoughts for the future, Acta Obstet Gynecol Scand Suppl, 155 (1992) 75-77.

[8] E.R. Smith, J.Q. Wang, D.H. Yang, X.X. Xu, Paclitaxel resistance related to nuclear envelope structural sturdiness, Drug Resist Updat, 65 (2022) 100881. https://doi.org/10.1016/j.drup.2022.100881

[9] E. Bayram, G. Khatib, U. Kucukgoz-Gulec, A.B. Guzel, M.A. Vardar, S. Paydas, Comparison of the effectiveness of liposomal doxorubicin and gemcitabine in patients with platinum-sensitive recurrent ovarian cancer receiving third-line chemotherapy, Eur Rev Med Pharmacol Sci, 27 (2023) 6618-6626. https://doi.org/10.26355/eurrev_202307_33132

[10] P.A. Buklaho, J. Kisluk, J. Niklinski, Diagnostics and treatment of ovarian cancer in the era of precision medicine - opportunities and challenges, Front Oncol, 13 (2023) 1227657. https://doi.org/10.3389/fonc.2023.1227657

[11] Y.N. Kim, B. Park, J.W. Kim, B.G. Kim, S.W. Kim, H.S. Kim, C.H. Choi, M.C. Lim, N. Yl Ngoi, D. Sp Tan, J.Y. Lee, Triplet maintenance therapy of olaparib, pembrolizumab and bevacizumab in women with BRCA wild-type, platinum-sensitive recurrent ovarian cancer: the multicenter, single-arm phase II study OPEB-01/APGOT-OV4, Nat Commun, 14 (2023) 5476. https://doi.org/10.1038/s41467-023-40829-2

[12] A.N. Gordon, M. Tonda, S. Sun, W. Rackoff, I. Doxil Study, Long-term survival advantage for women treated with pegylated liposomal doxorubicin compared with topotecan in a phase 3 randomized study of recurrent and refractory epithelial ovarian cancer, Gynecol Oncol, 95 (2004) 1-8. https://doi.org/10.1016/j.ygyno.2004.07.011

[13] M. Liu, D. Chan, H. Ngan, Gynecology and obstetrics mechanisms of chemoresistance in human ovarian cancer at a glance, Gynecol Obs, 2 (2012) 3-6.

[14] I. Meinhold-Heerlein, S. Hauptmann, The heterogeneity of ovarian cancer, Arch Gynecol Obstet, 289 (2014) 237-239. https://doi.org/10.1007/s00404-013-3114-3

[15] S. Domcke, R. Sinha, D.A. Levine, C. Sander, N. Schultz, Evaluating cell lines as tumour models by comparison of genomic profiles, Nat Commun, 4 (2013) 2126. https://doi.org/10.1038/ncomms3126

[16] N. Ahmed, K.L. Stenvers, Getting to know ovarian cancer ascites: opportunities for targeted therapy-based translational research, Front Oncol, 3 (2013) 256. https://doi.org/10.3389/fonc.2013.00256

[17] T.C. Hamilton, R.C. Young, W.M. McKoy, K.R. Grotzinger, J.A. Green, E.W. Chu, J. Whang-Peng, A.M. Rogan, W.R. Green, R.F. Ozols, Characterization of a human ovarian carcinoma cell line (NIH:OVCAR-3) with androgen and estrogen receptors, Cancer Res, 43 (1983) 5379-5389.

[18] M. Kobayashi, C. Salomon, J. Tapia, S.E. Illanes, M.D. Mitchell, G.E. Rice, Ovarian cancer cell invasiveness is associated with discordant exosomal sequestration of Let-7 miRNA and miR-200, J Transl Med, 12 (2014) 4. https://doi.org/10.1186/1479-5876-12-4

[19] A. Hallas-Potts, J.C. Dawson, C.S. Herrington, Ovarian cancer cell lines derived from non-serous carcinomas migrate and invade more aggressively than those derived from high-grade serous carcinomas, Sci Rep, 9 (2019) 5515. https://doi.org/10.1038/s41598-019-41941-4

[20] S. Sharma, M. Alharbi, M. Kobayashi, A. Lai, D. Guanzon, F. Zuniga, V. Ormazabal, C. Palma, K. Scholz-Romero, G.E. Rice, J.D. Hooper, C. Salomon, Proteomic analysis of exosomes reveals an association between cell

invasiveness and exosomal bioactivity on endothelial and mesenchymal cell migration in vitro, Clin Sci (Lond), 132 (2018) 2029-2044. https://doi.org/10.1042/CS20180425

[21] G.A. Rezniczek, J. Buggisch, J. Sobilo, A. Launay, S. Lerondel, A. Le Pape, M. Ouaissi, D. Gohler, M. Senkal, U. Giger-Pabst, C.B. Tempfer, Establishment of a Mouse Ovarian Cancer and Peritoneal Metastasis Model to Study Intraperitoneal Chemotherapy, Cancers (Basel), 12 (2020). https://doi.org/10.3390/cancers12123818

[22] M.G. Kim, J.H. Pak, W.H. Choi, J.Y. Park, J.H. Nam, J.H. Kim, The relationship between cisplatin resistance and histone deacetylase isoform overexpression in epithelial ovarian cancer cell lines, J Gynecol Oncol, 23 (2012) 182-189. https://doi.org/10.3802/jgo.2012.23.3.182

[23] C.W. Wang, C.L. Chen, C.K. Wang, Y.J. Chang, J.Y. Jian, C.S. Lin, C.J. Tai, C.J. Tai, Cisplatin-, Doxorubicin-, and Docetaxel-Induced Cell Death Promoted by the Aqueous Extract of Solanum nigrum in Human Ovarian Carcinoma Cells, Integr Cancer Ther, 14 (2015) 546-555. https://doi.org/10.1177/1534735415588826

[24] N.A. Patankar, J. Pritchard, M. van Grinsven, M. Osooly, M.B. Bally, Topotecan and doxorubicin combination to treat recurrent ovarian cancer: the influence of drug exposure time and delivery systems to achieve optimum

therapeutic activity, Clin Cancer Res, 19 (2013) 865-877. https://doi.org/10.1158/1078-0432.CCR-12-2459

[25] H.D. Jung, Y.J. Sung, H.U. Kim, Omics and Computational Modeling Approaches for the Effective Treatment of Drug-Resistant Cancer Cells, Front Genet, 12 (2021) 742902. https://doi.org/10.3389/fgene.2021.742902

[26] M. Ye, Y. Lin, S. Pan, Z.W. Wang, X. Zhu, Applications of Multi-omics Approaches for Exploring the Molecular Mechanism of Ovarian Carcinogenesis, Front Oncol, 11 (2021) 745808. https://doi.org/10.3389/fonc.2021.745808

[27] E. Hishinuma, M. Shimada, N. Matsukawa, D. Saigusa, B. Li, K. Kudo, K. Tsuji, S. Shigeta, H. Tokunaga, K. Kumada, K. Komine, H. Shirota, Y. Aoki, I.N. Motoike, J. Yasuda, K. Kinoshita, M. Yamamoto, S. Koshiba, N. Yaegashi, Wide-Targeted Metabolome Analysis Identifies Potential Biomarkers for Prognosis Prediction of Epithelial Ovarian Cancer, Toxins (Basel), 13 (2021). https://doi.org/10.3390/toxins13070461

[28] P. Yue, B. Han, Y. Zhao, Focus on the molecular mechanisms of cisplatin resistance based on multi-omics approaches, Mol Omics, (2023). https://doi.org/10.1039/d2mo00220e

[29] G. Gentric, Y. Kieffer, V. Mieulet, O. Goundiam, C. Bonneau, F. Nemati, I. Hurbain, G. Raposo, T. Popova, M.H. Stern, V. Lallemand-Breitenbach, S. Muller, T. Caneque, R. Rodriguez, A. Vincent-Salomon, H. de The, R. Rossignol, F. Mechta-Grigoriou, PML-Regulated Mitochondrial Metabolism Enhances

Chemosensitivity in Human Ovarian Cancers, Cell Metab, 29 (2019) 156-173 e110. https://doi.org/10.1016/j.cmet.2018.09.002

[30] N. Traverso, R. Ricciarelli, M. Nitti, B. Marengo, A.L. Furfaro, M.A. Pronzato, U.M. Marinari, C. Domenicotti, Role of glutathione in cancer progression and chemoresistance, Oxid Med Cell Longev, 2013 (2013) 972913. https://doi.org/10.1155/2013/972913

[31] V. Vichai, K. Kirtikara, Sulforhodamine B colorimetric assay for cytotoxicity screening, Nat Protoc, 1 (2006) 1112-1116. https://doi.org/10.1038/nprot.2006.179

[32] M. Hafner, M. Niepel, M. Chung, P.K. Sorger, Growth rate inhibition metrics correct for confounders in measuring sensitivity to cancer drugs, Nature Methods, 13 (2016) 521-527. https://doi.org/10.1038/nmeth.3853

[33] M. Hafner, M. Niepel, P.K. Sorger, Alternative drug sensitivity metrics improve preclinical cancer pharmacogenomics, Nat Biotechnol, 35 (2017) 500-502. https://doi.org/10.1038/nbt.3882

[34] K. Dettmer, N. Nurnberger, H. Kaspar, M.A. Gruber, M.F. Almstetter, P.J. Oefner, Metabolite extraction from adherently growing mammalian cells for metabolomics studies: optimization of harvesting and extraction protocols, Anal Bioanal Chem, 399 (2011) 1127-1139. https://doi.org/10.1007/s00216-010-4425-x

[35] J. Chong, D.S. Wishart, J. Xia, Using MetaboAnalyst 4.0 for Comprehensive and Integrative Metabolomics Data Analysis, Curr Protoc Bioinformatics, 68 (2019) e86. https://doi.org/10.1002/cpbi.86

[36] Z. Pang, J. Chong, G. Zhou, D.A. de Lima Morais, L. Chang, M. Barrette, C. Gauthier, P.E. Jacques, S. Li, J. Xia, MetaboAnalyst 5.0: narrowing the gap between raw spectra and functional insights, Nucleic Acids Res, 49 (2021) W388-W396. https://doi.org/10.1093/nar/gkab382

[37] B. Worley, R. Powers, Multivariate Analysis in Metabolomics, Curr Metabolomics, 1 (2013) 92-107. https://doi.org/10.2174/2213235X11301010092

[38] B. Worley, R. Powers, PCA as a practical indicator of OPLS-DA model reliability, Curr Metabolomics, 4 (2016) 97-103. https://doi.org/10.2174/2213235X04666160613122429

[39] C. Ruttkies, E.L. Schymanski, S. Wolf, J. Hollender, S. Neumann, MetFrag relaunched: incorporating strategies beyond in silico fragmentation, Journal of Cheminformatics, 8 (2016) 3. https://doi.org/10.1186/s13321-016-0115-9

[40] K. Duhrkop, H. Shen, M. Meusel, J. Rousu, S. Bocker, Searching molecular structure databases with tandem mass spectra using CSI:FingerID, Proc Natl Acad Sci U S A, 112 (2015) 12580-12585. https://doi.org/10.1073/pnas.1509788112

[41] K. Dührkop, M. Fleischauer, M. Ludwig, A.A. Aksenov, A.V. Melnik, M. Meusel, P.C. Dorrestein, J. Rousu, S. Böcker, SIRIUS 4: a rapid tool for turning tandem mass spectra into metabolite structure information, Nature Methods, 16 (2019) 299-302. https://doi.org/10.1038/s41592-019-0344-8

[42] T. Metsalu, J. Vilo, ClustVis: a web tool for visualizing clustering of multivariate data using Principal Component Analysis and heatmap, Nucleic Acids Res, 43 (2015) W566-570. https://doi.org/10.1093/nar/gkv468

[43] Z. Pang, G. Zhou, J. Ewald, L. Chang, O. Hacariz, N. Basu, J. Xia, Using MetaboAnalyst 5.0 for LC–HRMS spectra processing, multi-omics integration and covariate adjustment of global metabolomics data, Nature Protocols, 17 (2022) 1735-1761. https://doi.org/10.1038/s41596-022-00710-w

[44] L. Mardones, F.A. Zuniga, M. Villagran, K. Sotomayor, P. Mendoza, D. Escobar, M. Gonzalez, V. Ormazabal, M. Maldonado, G. Onate, C. Angulo, Concha, II, A.M. Reyes, J.G. Carcamo, V. Barra, J.C. Vera, C.I. Rivas, Essential role of intracellular glutathione in controlling ascorbic acid transporter expression and function in rat hepatocytes and hepatoma cells, Free Radic Biol Med, 52 (2012) 1874-1887. https://doi.org/10.1016/j.freeradbiomed.2012.02.017

[45] M.T. Climent, A. Serra, M. Llueca, A. Llueca, Surgery in Recurrent Ovarian Cancer: A Meta-Analysis, Cancers (Basel), 15 (2023). https://doi.org/10.3390/cancers15133470

[46] R. Pokhriyal, R. Hariprasad, L. Kumar, G. Hariprasad, Chemotherapy Resistance in Advanced Ovarian Cancer Patients, Biomark Cancer, 11 (2019) 1179299X19860815. https://doi.org/10.1177/1179299X19860815

[47] S.K. Bardal, J.E. Waechter, D.S. Martin, Chapter 20 - Neoplasia, in: S.K. Bardal, J.E. Waechter, D.S. Martin (Eds.) Applied Pharmacology, W.B. Saunders, Philadelphia, 2011, pp. 305-324. https://doi.org/https://doi.org/10.1016/B978-1-4377-0310-8.00020-8

[48] S. Pignata, C. Pisano, M. Di Napoli, S.C. Cecere, R. Tambaro, L. Attademo, Treatment of recurrent epithelial ovarian cancer, Cancer, 125 Suppl 24 (2019) 4609-4615. https://doi.org/10.1002/cncr.32500

[49] J.K. Bhardwaj, P. Bikal, S.N. Sachdeva, Chemotherapeutic drugs induced female reproductive toxicity and treatment strategies, J Biochem Mol Toxicol, 37 (2023) e23371. https://doi.org/10.1002/jbt.23371

[50] S. Ghosh, U. Chitgupi, U. Sunar, J.F. Lovell, Chemophototherapeutic Ablation of Doxorubicin-Resistant Human Ovarian Tumor Cells, Photochem Photobiol, 99 (2023) 844-849. https://doi.org/10.1111/php.13677

[51] D. Lorusso, I. Sabatucci, G. Maltese, S. Lepori, E. Tripodi, G. Bogani, F. Raspagliesi, Treatment of recurrent ovarian cancer with pegylated liposomal doxorubicin: a reappraisal and critical analysis, Tumori, 105 (2019) 282-287. https://doi.org/10.1177/0300891619839308

[52] K.L. Alatise, S. Gardner, A. Alexander-Bryant, Mechanisms of Drug Resistance in Ovarian Cancer and Associated Gene Targets, Cancers (Basel), 14 (2022). https://doi.org/10.3390/cancers14246246

[53] B. Thibault, L. Genre, A. Le Naour, C. Broca, E. Mery, G. Vuagniaux, J.P. Delord, N. Wiedemann, B. Couderc, DEBIO 1143, an IAP inhibitor, reverses carboplatin resistance in ovarian cancer cells and triggers apoptotic or necroptotic cell death, Sci Rep, 8 (2018) 17862. https://doi.org/10.1038/s41598-018-35860-z

[54] T. Singh, A. Neal, G. Dibernardo, N. Raheseparian, N.A. Moatamed, S. Memarzadeh, Efficacy of birinapant in combination with carboplatin in targeting platinum-resistant epithelial ovarian cancers, Int J Oncol, 60 (2022). https://doi.org/10.3892/ijo.2022.5325

[55] R. Diegmiller, L. Salphati, B. Alicke, T.R. Wilson, T.J. Stout, M. Hafner, Growth-rate model predicts in vivo tumor response from in vitro data, CPT Pharmacometrics Syst Pharmacol, 11 (2022) 1183-1193. https://doi.org/10.1002/psp4.12836

[56] Q. Li, J.F. Gao, B.L. Qi, PDCD1 strengthens the sensitivity of ovarian cancer to cisplatin chemotherapy by promoting apoptosis, J BUON, 22 (2017) 746-756.

[57] C.M. Beaufort, J.C. Helmijr, A.M. Piskorz, M. Hoogstraat, K. Ruigrok-Ritstier, N. Besselink, M. Murtaza, I.W.F. van, A.A. Heine, M. Smid, M.J. Koudijs, J.D. Brenton, E.M. Berns, J. Helleman, Ovarian cancer cell line panel (OCCP): clinical

importance of in vitro morphological subtypes, PLoS One, 9 (2014) e103988. https://doi.org/10.1371/journal.pone.0103988

[58] M. Kleih, K. Bopple, M. Dong, A. Gaissler, S. Heine, M.A. Olayioye, W.E. Aulitzky, F. Essmann, Direct impact of cisplatin on mitochondria induces ROS production that dictates cell fate of ovarian cancer cells, Cell Death Dis, 10 (2019) 851. https://doi.org/10.1038/s41419-019-2081-4

[59] P.M. Haverty, E. Lin, J. Tan, Y. Yu, B. Lam, S. Lianoglou, R.M. Neve, S. Martin, J. Settleman, R.L. Yauch, R. Bourgon, Reproducible pharmacogenomic profiling of cancer cell line panels, Nature, 533 (2016) 333-337. https://doi.org/10.1038/nature17987

[60] Y. Ariav, J.H. Ch'ng, H.R. Christofk, N. Ron-Harel, A. Erez, Targeting nucleotide metabolism as the nexus of viral infections, cancer, and the immune response, Sci Adv, 7 (2021). https://doi.org/10.1126/sciadv.abg6165

[61] R. Gorgoglione, V. Impedovo, C.L. Riley, D. Fratantonio, S. Tiziani, L. Palmieri, V. Dolce, G. Fiermonte, Glutamine-Derived Aspartate Biosynthesis in Cancer Cells: Role of Mitochondrial Transporters and New Therapeutic Perspectives, Cancers (Basel), 14 (2022). https://doi.org/10.3390/cancers14010245

[62] P. Borst, The malate-aspartate shuttle (Borst cycle): How it started and developed into a major metabolic pathway, IUBMB Life, 72 (2020) 2241-2259. https://doi.org/10.1002/iub.2367

[63] Z. Ji, Y. Shen, X. Feng, Y. Kong, Y. Shao, J. Meng, X. Zhang, G. Yang, Deregulation of Lipid Metabolism: The Critical Factors in Ovarian Cancer, Front Oncol, 10 (2020) 593017. https://doi.org/10.3389/fonc.2020.593017

[64] H. Shao, E.M. Mohamed, G.G. Xu, M. Waters, K. Jing, Y. Ma, Y. Zhang, S. Spiegel, M.O. Idowu, X. Fang, Carnitine palmitoyltransferase 1A functions to repress FoxO transcription factors to allow cell cycle progression in ovarian cancer, Oncotarget, 7 (2016) 3832-3846. https://doi.org/10.18632/oncotarget.6757

[65] M. Liu, Y. Liu, H. Feng, Y. Jing, S. Zhao, S. Yang, N. Zhang, S. Jin, Y. Li, M. Weng, X. Xue, F. Wang, Y. Yang, X. Jin, D. Kong, Clinical Significance of Screening Differential Metabolites in Ovarian Cancer Tissue and Ascites by LC/MS, Front Pharmacol, 12 (2021) 701487. https://doi.org/10.3389/fphar.2021.701487

[66] Y. Ahmed-Salim, N. Galazis, T. Bracewell-Milnes, D.L. Phelps, B.P. Jones, M. Chan, M.D. Munoz-Gonzales, T. Matsuzono, J.R. Smith, J. Yazbek, J. Krell, S. Ghaem-Maghami, S. Saso, The application of metabolomics in ovarian cancer management: a systematic review, Int J Gynecol Cancer, 31 (2021) 754-774. https://doi.org/10.1136/ijgc-2020-001862

[67] C. Ke, A. Li, Y. Hou, M. Sun, K. Yang, J. Cheng, J. Wang, T. Ge, F. Zhang, Q. Li, J. Li, Y. Wu, G. Lou, K. Li, Metabolic phenotyping for monitoring ovarian cancer patients, Sci Rep, 6 (2016) 23334. https://doi.org/10.1038/srep23334

[68] A. Bansal, M.C. Simon, Glutathione metabolism in cancer progression and treatment resistance, J Cell Biol, 217 (2018) 2291-2298. https://doi.org/10.1083/jcb.201804161

[69] R. Oun, Y.E. Moussa, N.J. Wheate, The side effects of platinum-based chemotherapy drugs: a review for chemists, Dalton Trans, 47 (2018) 6645-6653. https://doi.org/10.1039/c8dt00838h

[70] T.C. Johnstone, K. Suntharalingam, S.J. Lippard, The Next Generation of Platinum Drugs: Targeted Pt(II) Agents, Nanoparticle Delivery, and Pt(IV) Prodrugs, Chem Rev, 116 (2016) 3436-3486. https://doi.org/10.1021/acs.chemrev.5b00597

[71] V. Ghini, T. Senzacqua, L. Massai, T. Gamberi, L. Messori, P. Turano, NMR reveals the metabolic changes induced by auranofin in A2780 cancer cells: evidence for glutathione dysregulation, Dalton Trans, 50 (2021) 6349-6355. https://doi.org/10.1039/d1dt00750e

[72] L. Cosottini, L. Massai, V. Ghini, S. Zineddu, A. Geri, M. Mannelli, S. Ciambellotti, M. Severi, T. Gamberi, L. Messori, P. Turano, Bioconjugation of the gold drug auranofin to human ferritin yields a potent cytotoxin, Journal of Drug Delivery Science and Technology, 87 (2023) 104822. https://doi.org/https://doi.org/10.1016/j.jddst.2023.104822

[73] B. Niu, K. Liao, Y. Zhou, T. Wen, G. Quan, X. Pan, C. Wu, Application of glutathione depletion in cancer therapy: Enhanced ROS-based therapy,

ferroptosis, and chemotherapy, Biomaterials, 277 (2021) 121110. https://doi.org/10.1016/j.biomaterials.2021.121110

[74] S. Mathan Kumar, A. Dey, Regulation of Glutathione in Health and Disease with Special Emphasis on Chronic Alcoholism and Hyperglycaemia Mediated Liver Injury: A Brief Perspective, Springer Science Reviews, 2 (2014) 1-13. https://doi.org/10.1007/s40362-013-0015-6

4.2 Lipidomics profiling in Ovarian Cancer Cell Lines: lipid metabolism upregulation is pivotal to drug resistance behavior and cell survival.

En esta sección se presentan y discuten los resultados que dieron origen al artículo “Lipidomics profiling in Ovarian Cancer Cell Lines: lipid metabolism upregulation is pivotal to drug resistance behavior and cell survival”, el cual se encuentra bajo revisión en la revista Cancer Letters (CANLET-D-23-03947).

Lipidomics profiling in Ovarian Cancer Cell Lines: lipid metabolism upregulation is pivotal to drug resistance behavior and cell survival.

Pedro Alarcon-Zapata [a,b], Karin Toledo-Oñate [a], Andy J. Perez [c], Barbara Alarcon-Zapata [c], Lia Olivares-Caro [a], Hector Contreras [a], Valeska Ormazabal [d], Felipe A. Zuniga [a,*]

[a] Department of Clinical Biochemistry and Immunology, Faculty of Pharmacy, University of Concepcion. [b] Departamento de Ciencias Básicas, Facultad de Ciencias, Universidad Santo Tomás, Concepción, Chile. [c] Department of Instrumental Analysis, Faculty of Pharmacy, University of Concepcion. [d] Department of Pharmacology, Faculty of Biological Sciences, University of Concepcion.

[*] Corresponding author.

E-mail address: fzuniga@udec.cl (F.A. Zuniga).

Abstract

In ovarian cancer, cellular metabolism, particularly glycolysis and lipid metabolism, plays a critical role in tumor proliferation and chemoresistance. This study provides a comprehensive lipidomic analysis comparing two ovarian cancer cell lines, OVCAR-3 and SK-OV-3, focusing on the impact of glycolysis inhibition on lipid metabolism. Utilizing liquid chromatography-mass spectrometry (LC-MS) lipidomics and multivariate statistical analyses, including Principal Component Analysis (PCA) and Orthogonal Partial Least Squares Discriminant Analysis (OPLS-DA), we elucidated distinct lipidomic profiles between these cell lines.

The study revealed a significant reliance of OVCAR-3 cells on glycolysis for survival, indicated by a pronounced decrease in cell viability upon treatment with the glycolysis inhibitor 2-deoxy-D- glucose (2-DG). In contrast, SK-OV-3 cells exhibited sustained viability despite reduced proliferation, suggesting an alternative metabolic pathway for energy production. Further, our lipidomic analysis identified 27 significant lipids across various subclasses, predominantly upregulated in SK-OV-3 cells. This included an abundance of glycerophospholipids, ether-linked phospholipids, and oxidized sphingomyelins, marking a distinct metabolic phenotype.

PCA and OPLS-DA models further highlighted the stark metabolic differences between the cell lines, demonstrating a clear separation based on lipidomic profiles. The SK-OV-3 cells showed an upregulation in most lipid categories,

indicating a robust lipid metabolism, in contrast to OVCAR-3 cells. The subclass categorization and normalized intensity plots provided insights into the specific lipid subclasses upregulated in each cell line, with glycerophospholipids being the most abundant in SK-OV-3. Our findings underscore the metabolic flexibility of ovarian cancer cells in response to glycolytic inhibition and reveal the potential of targeting lipid metabolism in ovarian cancer therapeutics. The distinct lipidomic profiles observed suggest new avenues for research into the metabolic vulnerabilities of different ovarian cancer subtypes.

Keywords: Ovarian cancer, lipidomics, glycerophospholipids, SK-OV-3 cells.

1. Introduction

Ovarian cancer (OC) is one of the deadliest malignancies affecting women. It ranks as the fifth leading cause of cancer-related deaths among women worldwide and is the second most common cause of mortality among all gynecologic malignancies [1, 2]. Unfortunately, OC is associated with a five-year relative survival rate ranging between 30% and 40%, highlighting its high lethality [3, 4]. Moreover, less than 20% of patients respond favorably to highly resistant chemotherapy, further reducing highlighting its high lethality in the survival rate [5, 6].

A significant factor contributing to the poor prognosis of ovarian cancer is the frequent diagnosis of the disease at advanced stages, which worsens its severity [7]. Ovarian cancer rapidly spreads within the peritoneal cavity, promoting metastasis. This process is facilitated by significant metabolic shifts, including alterations in glycometabolism, amino acid metabolism, and lipid metabolism, contributing to the aggressiveness of the disease [8].

Previously, we utilized a metabolomics approach to characterize the sensitivity and resistance of ovarian cancer cells to chemotherapy, specifically OVCAR-3 and SK-OV-3 cells representing sensitive and resistant phenotypes, respectively. Our findings indicated that glycolytic metabolism was associated with the sensitive OVCAR-3 cells, while lipid metabolism was linked to the resistant SK-OV-3 cells [9].

Lipid metabolism plays a crucial role in carcinogenesis, promoting energy for cancer cell growth, acquiring drug resistance, and contributing to carcinogenic signaling within the tumor microenvironment [10]. In OC, a high correlation exists with Fatty Acid uptake from food or adipocyte lipolysis induction, leading to increased β-oxidation and promoting tumor growth with a poor prognosis [11]. Conversely, a high lipid unsaturation activity has been reported in ovarian cancer stem cells, which is associated with drug resistance and tumor relapse [12]. Given the importance of lipid metabolism in ovarian cancer and its close relationship with chemoresistance, it is crucial to elucidate whether specific lipid families contribute to changes associated with drug resistance. Our study utilized lipidomics to elucidate the lipid metabolic profiles of OVCAR-3 and SK-OV-3 cells. We aim to deepen our understanding of the relationship between lipid metabolism and drug sensitivity, enhance our comprehension of ovarian cancer lipid metabolism, and identify potential strategies for overcoming drug resistance.

2. Material and methods

2.1. Chemical and reagents

Trichloroacetic acid (TCA) and acetic acid were acquired from Winkler, Chile, Sulforhodamine B (SRB), Tris Base, and 2-Deoxy-D-glucose D8375 (2-DG), were purchased from Sigma-Aldrich. Fetal bovine serum was purchased from Hyclone, Cytiva. Solutions of trypsin TrypLE^{TM} and Roswell Park Memorial

Institute 1640 (RPMI-1640) were procured from Gibco. For LC-MS analysis, water, formic acid, methanol, Methyl tert-butyl ether (MTBE), acetonitrile, isopropanol (IPA), and ammonium formate of LC/MS grade were obtained from Sigma-Aldrich.

2.2. Cell culture

2.2.1. Cell lines

Human epithelial ovarian adenocarcinoma cell lines OVCAR-3 (HTB-161) and SK-OV-3 (HTB-77) were acquired from the American Type Culture Collection. The cells were cultured in an RPMI-1640 with Glutamine and Sodium Pyruvate medium containing 10% fetal bovine serum and 100 units/mL penicillin-streptomycin antibiotic mixture in a 95% relative humidity atmosphere containing 5% CO_2 at 37°C and harvested at confluence using TrypLE^{TM}.

2.2.2. Effect of glycolysis inhibition on cell proliferation.

To investigate the effect of glycolysis inhibition we used a 2-DG treatment on cell proliferation. OVCAR-3 and SK-OV-3 cells were evenly seeded in a 96-well plate, with a concentration of 5×10^3 cells per well in 100 µL of cell suspension. Cell viability was assessed using the Sulforhodamine B (SRB) method [13]. The cells were treated with 50 mM 2-DG for five days, and cell viability was determined per day. For the SRB method, cells were fixed with 10%

(w/v) Trichloroacetic acid (TCA) and stained with 0.057% (w/v) SRB in 1% (v/v) acetic acid. After the stipulated incubation period, the bound dye was dissolved in a 10 mM Tris base, and absorbance was measured at 510 nm using a multiplate reader (Synergy 2, BioTek Instruments). Finally, the results are presented by cell number.

2.3 Lipidomics analysis

2.3.1 Samples Extraction

The sample extraction followed a previously established solvent-scrapping protocol with some modifications [14]. The SK-OV-3 and OVCAR-3 cells were seeded into 100 mm plates, each consisting of four replicate wells and two counting wells. The counting wells were trypsinized and counted, and 8×10^6 cells were obtained for each replicate. The media was removed from the wells and washed twice with water before removal.

For lipidome extraction, a 2 mL mixture of MTBE, methanol, and water (5:3:2) was added to each plate, and cells were scraped off. The samples were then briefly placed in liquid nitrogen. Next, cell disruption was performed using a Precellys Evolution Homogenizer (Bertin Instrument) with two cycles of 90 seconds at 6000 rpm. Subsequently, the cells were centrifuged at 13000 x g at 4 °C for 15 minutes, and the resulting supernatants were transferred to new tubes for liquid-liquid extraction by adding 400 µL of water and an equal volume of

MTBE. Each sample was mixed with the Precellys Evolution Homogenizer for two cycles of 90 seconds at 4500 rpm. After centrifugation at 13,000 x g at 4 °C for 15 minutes, the two phases were separated with a distinct interface. The hydrophilic (top layer) and hydrophobic (bottom, lipidomics) fractions were carefully transferred to new tubes and dried in a vacuum centrifuge using a Refrigerated Centrivap Concentrator at 4 °C. The dried extracts were stored at -80 °C until further analysis.

Before analysis, the hydrophobic extracts with 200 µL of cold 80% methanol/IPA were then homogenized using a Precellys Evolution Homogenizer and centrifuged at 13,000 rpm at 4 °C for 5 minutes. The supernatant was transferred to 150 µL inserts in 1.5 mL amber vials, and with 50 µL of each sample, the Quality Controls (QCs) were built. These vials were placed in a liquid chromatography autosampler maintained at 4°C, following a pre-determined random sequence that began with three blank samples, including QCs.

2.3.2 LC-MS Analysis

Lipidomics analysis was conducted using a UHPLC-DAD Bruker Elute LC system coupled to a Q-TOF spectrometer Compact (Bruker, Bremen, Germany). The control system utilized was Compass HyStar (Bruker), and data acquisition was managed with Bruker otofControl 4.1.402.322-7977-vc110 6.3.3.11 software. Data analysis was performed using Compass DataAnalysis 4.4.200 (Bruker)

software and MetaboScape 3.0 (Bruker Daltonics, Bremen, Germany). The chromatographic column utilized in this study was a Phenomenex column Kinetex® C18, with dimensions of 100 x 4.6 mm and particle size of 2.6 µm, located in Torrance, CA, USA. The column was maintained at a stable temperature of 60 °C throughout the analysis.

The mobile phase consisted of two solvents: solvent A, a mixture of acetonitrile and water in a 60:40 ratio, containing 0.1% formic acid and 10 mM ammonium formate, and solvent B, a combination of isopropanol and acetonitrile in a 90:10 ratio, also containing 0.1% formic acid and 10 mM ammonium formate. The flow rate was set at 0.6 mL/min, and each injection volume was 10 µL. The gradient of mobile phase B was as follows: starting from 15%, it increased to 30% over 2 minutes, then to 48% within 0.5 minutes, followed by 82% within 8.5 minutes, and reaching 99% within 0.5 minutes. After holding at 99% for 0.5 minutes, it decreased to 15% in 0.1 minutes and finally maintained at 15% for 2.9 minutes, with a 3-minute stabilization period.

For the mass spectrometry (MS) analysis, the instrument operated under positive ionization mode (ESI +4500 V) and negative ionization mode (ESI -3500V). The dry gas flow rate was 9 L/min, and the nebulizer pressure was maintained at 2 Bar. The temperature was set to 200°C, and the end capillary voltage was adjusted to 500 V. Collision energy was used in stepping mode in the 20-50 eV range. The Auto MS/MS mode with 2 precursor ions per cycle was

employed. The scan range was set from 50 to 1500 m/z, and the scan time was 0.2 seconds in centroid mode. For internal calibration, sodium formate with 10% formic acid and a concentration of 1 M was used, ensuring a mass accuracy of less than 3 ppm.

2.3.3 Data processing and statistics.

The bucket table was processed in MS-DIAL ver. 4.70. This software transformed the raw data into a matrix with the features (m/z – retention time (tR) pairs and normalized peak intensity) (file .txt). The workflow included mass recalibration, tR alignment, feature extraction (m/z – tR pairs), adducts administration, QCs normalization, blanks filtered, import of MS/MS spectra, and generation of the Bucket Table. In the process of lipid annotation, the identification of metabolites was accomplished by comparing the obtained spectra with the LipidBlast database [15], only ms/ms identification was considered in the analysis.

Before, the buckets tables were exported to the MetaboAnalyst 5.0 online software for the analysis pipeline [16, 17]. After uploading, the data was filtered on standard deviation, and Pareto scaling. Then, fold change analysis was used to visualize differences by lipids categories. An unsupervised model was used, applying principal component analysis (PCA) to uncover inherent cluster patterns in the data [18]. The results showed a natural separation of the data with PCA reliability, followed by a supervised method to enforce class separation [19]. The

supervised modeling method, Orthogonal Projection to Latent Structures Discriminant Analysis (OPLS-DA), was then applied to the dataset to discover correlated features and select significant characteristic features of the group using an S-plot. The regression method used LC-MS data as the X, and the binary vector Y was formed with 0 for the OVCAR-3 class and 1 for the SK-OV-3 class.

2.4. Statistical Analysis.

Graphs and statistical analysis of the data were performed using GraphPad Prism 8. Results are expressed as either mean ± standard error of the mean (SEM). Statistical differences between the two groups were analyzed using the Mann-Whitney test, with a *p*-value <0.05 considered statistically significant.

3. Results

3.1 Glucose uptake inhibition by 2-DG decreases cell proliferation in OvCa cells.

In oncology, the inhibition of glycolysis impairs cellular proliferation and compromises viability. First, we elucidate the consequences of glycolytic interference on the proliferative capacity of OVCAR-3 and SK-OV-3 cells. Cells were exposed to 50 mM 2-deoxy-D-glucose (2-DG), a glycolytic inhibitor, over five days. An immediate suppressive effect on cellular proliferation was noted from the initial day of 2-DG treatment in both cell lines. Notwithstanding, subsequent days revealed divergent proliferation patterns between the two. Specifically,

OVCAR-3 cells exhibited a reduction in cell count from an initial 20,000 to approximately 10,000 cells per well post the first day of 2-DG administration. The decline in cell viability persisted, with a significant diminution to roughly 1,500 cells per well by day five of treatment, as depicted in Figure 1A.

In contrast, SK-OV-3 cells exhibited a marked inhibition of proliferation commencing from the initial day of treatment with 50 mM 2-DG. However, in divergence from the OVCAR-3 cell response, SK-OV-3 cells maintained a stable cell count throughout the subsequent incubation period, indicating an arrest in proliferation without a further decline in cell numbers (Fig. 1B). These observations underscore the pronounced dependency of OVCAR-3 cells on glycolysis for proliferation and survival. In contrast, the SK-OV-3 cells, despite a reduction in proliferation, demonstrated sustained viability throughout treatment, implying reliance on alternative metabolic pathways for energy production.

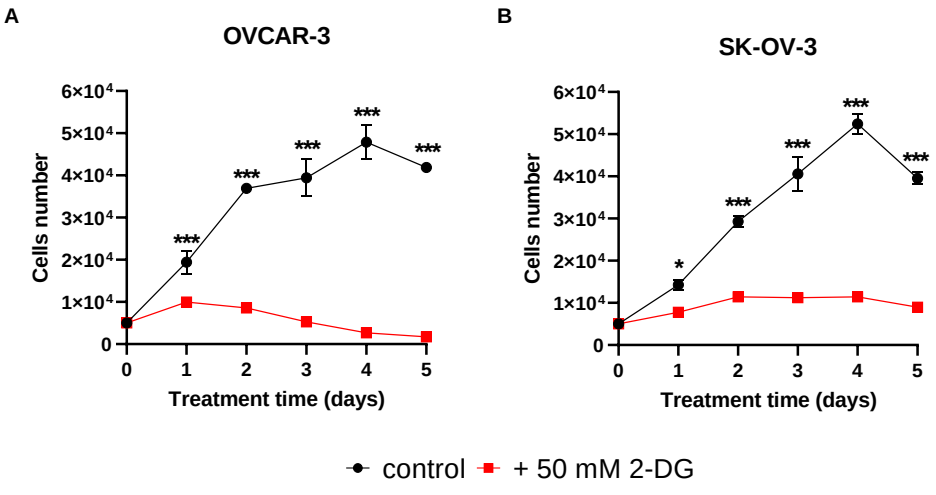

Figure 4.2.1: Proliferation curve of OVCAR-3 and SK-OV-3 cells treated with 2-DG.

The cells were exposed to 50 mM of 2-DG for five days. (A) OVCAR-3 cells treated with 2-DG; (B) SK-OV-3 cells treated with 2-DG. The black lines represent cells control without treatment, and the red lines indicate cells treated. The experiments were realized in triplicate, and error bars show the mean with SEM. (**) p <0.01, y (***) p <0.001.

3.2. Lipidomics differences between OVCAR-3 and SK-OV-3 cells.

3.2.1 Lipidomic analysis unveils a complete upregulation of lipidic metabolism in SK-OV-3 cells rather than OVCAR-3 cells.

Inhibition of glycolysis in SK-OV-3 cells intimates their potential to utilize alternative metabolic pathways for survival. In light of the robust association between lipid metabolism and cancer chemoresistance and our recent metabolomic analysis revealing divergent profiles of drug sensitivity in OVCAR-3 and drug resistance in SK-OV-3 cells—including the upregulation of metabolites related to fatty acid metabolism—we opted to investigate lipid metabolism through LC-MS lipidomics further. Our initial investigations, employing fold change analysis, discerned variations between the two cell lines across different lipid categories identified using the LipidBlast database and segregated by LC-MS ionization modes. We quantified 4.8% fatty acids, 7.8% sterol lipids, 10.2% sphingolipids, 22.8% glycerolipids, and a predominant 55.5% glycerophospholipids (Fig. 2A). Intriguingly, analyses using both ionization modes revealed an overexpression of all lipid categories in SK-OV-3 cells, highlighting

the crucial role of lipid metabolism in the sustenance of these cells (Fig. 2B and 2C).

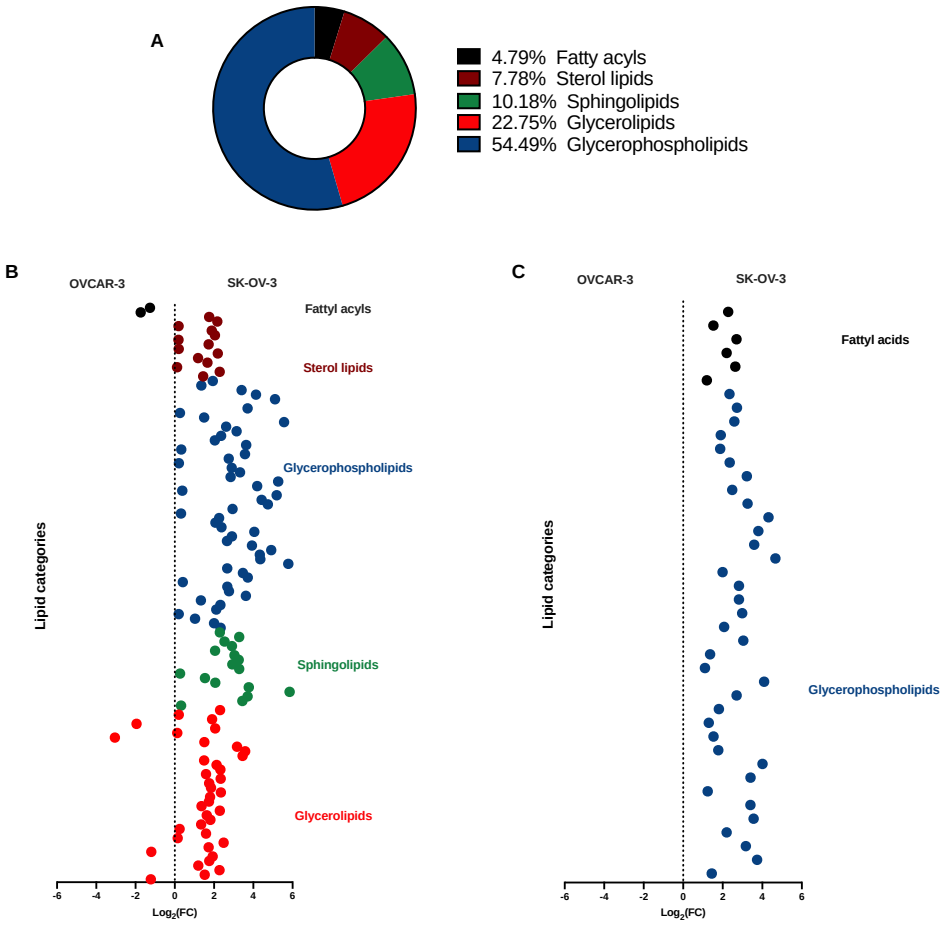

Figure 4.2.2: Comparative lipidomic analysis between OVCAR-3 and SK-OV-3 cells. Differential lipid profiles were elucidated through fold change analysis. The lipid categories are denoted by colors in the following manner: fatty acyls (black), sterol lipids (brown), sphingolipids (green), glycerolipids (red), and glycerophospholipids (blue). (A) Represents the proportion of lipid categories quantified in both cell lines; (B) Depicts fold change in lipid categories as determined by positive electrospray ionization (+ESI), with left-side dots indicating lipids preferentially upregulated in OVCAR-3 cells and right-side dots showing those in SK-OV-3 cells; (C) Illustrates fold change in lipid categories ascertained by negative electrospray ionization (–ESI), with the left-

side dots and right-side dots similarly representing lipids upregulated in OVCAR-3 and SK-OV-3 cells, respectively.

To elucidate the specific lipids predominantly upregulated in both cell lines and under each acquisition mode, we employed unsupervised multivariate Principal Component Analysis (PCA) (Fig. 3). The score plots, delineating cell distribution across the first three Principal Components (PCs), manifested a pronounced divergence between OVCAR-3 and SK-OV-3 cells along PC1, explaining 92.0% and 88.6% of the total variance in the +ESI and –ESI modes, respectively (Fig. 3A and B). Subsequent Orthogonal Partial Least Squares Discriminant Analysis (OPLS-DA) enabled the discrimination between the cell lines. Consistent with PCA findings, the OPLS-DA score plots indicated a complete bifurcation of the two cell lines and ionization methods (Figs. 3C-D). The S-plots from the OPLS-DA models highlighted the lipids that most contributed to the distinction between the OVCAR-3 and SK-OV-3 cells (Figs. 3E and 3F), with lipids on the right end being characteristic of SK-OV-3 cells, and those on the left, of OVCAR-3 cells. Analysis revealed 21 significant features in +ESI and 14 in –ESI associated with the SK-OV-3 phenotype. Notably, no notable features indicative of upregulation were discerned in OVCAR-3 cells. This outcome corroborates the fold change analysis, indicating a pronounced enhancement of lipid metabolism in SK-OV-3 cells in contrast to its suppression in OVCAR-3 cells.

Detailed chemical data for each significant lipid metabolite are presented in Table 1.

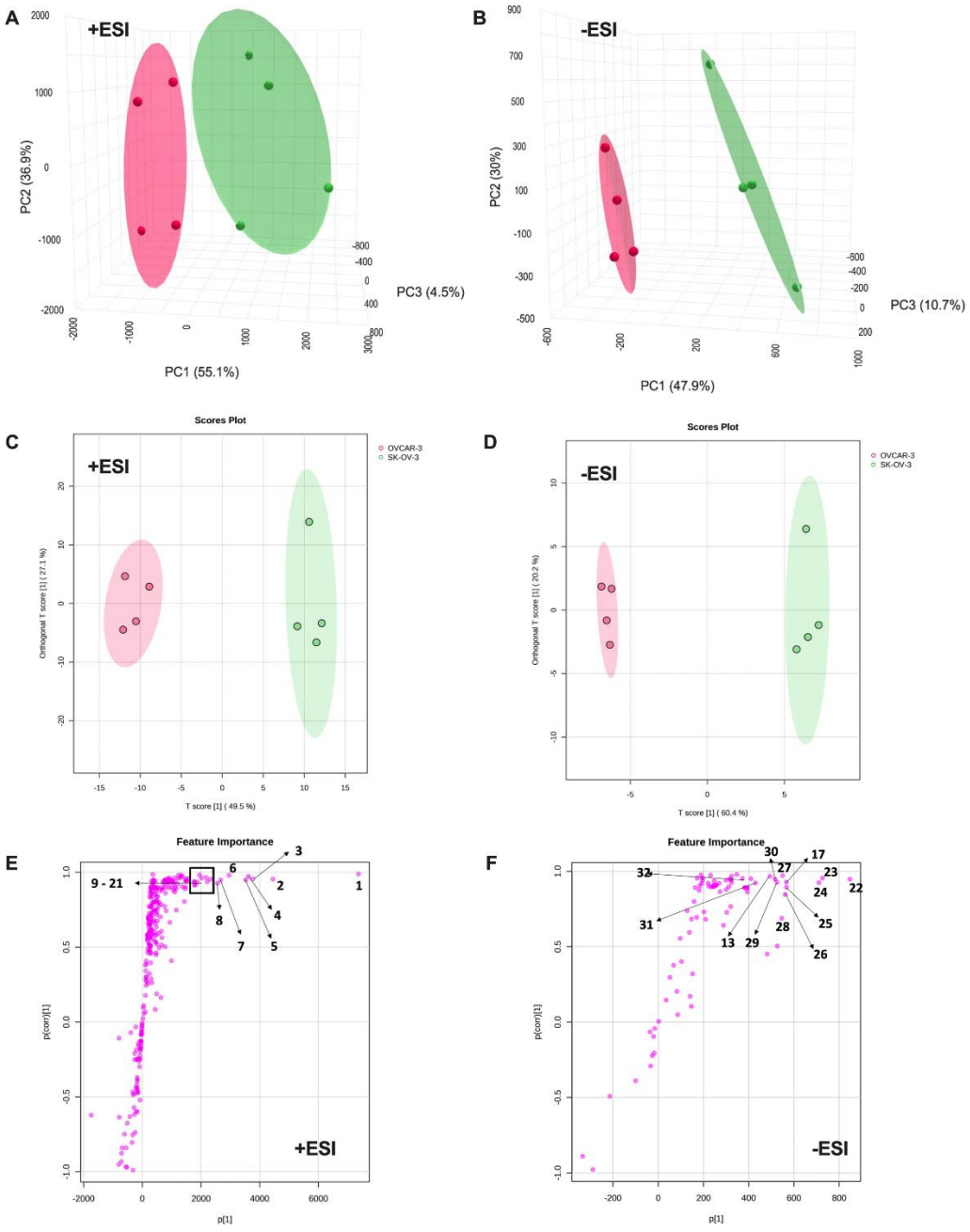

Figure 4.2.3: LC-MS lipidomic data analysis for OVCAR-3 and SK-OV-3 cells in both +ESI and –ESI modes.

PCA score plots reveal clustering within the first three principal components (PC1-PC3), with red circles denoting OVCAR-3 and green circles representing SK-OV-3 cells; shaded regions indicate 95% confidence intervals for (A) +ESI and (B) –ESI modes. OPLS-DA score plots illustrate the distinction between the cell lines (red for OVCAR-3, green for SK-OV-3), each with their respective 95% confidence intervals, in (C) +ESI and (D) –ESI modes. The x-axis displays the Y-predictive component (T score [1]), highlighting variation tied to class separation, while the y-axis depicts orthogonal variation unrelated to class distinction. S-plots (E) for +ESI and (F) for –ESI, assigned according to Table 1, exhibit significant features impacting the model's predictive component through a combined covariance (p[1]) and correlation (p(corr)[1]) profile, with covariance illustrating the predictive contribution and correlation (ranging between ±1) indicating prediction reliability for class 1 (SK-OV-3). Features positioned on the right of S-plots are highly correlated with SK-OV-3 (Y = 1) and vice versa for OVCAR-3. The selection of significant metabolites was based on high covariance (thresholds: > |1500| for +ESI; > |400| for –ESI) and correlation (> |0.6|).

Table 4.2.1: Identification of significant features categorized by lipid subclass ontology in SK-OV-3 obtained by lipidomics analysis.

n	Rt (min)	Lipid identification	Ontology	Mol. formula	Average m/z	Ref. m/z	Adduct	InChi-Key
1	9.49	PC 34:1|PC 16:0_18:1	PC	$C_{42}H_{82}NO_8P$	760.5782	760.5851	$[M+H]^+$	WTJKGGKOPKCXLL-UHFFFAOYSA-N
2	8.85	PC 32:1|PC 16:0_16:1	PC	$C_{40}H_{78}NO_8P$	732,5488	732,5538	$[M+H]^+$	QIBZFHLFHCIUOT-UHFFFAOYSA-N
3	9.86	PC 34:1	PC	$C_{42}H_{82}NO_8P$	760,5781	760,5851	$[M+H]^+$	WTJKGGKOPKCXLL-UHFFFAOYSA-N
4	8.61	SM 34:2;O2|SM 18:2;O2/16:0	SM+O	$C_{39}H_{79}N_2O_6P$	703,5673	703.5749	$[M+H]^+$	RWKUXQNLWDTSLO-UHFFFAOYSA-N
5	8.72	PC 30:0|PC 14:0_16:0	PC	$C_{38}H_{76}NO_8P$	706.5324	706.5381	$[M+H]^+$	RFVFQQWKPSOBED-UHFFFAOYSA-N
6	9.44	PC 32:0|PC 16:0_16:0	PC	$C_{40}H_{80}NO_8P$	734.5658	734.5694	$[M+H]^+$	KILNVBDSWZSGLL-UHFFFAOYSA-N
7	8.99	PE P-36:4|PE P-16:0_20	EtherPE(P)	$C_{41}H_{74}NO_7P$	724.5234	724.5276	$[M+H]^+$	YITZQGLIICATLN-UHFFFAOYSA-N
8	10.44	PC O-34:1|PC O-16:1_18	EtherPC	$C_{42}H_{84}NO_7P$	746.5981	746.6058	$[M+H]^+$	SVSLBZPEDBYFGG-UHFFFAOYSA-N

9	10.59	PC O-34:1|PC O-16:0_18:1	EtherPC	$C_{42}H_{84}NO_7P$	746.6019	746.6058	$[M+H]^+$	SIEDNCDNGMIKST-UHFFFAOYSA-N
10	8.76	PE P-38:6|PE P-16:0_22:6	EtherPE(P)	$C_{43}H_{74}NO_7P$	748.5236	748.5276	$[M+H]^+$	WVGALBKSWOUIE Z-UHFFFAOYSA-N
11	10.59	PC 36:1|PC 18:0_18:1	PC	$C_{44}H_{86}NO_8P$	788.6093	788.6164	$[M+H]^+$	ATHVAWFAEPLPP Q-UHFFFAOYSA-N
12	9.03	PE P-38:5|PE P-16:0_22:5	EtherPE(P)	$C_{43}H_{76}NO_7P$	750.5377	724.5276	$[M+H]^+$	GZEZURLIXRQSDE-UHFFFAOYSA-N
13	9.31	PE 38:4|PE 18:0_20:4	PE	$C_{43}H_{78}NO_8P$	768.5559	768.5538	$[M+H]^+$ $[M+H]^-$	YEHAZLUVAZKVR O-UHFFFAOYSA-N
14	8.74	PC 36:4|PC 16:0_20:4	PC	$C_{44}H_{80}NO_8P$	782.5635	782.5694	$[M+H]^+$	JAVWFBAAZSHHA D-UHFFFAOYSA-N
15	9.74	PE P-34:1|PE P-16:0_18:1	EtherPE(P)	$C_{39}H_{76}NO_7P$	702.5398	702.5432	$[M+H]^+$	ZVVYJAAMWXATN Y-UHFFFAOYSA-N
16	11.04	SM 42:2;O2|SM 18:1;O2/24:1	SM+O	$C_{47}H_{93}N_2O_6P$	813.6773	813.6844	$[M+H]^+$	WKZHECFHXLTOL J-UHFFFAOYSA-N
17	10.25	PC O-34:2|PC O-16:1_18:1	EtherPC	$C_{42}H_{82}NO_7P$	744.5843	744.5902	$[M+H]^+$ $[M+H]^-$	WDQJCKHLEYAET E-UHFFFAOYSA-N
18	9.15	PC 36:3	PC	$C_{44}H_{82}NO_8P$	782.5635	782.5694	$[M+H]^+$	GDWULUGDXGHJI J-UHFFFAOYSA-N
19	8.65	PE 38:5|PE 18:1_20:4	PE	$C_{43}H_{76}NO_8P$	766.5325	766.5381	$[M+H]^+$	ZYMZKMQPPJPQH Y-UHFFFAOYSA-N
20	8.81	SM 34:0;O2	SM+O	$C_{39}H_{81}N_2O_6P$	705.5849	705.5905	$[M+H]^+$	JIOJUELCHJZSCJ-UHFFFAOYSA-N
21	9.72	PE P-38:4|PE P-18:0_20:4	EtherPE(P)	$C_{43}H_{78}NO_7P$	752.5541	752.5589	$[M+H]^+$	ZTZQZGHJLWFLF Q-UHFFFAOYSA-N
22	9.52	RIKEN N-VS1 ID-6109 from Mouse_Plasma_ApoEKO_N_F1DHA	-	-	804.5746	804.5569	$[M+H]^-$	-
23	9.00	PE O-36:5|PE O-16:1_20:4	EtherPE	$C_{41}H_{74}NO_7P$	722.5118	722.5130	$[M+H]^-$	YITZQGLIICATLN-UHFFFAOYSA-N
24	1.50	Unknown	-	-	243.0629	-	$[M+H]^-$	-
25	7.85	PI 38:4|PI 18:0_20:4	PI	$C_{47}H_{83}O_{13}P$	885.5491	885.5499	$[M+H]^-$	OJESNYFIPWSOP O-UHFFFAOYSA-N
26	5.28	FA 20:4	FA	$C_{20}H_{32}O_2$	303.2502	303.2330	$[M+H]^-$	HQPCSDADVLFHH O-UHFFFAOYSA-N
27	8.77	PE O-38:7|PE O-16:1_22:6	EtherPE	$C_{43}H_{74}NO_7P$	746.5106	746.130	$[M+H]^-$	WVGALBKSWOUIE Z-UHFFFAOYSA-N
28	6.79	FA 18:0	FA	$C_{18}H_{36}O_2$	283.2617	283.2643	$[M+H]^-$	QIQXTHQIDYTFRH-UHFFFAOYSA-N
29	1.48	Unknown	-	-	481.1602	-	$[M+H]^-$	-
30	9.05	PE O-38:6|PE O-16:1_22:5	EtherPE	$C_{43}H_{76}NO_7P$	748.5269	748.5287	$[M+H]^-$	GZEZURLIXRQSDE-UHFFFAOYSA-N
31	1.49	Unknown	-	-	481.1602	-	$[M+H]^-$	-
32	9.74	PE O-38:5|PE O-18:1_20:4	EtherPE	$C_{43}H_{78}NO_7P$	750.5433	750.5443	$[M+H]^-$	ZTZQZGHJLWFLF Q-UHFFFAOYSA-N

3.2.2 Fatty acids, glycerophospholipids, and sphingolipids are strongly associated with metabolism in SK-OV-3 cells.

Informed by our statistical analyses, we refined our data categorization to include only the twenty-seven lipids identified by the LipidBlast database and deemed significant within distinct lipid subclass nomenclatures [15]. The findings are delineated by subclass percentages and depicted through comparative normalized intensity plots for both cell lines. Within the fatty acid category, two free fatty acids demonstrated upregulation (7%) (Fig. 4A). Among the glycerophospholipids, which were more prevalent in SK-OV-3 relative to other lipid families, eight phosphatidylcholines exhibited a significant increment (30%) (Fig. 4B), alongside two ether-linked phosphatidylcholines (2%) (Fig. 4C), two phosphatidylethanolamines (7%) (Fig. 4D), five ether-linked phosphatidylethanolamines (19%) (Fig. 4E), one phosphatidylinositol (4%) (Fig. 4F), and four ether-linked oxidized phosphatidylethanolamines (15%) (Fig. 4G). Of the sphingolipid category, three oxidized sphingomyelins were identified (11%) (Fig. 4H).

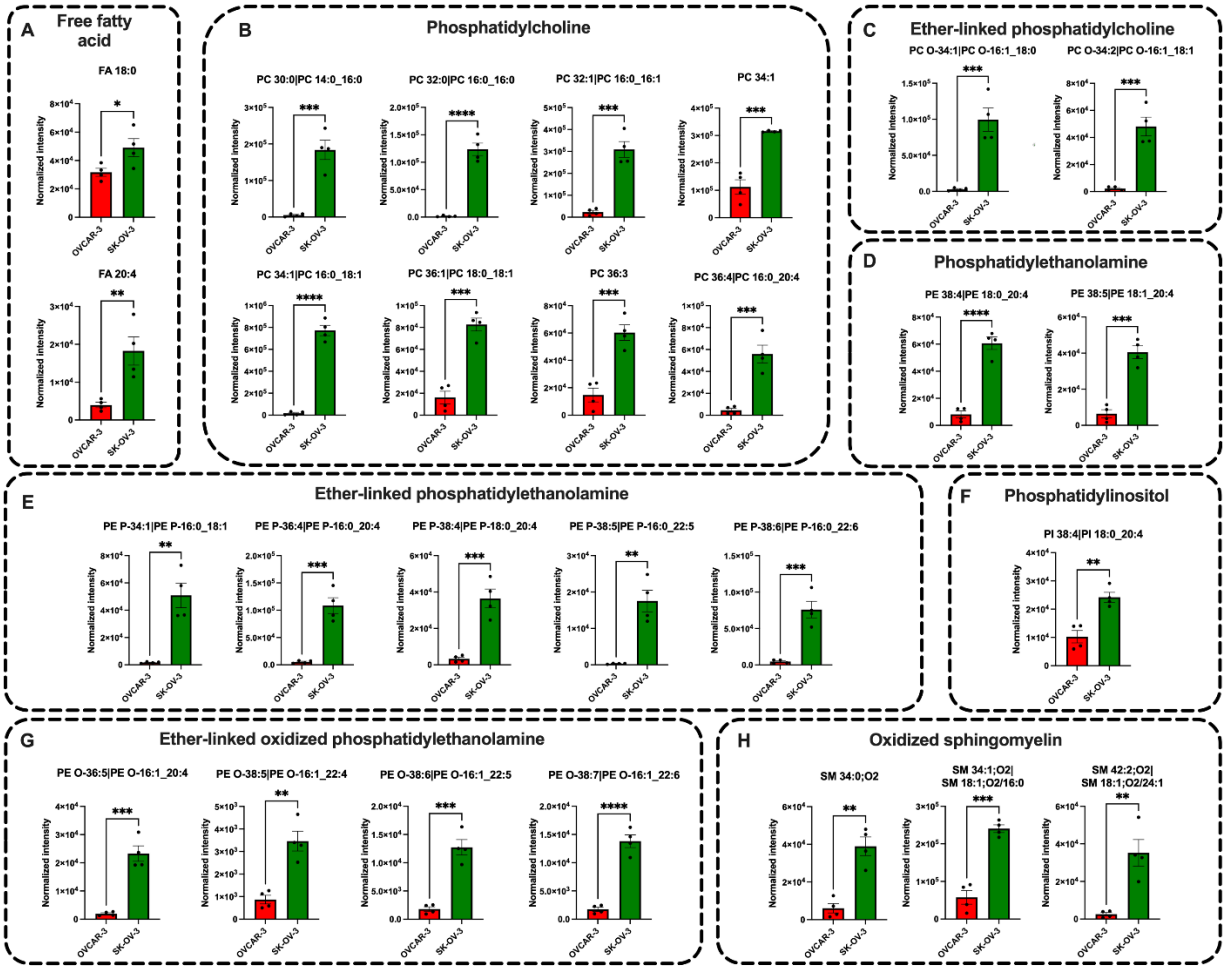

Table 4.2.2: Differential lipid subclass upregulation in OVCAR-3 and SK-OV-3 cells.

The figure presents normalized intensity data for (A) free fatty acids, (B) phosphatidylcholines, (C) ether-linked phosphatidylcholines, (D) phosphatidylethanolamines, (E) ether-linked phosphatidylethanolamines, (F) phosphatidylinositol, and (G) oxidized sphingomyelins. The subclasses are illustrated with red bars for OVCAR-3 and green bars for SK-OV-3 cells. All values are expressed as mean ± standard error of the mean (SEM) for n=4 biological replicates. Statistical significance is indicated by (*) p <0.05, (**) p <0.01, (***) p <0.001, and (****) p <0.0001.

4. Discussion

In this study, we assessed the dependence on glycolytic metabolism in ovarian cancer cell lines previously characterized as chemosensitive (OVCAR-3) and chemoresistant (SK-OV-3) [9]. Our data reveal that SK-OV-3 cells do not rely solely on glycolysis for survival. This led us to explore whether variances in lipidomic profiles could elucidate the role of lipid metabolism in sustaining cellular viability. Notably, we identified a marked elevation in lipid concentrations, particularly glycerophospholipids, and sphingolipids, in SK-OV-3 cells, whereas lipid metabolism appeared markedly diminished in OVCAR-3 cells. These findings align with recent observations in SK-OV-3 demonstrating heightened lipid biosynthesis, as lipid droplets indicate. Further, the inhibition of this biosynthetic pathway using statins has been documented to suppress cell proliferation, migration, and invasion, concurrently augmenting chemosensitivity both *in vitro* and *in vivo* [20].

To understand their metabolic implications, we delved deeper into the lipidomic profiles, focusing on the subclasses most significantly represented in SK-OV-3 cells. We identified a fascinating interplay between glycolytic metabolism and the phosphatidylcholine cycle. Glycolytic by products like dihydroxyacetone phosphate and glyceraldehyde 3-phosphate contribute to the formation of glycerol 3-phosphate, a precursor for phosphatidate and diacylglycerol (DAG), which is involved in phosphatidylcholine (PtdCho) biosynthesis. Additionally, 3-phosphoglycerate, another glycolytic intermediate,

serves as a precursor for sphingolipids, including their oxidized forms detected in our study [21].

We observed an enrichment of lipid droplets in SK-OV-3 cells, previously reported in the literature. These cells exhibited an abundance of phosphatidylcholine (PC), a precursor to potent lipid mediators like prostaglandin E2 (PGE2), lysophosphatidic acid (LPA), and platelet-activating factor (PAF). These mediators modify the tumor microenvironment and play roles in immune evasion, promoting cancer cell proliferation and survival. Intriguingly, we found elevated levels of phosphatidylinositol (PI), known to decrease in ovarian cancer as the cell generates second messengers from phosphatidylinositol to activate the PI3K/AKT signaling pathway, crucial for tumor survival [22].

Our study also highlighted the presence of oxidized lipids, which may participate in fatty acid (FA) biosynthesis, promoting ATP production through beta-oxidation. PtdCho undergoes hydrolysis by phospholipase A2 (PLA2), yielding lysophosphatidylcholine (lyso-PC) and arachidonic acid (AA). COX2 enzymes catalyze AA to PGE2, and lyso-PC acetyltransferases (LPCATs) convert lyso-PC to PAF. Alternatively, lyso-PC is hydrolyzed by autotaxin (ATX) to form LPA. These lipid mediators, including PGE2, PAF, and LPA, bind to specific receptors, promoting cancer cell proliferation, survival, and migration. PtdCho is also hydrolyzed by phosphatidylcholine phospholipase C (PC- PLC) and D (PC-PLD), generating diacylglycerol (DAG) and phosphatidic acid (PA), which activate

the protein kinase C (PKC) pathway and are crucial for mTOR activity, respectively. These catabolic products are implicated in therapy resistance [23]. Hydrolysis products of PI and its phosphorylated derivatives such as PIP, PIP2, and PIP3 are second messengers that activate the PI3K/AKT signaling pathway, significant in cancer treatment modalities like chemotherapy and radiotherapy [24, 25].

5. Conclusion

In conclusion, our data indicate that chemoresistant SK-OV-3 cells utilize glycolysis for lipid biosynthesis, accumulating lipid droplets that support energy production through beta-oxidation. In response to drug treatment, these cells generate secondary mediators facilitating cell survival, proliferation, and immune evasion.

CRediT author statement

PA-Z: Conceptualization, Methodology, Software. PA-Z, FZ: Data curation, Writing- Original draft preparation. PA-Z, KT-O, HC, BA-Z, LO-C: Visualization, Investigation. FZ, AP, VO: Supervision. PA-Z, HC, KT-O: Software, Validation. FZ, VO: Writing- Reviewing and Editing.

Declaration of competing interests

The authors declare that they have no known competing financial interests or personal relationships that could have appeared to influence the work reported in this paper.

Ethics approval

This article contains no studies with human participants or animals performed by authors.

Funding

This work was supported by the ANID Doctorado Nacional [21201654], (PA-Z); Fondequip-EQM-[170023], AP; FONDECYT Regular [1170809], CS. FONDECYT Iniciación [11190522], VO; and VRID-UDEC [220.072.043-M], FZ.

References

[1] Luvero D, Plotti F, Aloisia A, Montera R, Terranova C, Carlo De Cicco N, et al. Ovarian cancer relapse: From the latest scientific evidence to the best practice. Crit Rev Oncol Hematol. 2019;140:28-38. https://doi.org/10.1016/j.critrevonc.2019.05.014

[2] Sung H, Ferlay J, Siegel RL, Laversanne M, Soerjomataram I, Jemal A, et al. Global Cancer Statistics 2020: GLOBOCAN Estimates of Incidence and Mortality Worldwide for 36 Cancers in 185 Countries. CA Cancer J Clin. 2021;71:209-49. https://doi.org/10.3322/caac.21660

[3] Kumar N. SAK. Advances in Tumour Biomarkers for Screening, Diagnosis and Management of Ovarian Malignancies. Journal of Clinical and Diagnostic Research. 2018;12:QE01 - QE7. https://doi.org/10.7860/JCDR/2018/34896.11453

[4] Berek JS, Renz M, Kehoe S, Kumar L, Friedlander M. Cancer of the ovary, fallopian tube, and peritoneum: 2021 update. Int J Gynaecol Obstet. 2021;155 Suppl 1:61-85. https://doi.org/10.1002/ijgo.13878

[5] Liu M, Chan D, Ngan H. Gynecology and obstetrics mechanisms of chemoresistance in human ovarian cancer at a glance. Gynecol Obs. 2012;2:3-6.

[6] Meinhold-Heerlein I, Hauptmann S. The heterogeneity of ovarian cancer. Arch Gynecol Obstet. 2014;289:237-9. https://doi.org/10.1007/s00404-013-3114-3

[7] Huang J, Chan WC, Ngai CH, Lok V, Zhang L, Lucero-Prisno DE, 3rd, et al. Worldwide Burden, Risk Factors, and Temporal Trends of Ovarian Cancer: A Global Study. Cancers (Basel). 2022;14. https://doi.org/10.3390/cancers14092230

[8] Ji Z, Shen Y, Feng X, Kong Y, Shao Y, Meng J, et al. Deregulation of Lipid Metabolism: The Critical Factors in Ovarian Cancer. Front Oncol. 2020;10:593017. https://doi.org/10.3389/fonc.2020.593017

[9] Alarcon-Zapata P, Perez AJ, Toledo-Onate K, Contreras H, Ormazabal V, Nova-Lamperti E, et al. Metabolomics profiling and chemoresistance mechanisms in ovarian cancer cell lines: Implications for targeting glutathione pathway. Life Sci. 2023;333:122166. https://doi.org/10.1016/j.lfs.2023.122166

[10] Liu X, Zhang P, Xu J, Lv G, Li Y. Lipid metabolism in tumor microenvironment: novel therapeutic targets. Cancer Cell Int. 2022;22:224. https://doi.org/10.1186/s12935-022-02645-4

[11] Bian X, Liu R, Meng Y, Xing D, Xu D, Lu Z. Lipid metabolism and cancer. J Exp Med. 2021;218. https://doi.org/10.1084/jem.20201606

[12] Li J, Condello S, Thomes-Pepin J, Ma X, Xia Y, Hurley TD, et al. Lipid Desaturation Is a Metabolic Marker and Therapeutic Target of Ovarian Cancer Stem Cells. Cell Stem Cell. 2017;20:303-14 e5. https://doi.org/10.1016/j.stem.2016.11.004

[13] Vichai V, Kirtikara K. Sulforhodamine B colorimetric assay for cytotoxicity screening. Nat Protoc. 2006;1:1112-6. https://doi.org/10.1038/nprot.2006.179

[14] Dettmer K, Nurnberger N, Kaspar H, Gruber MA, Almstetter MF, Oefner PJ. Metabolite extraction from adherently growing mammalian cells for metabolomics studies: optimization of harvesting and extraction protocols. Anal Bioanal Chem. 2011;399:1127-39. https://doi.org/10.1007/s00216-010-4425-x

[15] Liebisch G, Fahy E, Aoki J, Dennis EA, Durand T, Ejsing CS, et al. Update on LIPID MAPS classification, nomenclature, and shorthand notation for MS-derived lipid structures. J Lipid Res. 2020;61:1539-55. https://doi.org/10.1194/jlr.S120001025

[16] Chong J, Wishart DS, Xia J. Using MetaboAnalyst 4.0 for Comprehensive and Integrative Metabolomics Data Analysis. Curr Protoc Bioinformatics. 2019;68:e86. https://doi.org/10.1002/cpbi.86

[17] Pang Z, Chong J, Zhou G, de Lima Morais DA, Chang L, Barrette M, et al. MetaboAnalyst 5.0: narrowing the gap between raw spectra and functional insights. Nucleic Acids Res. 2021;49:W388-W96. https://doi.org/10.1093/nar/gkab382

[18] Worley B, Powers R. Multivariate Analysis in Metabolomics. Curr Metabolomics. 2013;1:92-107. https://doi.org/10.2174/2213235X11301010092

[19] Worley B, Powers R. PCA as a practical indicator of OPLS-DA model reliability. Curr Metabolomics. 2016;4:97-103. https://doi.org/10.2174/2213235X04666160613122429

[20] Chen Y, Xu Y, Wang J, Prisinzano P, Yuan Y, Lu F, et al. Statins Lower Lipid Synthesis But Promote Secretion of Cholesterol-Enriched Extracellular Vesicles and Particles. Front Oncol. 2022;12:853063. https://doi.org/10.3389/fonc.2022.853063

[21] Iorio E, Caramujo MJ, Cecchetti S, Spadaro F, Carpinelli G, Canese R, et al. Key Players in Choline Metabolic Reprograming in Triple-Negative Breast Cancer. Front Oncol. 2016;6:205. https://doi.org/10.3389/fonc.2016.00205

[22] Rani S, Lai A, Nair S, Sharma S, Handberg A, Carrion F, et al. Extracellular vesicles as mediators of cell-cell communication in ovarian cancer and beyond - A lipids focus. Cytokine Growth Factor Rev. 2023;73:52-68. https://doi.org/10.1016/j.cytogfr.2023.06.004

[23] Saito RF, Andrade LNS, Bustos SO, Chammas R. Phosphatidylcholine-Derived Lipid Mediators: The Crosstalk Between Cancer Cells and Immune Cells. Front Immunol. 2022;13:768606. https://doi.org/10.3389/fimmu.2022.768606

[24] Albini A, Sporn MB. The tumour microenvironment as a target for chemoprevention. Nat Rev Cancer. 2007;7:139-47. https://doi.org/10.1038/nrc2067

[25] Marat AL, Haucke V. Phosphatidylinositol 3-phosphates-at the interface between cell signalling and membrane traffic. EMBO J. 2016;35:561-79. https://doi.org/10.15252/embj.201593564

CONCLUSIONES GENERALES

El cáncer de ovario, una de las malignidades ginecológicas más mortales, se diagnostica principalmente en etapas avanzadas, contribuyendo a una baja tasa de supervivencia a 5 años. Además, la alta recurrencia después del tratamiento se debe a mecanismos de quimiorresistencia.

La propuesta de trabajo fue investigar el papel de los metabolitos en los mecanismos de resistencia a agentes antineoplásicos en células de cáncer de ovario mediante una estrategia analítica basada en metabolómica utilizando UHPLC-HR-QTOF-MS, con el fin de comprender mejor las vías metabólicas alteradas y su impacto en los parámetros farmacológicos.

Nuestro estudio de metabolómica utilizando células de cáncer de ovario OVCAR-3 y SK-OV-3, como modelos de células sensibles y resistentes a agentes antineoplásicos entregó las siguientes conclusiones que responden a la hipótesis establecida:

1. Nuestros resultados han identificado las principales vías metabólicas que diferencian entre las células sensibles (OVCAR-3) y resistentes (SK-OV-3) a agentes antineoplásicos.
2. La metabolómica demostró ser una herramienta poderosa para identificar metabolitos claves y vías que contribuyen a la quimiorresistencia.

3. La eliminación del glutatión generó un cambio notable en la resistencia a los agentes antineoplásicos y aumentó significativamente los parámetros farmacológicos, transformando además la respuesta celular de citostática a citotóxica.
4. Las células SK-OV-3, resistentes a agentes antineoplásicos, no son dependientes de la glucólisis y presentan un aumento en la biosíntesis de lípidos, que podrían respaldar la producción de energía a través de la beta-oxidación.
5. Aunque nuestro estudio actual se centró en modelos celulares, las conclusiones obtenidas ofrecen perspectivas prometedoras para la investigación traslacional y futuras aplicaciones clínicas.

PRODUCTIVIDAD

1. Publicaciones científicas.

- Metabolomics profiling and chemoresistance mechanisms in ovarian cancer cell lines: Implications for targeting glutathione pathway.

Pedro Alarcon-Zapata, Andy J. Perez, Karin Toledo-Oñate, Hector Contreras, Valeska Ormazabal, Estefania Nova-Lamperti, Claudio A. Aguayo, Carlos Salomon, Felipe A. Zuniga.

Paper publicado en *Life Sciences* el 10 de octubre de 2023. Life Sciences 333 (2023) 122166. https://doi.org/10.1016/j.lfs.2023.122166.

- Lipidomics profiling in Ovarian Cancer Cell Lines: lipid metabolism upregulation is pivotal to drug resistance behavior and cell survival.

Pedro Alarcon-Zapata, Karin Toledo-Oñate, Andy J. Perez, Barbara Alarcon-Zapata, Lia Olivares-Caro, Hector Contreras, Valeska Ormazabal, Felipe A. Zuniga.

Paper enviado a *Cancer Letters* (CANLET-D-23-03947).

2. Participación en otras publicaciones.

- Contreras, H., **Alarcón-Zapata, P.,** Nova-Lamperti, E., Ormazabal, V., Varas-Godoy, M., Salomon, C., & Zuniga, F. A. (2023). Comparative study of size exclusion chromatography for isolation of small extracellular vesicle from cell-conditioned media, plasma, urine, and saliva. Frontiers in Nanotechnology, 5, 1146772.
- Garzoli, S., **Alarcón-Zapata, P**., Seitimova, G., Alarcón-Zapata, B., Martorell, M., Sharopov, F., ... & Vitalini, S. (2022). Natural essential oils as a new therapeutic tool in colorectal cancer. Cancer Cell International, *22*(1), 1-20.
- Butnariu, M., Quispe, C., Herrera-Bravo, J., Helon, P., Kukula-Koch, W., López, V., Les, F., Valdés, C., **Alarcón-Zapata, P**., … & Cho, W. C. (2022). The effects of thymoquinone on pancreatic cancer: Evidence from preclinical studies. Biomedicine & Pharmacotherapy, *153*, 113364.
- Escobar DF, Díaz P, Díaz-Dinamarca D, Puentes R, **Alarcón P**, Alarcón B, Rodríguez I, Manzo RA, Soto DA, Lamperti L, Díaz J, García-Escorza HE and Vasquez AE. (2021) Validation of a Methodology for the Detection of Severe Acute Respiratory Syndrome Coronavirus 2 in Saliva by Real-Time Reverse Transcriptase-PCR. Front. Public Health 9:743300.
- Sharifi-Rad J, Quispe C, Rahavian A, Pereira Carneiro JN, Rocha JE, Alves Borges Leal AL, Bezerra Morais Braga MF, Melo Coutinho HD, Ansari Djafari A, **Alarcón-Zapata P**, Martorell M, Antika G, Tumer TB,

Cruz-Martins N, Helon P, Paprocka P, Koch W, Docea AO and Calina D. (2021) Bioactive Compounds as Potential Agents for Sexually Transmitted Diseases Management: A Review to Explore Molecular Mechanisms of Action. Front. Pharmacol. 12:674682.

- Martorell, M., Lucas, X., **Alarcón-Zapata, P.,** Capó, X., Quetglas-Llabrés, M. M., Tejada, S., & Sureda, A. (2020). Targeting Xanthine Oxidase by Natural Products as a Therapeutic Approach for Mental Disorders. Current Pharmaceutical Design.

3. Participación en proyectos.

- "Identificación de los principales metabolitos plasmáticos asociados a severidad de covid-19, a través de una estrategia metabolómica basada en UHPLC-QTOF-MS/MS".

Proyecto ANID COVID0370. Universidad de Concepción. Participación como profesional de investigación.

4. Participación en congresos.

- Identificación de biomarcadores metabólicos asociados a quimiorresistencia en células de cáncer de ovario mediante metabolómica.

Alarcón-Zapata P, Pérez AJ, Contreras H., Toledo K., Tapia K., Valenzuela F., Cordonier M., Acevedo M., Nova-Lamperti E., Ormazabal V., Zúñiga F. 20 Congreso Chileno de Química Clínica, Santiago, Chile. (2022). Presentación en modalidad ORAL.

Obtención del Premio Sociedad Chilena de Química Clínica al mejor trabajo de investigación.

- Metabolomic analysis by UHPLC-HR-QTOF-MS on ovarian cancer cells with different chemosensitivity.

Alarcón-Zapata P, Pérez AJ, Nova-Lamperti E, Sharma S, Ormazabal V, Hooper J, Salomon C, Zúñiga FA. Congreso Sociedad Chilena de Ciencias Fisiológicas y Asociación Latinoamericana de Ciencias Fisiológicas, *online* (2020). Presentación en modalidad POSTER *online*.

- Proteomic analysis of *Lactobacillus fermentum* UCO-979C lysate on human gastric adenocarcinoma cells.

Alarcón-Zapata, P.; Alarcón-Zapata, B; Parra, C; Ormazabal, V; García, A.; Zúñiga, F.A. XL Congreso Anual de la Sociedad de Farmacología de Chile (SOFARCHI), Santa Cruz, Chile. (2018). Presentación en modalidad POSTER.

ANEXOS

Table S1: Annotation of significant metabolites in OVCAR-3 and SK-OV-3 obtained by C18 column.

n	Rt (min)	Metabolite identification	Metabolite class	Mol. formula	Theor m/z	Found m/z	m/z error (ppm)[a]	MS/MS m/z	Adduct (ESI mode)	InChi-Key	Cell Upregulated	Ident. Level (A-D)
1	5.87	1-[5-(4-mesylphenyl)-2-pyrazolin-1-yl]-2,2-dimethyl-propan-1-one	-	$C_{15}H_{20}N_2O_3S$	308.1193	307.1120	1.95	229.1, 158.1, 137.1, 117.0, 98.0	$[M-H]^-$ $[M-H]^+$	BNEBONHNRMQHEE-UHFFFAOYSA-N	SK-OV-3	B
2	5.87	3-[1-(methanesulfonamido)-5-m-phenetyl-pyrrol-2-yl]propionic acid	-	$C_{16}H_{20}N_2O_5S$	352.1094	351.1021	0.69	353.0, 307.1, 273.1, 229.1, 137.7, 117.0	$[M-H]^-$ $[M-H]^+$	AMNAHJKULWSFBK-UHFFFAOYSA-N	SK-OV-3	B
3	1.46	Unknow	-	$C_{18}H_{18}O_9$	378.0931	377.0858	5.56	377.1, 263.1, 237.1, 221.1, 179.0, 161.0, 143.0, 119.0, 101.0	$[M-H]^-$	-	SK-OV-3	C
4	5.87	Unknow	-	$C_{14}H_{18}N_2O$	230.1418	229.1345	0.51	137.1	$[M-H]^-$	-	SK-OV-3	C
5	4.95	Unknow	-	-	1312.5758	655.2806	-	n.d	$[M-H-H]^{2-}$	-	SK-OV-3	D
6	11.53	Unknow	-	$C_{20}H_{36}N_6O_2$	392.2920	391.2837	3.14	391.3, 355.3, 345.3, 327.3, 311.2	$[M-H]^-$	-	SK-OV-3	C

7	5.86	2-[[16-[(8-sulfo-2-quinolyl)methyl]-1,4,10,13-tetraoxa-7,16-diazacyclooctadec-7-yl]methyl]quinoline-8-sulfonic acid	-	$C_{32}H_{40}N_4O_{10}S_2$	704.2171	703.2098	0.32	351.1, 307.1, 273.1, 229.1, 137.1	$[M-H]^-$	NWUAODCFJLEZEP-UHFFFAOYSA-N	SK-OV-3	B
8	7.37	2-cyano-N-(cyanomethyl)-2-[3-ethyl-5-[[3-[(2-indolin-1-ylacetyl)amino]anilino]methylene]-4-keto-thiazolidin-2-ylidene]acetamide	-	$C_{27}H_{25}N_7O_3S$	527.1719	526.1646	7.17	526.2, 408.1, 350.1, 333.1, 307.1, 289.1, 255.1, 236.0, 208.0, 192.0, 168.1, 158.1, 149.0, 127.1	$[M-H]^-$	VBUJIGKATMCVFL-UHFFFAOYSA-N	SK-OV-3	B
9	3.12	Pantothenate	Vitamins	$C_9H_{17}NO_5$	219.1109	218.1036	1.85	218.1, 146.1, 116.7, 99.0, 88.0	$[M-H]^-$	GHOKWGTUZJEAQD-ZETCQYMHSA-N	SK-OV-3	B
10	3.62	Tryptophan	L-alpha-amino acid	$C_{11}H_{12}N_2O_2$	204.0898	203.0825	1.05	203.1, 186.0, 159.1, 142.1, 130.1, 121.0, 116.0	$[M-H]^-$	QIVBCDIJIAJPQS-VIFPVBQESA-N	SK-OV-3	B
11	4.74	Unknow	-	$C_{15}H_{18}N_2O_2S$	290.1093	289.1021	1.44	241.1, 171.1, 157.1	$[M-H]^-$	-	SK-OV-3	C
12	1.49	Unknow	-	$C_{20}H_{40}N_2O_{15}S$	580.2145	579.2072	0.66	579.2, 237.1	$[M-H]^-$	-	SK-OV-3	B
13	5.90	2-[3-[2-[3-[2-[4-amino-2-(methylthio)-5-nitro-anilino]ethyl]-4-imidazolin-1-yl]ethyl]-4-imidazolin-1-yl]ethyl-[4-amino-2-(methylthio)-5-nitro-phenyl]amine	-	$C_{26}H_{36}N_{10}O_4S_2$	616.2373	615.2300	0.35	307.1, 229.1, 189.1, 137.1, 98.0	$[M-H]^-$	OBQONIDWRDMTAG-UHFFFAOYSA-N	SK-OV-3	B
14	3.13	Unknow	-	-	482.1138	481.1066	-	481.1, 338.0,	$[M-H]^-$	-	SK-OV-3	C

								304.1, 272.1, 254.1, 226.1, 210.1, 176.0, 153.1, 143.0, 128.0, 98.1				
15	4.90	Methylhippuric acid	N-acylglycine	$C_{10}H_{11}NO_3$	193.0738	192.0665	0.04	102.9	$[M-H]^-$	YOEBAVRJHRCKRE-UHFFFAOYSA-N	SK-OV-3	B
16	4.74	4-[(E)-(2-methyl-1H-indol-3-yl)methyleneamino]-3-(4-pyridyl)-1H-1,2,4-triazole-5-thione	-	$C_{17}H_{14}N_6S$	334.0993	333.0920	2.28	289.1, 245.1, 237.1, 211.1, 171.1, 157.1, 131.0	$[M-H]^-$	JMZWXKNFUAEBCC-VXLYETTFSA-N	SK-OV-3	B
17	5.93	Unknow	-	$C_{16}H_{18}N_2O_4S$	334.0988	333.0916	2.55	255.1, 237.1, 211.1, 201.1, 171.1, 157.1, 116.0	$[M-H]^-$	-	SK-OV-3	C
18	5.59	Unknow	-	-	428.2267	427.2194	-	427.2, 409.2, 397.2, 353.2, 296.1, 266.1, 242.2, 226.1, 208.1, 187.1, 166.1, 143.1, 237.0, 109.0	$[M-H]^-$	-	SK-OV-3	C
19	2.93	Phenylalanine	Amino acids	$C_9H_{11}NO_2$	165.0786	164.0713	3.03	164.1, 147.0, 119.0,	$[M-H]^-$	VVHOUVWJCQOYGG-REOHCLBHSA-N	SK-OV-3	B

								103.0, 96.9				
20	8.07	N-[1-[[(4S)-3-methylol-1-(6H-1,3-oxazin-2-ylsulfonyl)azepan-4-yl]carbamoyl]butyl]-5-nitro-2-furamide	-	$C_{21}H_{29}N_5O_9S$	527.1722	526.1649	6.98	482.2, 438.2, 350.1, 289.1, 255.1,245.1, 236.0, 192.0, 158.0, 137.1, 127.1, 117.0	$[M-H]^-$	QNCHYYQOGATAFJ-PCKAHOCUSA-N	SK-OV-3	B
21	5.86	Unknow	-	$C_{15}H_{18}N_2O_3$	274.1317	273.1245	0.73	227.2, 137.1	$[M-H]^-$	-	SK-OV-3	C
22	5.88	Unknow	-	$C_{28}H_{32}N_{14}O_2S_2$	660.2287	659.2215	1.68	n.d	$[M-H]^-$	-	SK-OV-3	D
23	4.74	Unknow	-	-	668.1998	667.1926	-	333.1, 289.1, 131.0	$[M-H]^-$	-	SK-OV-3	C
24	2.93	Unknow	-	-	119.0710	120.0783	-	103.0	$[M-H]^+$	-	SK-OV-3	D
25		Benzylpenicillin	Carboxylic acids and derivatives	$C_{16}H_{18}N_2O_4S$	334.0959	335.1029	8.08	335.1, 289.1, 243.1, 190.0, 159.1, 128.0, 113.0, 91.0	$[M-H]^+$	JGSARLDLIJGVTE-MBNYWOFBSA-N	SK-OV-3	B
26	5.86	4-[4-[[[2-(4-Oxo-1,3-thiazolidin-3-yl)acetyl]amino]methyl]phenoxy]butanoic acid	-	$C_{16}H_{20}N_2O_5S$	352.1066	353.1140	5.96	335.1, 309.1, 292.1, 263.1, 217.1, 202.0, 174.0, 160.0, 128.0, 114.0, 91.0	$[M-H]^+$	QFJNZWWNDAUXPR-UHFFFAOYSA-N	SK-OV-3	B
27	3.94	3-Indoleacrylate	Indoles and derivatives	$C_{11}H_9NO_2$	187.0626	188.0701	2.79	170.1, 146.1, 118.1,	$[M-H]^+$	PLVPPLCLBIEYEA-	SK-OV-3	B

								115.0, 104.14, 91.0		AATRIKPKSA-N		
28	5.86	Unknow	-	$C_6H_9NO_2S$	159.0357	160.0429	0.67	n.d	$[M-H]^+$	-	SK-OV-3	B
29	3.94	Unknow	-		113.0821	114.0889	-	114.1	$[M-H]^+$	-	SK-OV-3	B
30	2.93	Phenylalanine	Aminoacids	$C_9H_{11}NO_2$	165.0788	166.0864	0.73	120.1, 107.0, 103.0, 91.0	$[M-H]^+$	VVHOUVWJCQOYGG-REOHCLBHSA-N	SK-OV-3	B
31	1.41	Unknow	-	$C_{10}H_{16}N_6O_9$	364.0971	365.1044	1.96	365.1	$[M-H]^+$	-	SK-OV-3	C
32	1.44	4-O-[4-O-beta-D-Mannopyranosyl-2-(acetylamino)-2-deoxy-beta-D-glucopyranosyl]-2-(acetylamino)-2-deoxy-1-thio-beta-D-glucopyranose	-	$C_{22}H_{38}N_2O_{15}S$	602.1971	603.2041	3.16	603.2, 365.1, 283.1, 261.1, 239.1	$[M-H]^+$	COLNVLDHVKWLRT-QMMMGPOBSA-N	SK-OV-3	B
33	5.89	Unknow	-	$C_7H_{11}NO_2S$	173.0508	174.0581	1.78	90.1	$[M-H]^+$	PLVPPLCLBIEYEA-AATRIKPKSA-N	SK-OV-3	B
34	1.33	Unknow	-	-	260.0795	261.0868	-	261.1, 203.0, 174.0, 157.1, 131.1, 100.1	$[M-H]^+$	-	SK-OV-3	D
35	1.88	2-Phenylacetamide	Phenylacetamides	C_8H_9NO	135.0668	136.0740	11.12	n.d	$[M-H]^+$	LSBDFXRDZJMBSC-UHFFFAOYSA-N	SK-OV-3	B
36	1.89	Phenylpyruvate	Phenylpyruvic Acids	$C_9H_8O_3$	164.0471	165.0549	0.63	123.0, 95.0, 91.0	$[M-H]^+$	BTNMPGBKDVTSJY-UHFFFAOYSA-N	SK-OV-3	B
37	3.69	Unknow	-	$C_{16}H_{18}N_2O_4S$	334.0958	335.1031	8.71	335.1, 289.1, 257.1, 203.1, 159.1, 114.0, 91.0	$[M-H]^+$	-	SK-OV-3	C

38	1.22	Unknow	-	-	260.0790	283.0682	-	301.1, 283.1, 239.0	$[M-Na]^+$	-	SK-OV-3	B
39	2.25	L-isoleucine	Amino acids, peptides, and analogues	$C_6H_{13}NO_2$	131.0928	132.1001	12.49	n.d	$[M-H]^+$	-	SK-OV-3	B
1'	1.45	Unknow	-	$C_{16}H_{14}O_2$	238.0985	237.0912	3.76	237.1	$[M-H]^-$	-	OVCAR-3	C
2'	1.74	Glutathione	Oligopeptide	$C_{10}H_{17}N_3O_6S$	307.0841	306.0767	0.38	306.1, 288.1, 272.1, 260.1, 254.1, 242.1, 228.1, 210., 197.0, 179.0, 166.1, 160.0, 153.1, 143.0, 135.0, 128.0, 123.0, 112.0, 99.0	$[M-H]^-$	RWSXRVCMGQZWBV-WDSKDSINSA-N	OVCAR-3	B
3'	6.60	[4-[2-(4-carbethoxythiazol-2-yl)-2-(pivaloylamino)ethyl]phenyl] sulfamic acid	-	$C_{19}H_{25}N_3O_6S_2$	455.1185	454.1112	1.37	454.1, 410.1, 376.1, 342.1, 332.1, 298.1, 255.1, 229.1, 241.1, 180.1, 158.0	$[M-H]^-$	WDRLFWGIWNRZOQ-UHFFFAOYSA-N	OVCAR-3	B
4'	1.59	UDP-N-acetyl-D-galactosamine	Nucleoside Diphosphate Sugars	$C_{17}H_{27}N_3O_{17}P_2$	607.0809	606.0737	0.96	606.1, 402.9, 384.9, 362.0, 323.0, 295.0, 272.9, 237.1,	$[M-H]^-$	LFTYTUAZOPRMMI-UHFFFAOYSA-N	OVCAR-3	B

								176.9, 158.9, 96.9				
5’	1.95	N-Acetylaspartylglutamic acid	Dipeptides	$C_{11}H_{16}N_2O_8$	304.0902	285.0732	1.92	306.1, 285.1, 272.1, 255.2, 242.1, 226.0, 210.1, 182.0 155.0, 146.0, 128.0, 110.0, 102.0, 96.0	$[M-H-H_2O]^-$	OPVPGKGADVGKTG-BQBZGAKWSA-N	OVCAR-3	B
6’	1.88	N-Acetylaspartylglutamic acid	Dipeptides	$C_{11}H_{16}N_2O_8$	304.0896	303.0823	1.92	306.1, 285.1, 272.1, 255.2, 242.1, 237.1, 226.0, 210.1, 182.0, 155.0, 146.0, 138.1, 128.0, 110.0, 102.1, 96.0	$[M-H]^-$	OPVPGKGADVGKTG-BQBZGAKWSA-N	OVCAR-3	B
7’	1.73	N-acetyl-L-aspartate	Amino Acid	$C_6H_9NO_5$	175.0479	174.0406	0.60	174.0, 156.0, 130.0, 115.0, 96.9, 88.0	$[M-H]^-$	OTCCIMWXFLJLIA-BYPYZUCNSA-L	OVCAR-3	B
8’	1.92	beta-Citrylglutamate	N-acyl-L-alpha-amino acid	$C_{11}H_{15}NO_{10}$	321.0699	320.0626	0.60	302.0, 284.0, 240.0, 216.0, 196.1, 172.1, 146.0,	$[M-H]^-$	GAQNUGISBQJMKO-YFKPBYRVSA-N	OVCAR-3	B

								128.0, 110.0				
9’	1.33	Unknow	-	$C_8H_{20}O_4S_3$	276.0533	277.0606	2.47	277.1, 221.0, 104.1, 96.9	$[M-H]^+$	-	OVCAR-3	C
10’	1.24	Glycerophosphocholine	Glycerophosphates	$C_8H_{20}NO_6P$	257.1011	280.0900	4.75	n.d	$[M-Na]^+$	SUHOQUVVVLNYQR-UHFFFAOYSA-N	OVCAR-3	B
11’	1.28	Unknow	-	$C_5H_{15}O_3PS_2$	218.0193	219.0266	3.49	147.1, 130.0, 101.1	$[M-H]^+$	-	OVCAR-3	C
12’	1.42	Unknow	-	$C_4H_9N_3O_2$	131.0669	132.0742	18.9	n.d	$[M-H]^+$	-	OVCAR-3	D
13’	1.49	Unknow	-	$C_4H_9N_3O_2$	131.0671	132.0744	17.46	n.d	$[M-H]^+$	-	OVCAR-3	D
14’	1.74	Cysteinylglycine	Dipeptide	$C_5H_{10}N_2O_3S$	178.0411	179.0483	0.02	94.1	$[M-H]^+$	ZUKPVRWZDMRIEO-VKHMYHEASA-N	OVCAR-3	B
15’	1.45	Glutamine	Aminoacid	$C_5H_{10}N_2O_3$	146.0684	147.0757	4.53	130.0	$[M-H]^+$	ZDXPYRJPNDTMRX-VKHMYHEASA-N	OVCAR-3	B

[a]Mean accurate mass error for negative and positive ESI acquisition modes, respectively.

n.d.: not detected; InChi-Key: IUPAC international chemical identifier according to PubChem; Level of identification (A-D): A-standard or NMR, B-MS/MS, C-MS^E, D-MS only.

Table S2: Annotation of significant metabolites in OVCAR-3 and SK-OV-3 obtained by HILIC column.

n	Rt (min)	Metabolite identification	Metabolite class	Mol. formula	Theor m/z	Found m/z	m/z error (ppm)[a]	MS/MS m/z	Adduct (ESI mode)	InChi-Key	Cell Upregulated	Ident. Level (A-D)
1	1.39	1-[[4-[2-[Hexyl(methyl)amino]ethoxy]phenyl]methyl]-2-(4-hydroxyphenyl)-3-methylindol-5-ol	-	$C_{31}H_{38}N_2O_3$	486.2886	485.2814	0.20	487.3, 486.285, 485.3, 469.2	$[M-H]^-$	WUKMLNGOECUKLO-UHFFFAOYSA-N	SK-OV-3	B
2	14.17	Unknow	-	-	684.2286	683.2213	-	n.d	$[M-H]^-$	-	SK-OV-3	D
3	13.9	Benzyl 2-O,3-O,6-O-triacetyl-4-O-(3-O,4-O,6-O-triacetyl-beta-D-galactopyranosyl)-beta-D-glucopyranoside	O-glycosyl compounds	$C_{31}H_{40}O_{17}$	684.2278	683.2206	8.23	683.2, 623.2, 341.1, 323.1, 281.1, 263.1, 221.1, 179.1, 161.0, 143.0, 119.0, 101.0	$[M-H]^-$	RQRQTTJTTODXNM-KZXUBJNASA-N	SK-OV-3	B
4	1.51	Unknow	-	$C_6H_{10}O_3$	130.0626	129.0553	4.90	129.1	$[M-H]^-$	-	SK-OV-3	C
5	14.17	6-O-β-D-Galactofuranosyl-α-D-mannopyranose	Glycosylmannose	$C_{12}H_{22}O_{11}$	342.1145	341.1072	6.53	237.1, 221.1, 183.0, 179.0, 161.0,	$[M-H]^-$	MFBRTXIZJUHGPH-KGXCRCOUSA-N	SK-OV-3	B

								149.0, 143.0, 125.0, 115.0, 101.0, 97.0				
6	14.27	[(2S,3S,4R,5R)-1-Acetamidooxy-3,4,5,6-tetrahydroxyhexan-2-yl] (2R,3R,4S,5R)-2-acetamido-2,3,4,5,6-pentahydroxyhexanoate	-	$C_{16}H_{30}N_2O_{14}$	474.1664	473.1591	5.73	473.2, 179.0, 161.0, 131.0, 113.0	$[M-H]^-$	DCXXVCMXHGTBLX-PTEZTYNVSA-N	SK-OV-3	B
7	14.17	2,3,4,5,6-Pentahydroxy-7-[(2S,3R,4S,5S,6R)-3,4,5-trihydroxy-6-(hydroxymethyl)oxan-2-yl]oxyheptanoic acid	-	$C_{13}H_{24}O_{13}$	388.1211	387.1138	6.16	341.1, 281.1, 263.1, 221.1, 179.0, 161.0, 149.0, 143.0, 125.0, 113.0, 101.0	$[M-H]^-$	CDXJPGDTQSCRGD-BAMMHMRTSA-N	SK-OV-3	B
8	3.01	(2S)-2-[(2-Amino-3-prop-2-enylsulfanylpropanoyl)amino]-3-phenylpropanoic acid	-	$C_{15}H_{20}N_2O_3S$	308.1191	307.1118	3.17	309.2, 229.1, 158.1, 137.1, 117.0	$[M-H]^-$	PGVVGYMSTAHNES-ABLWVSNPSA-N	SK-OV-3	B
9	13.9	beta-D-Glcp-(1->6)-alpha-D-Manp	D-glucosyl-D-mannose	$C_{12}H_{22}O_{11}$	342.1137	341.1065	7.14	300.0, 237.1, 161.0, 143.0, 125.0, 113.0, 101.0, 97.0	$[M-H]^-$		SK-OV-3	B
10	13.9	2,3,4,5,6-Pentahydroxy-7-[(2S,3R,4S,5S,6R)-3,4,5-trihydroxy-6-(hydroxymethyl)oxan-2-yl]oxyheptanoic acid	-	$C_{13}H_{24}O_{13}$	388.1191	387.1118	6.35	341.1, 263.1, 221.1, 179.0, 161.0, 149.0, 143.0, 131.0, 119.0, 101.0	$[M-H]^-$	CDXJPGDTQSCRGD-BAMMHMRTSA-N	SK-OV-3	B

11	14.16	Unknow	-	$C_6H_{12}O_6$	180.0616	161.0441	11.45	99.9	$[M-H-H_2O]^-$	-	SK-OV-3	C
12	1.79	2,3-Bis(ethenoxy)butanedioic acid	-	$C_8H_{10}O_6$	202.0449	201.0376	14.13	201.0, 129.0, 111.0, 89.0	$[M-H]^-$	NAJBXIFWYVLCGM-UHFFFAOYSA-N	SK-OV-3	B
13	1.50	2-Aminoadenosine	Purine nucleoside	$C_{10}H_{14}N_2O_6$	282.1080	281.1008	0.22	281.1, 241.0, 184.0, 169.0, 153.0, 129.0	$[M-H]^-$	ZDTFMPXQUSBYRL-UUOKFMHZSA-N	SK-OV-3	B
14	4.84	Uridine	Pyrimidine Nucleosides	$C_9H_{12}N_6O_4$	244.0687	243.0614	3.51	243.1, 200.1, 185,1, 173.1, 152.0, 140.0, 133.0, 122.0, 115.0 114.0, 98.0	$[M-H]^-$	DRTQHJPVMGBUCF-XVFCMESISA-N	SK-OV-3	B
15	13.28	Glutathione	Oligopeptide	$C_{10}H_{17}N_3O_6S$	307.0813	306.0740	6.99	306.1, 288.0, 272.1, 260.1, 254.1, 242.1, 237.1, 228.1, 210.1, 197.0, 185.0, 179.0, 167.0, 160.0, 153.1, 143.0, 135.0, 128.0, 123.0, 109.0, 99.0	$[M-H]^-$	RWSXRVCMGQZWBV-WDSKDSINSA-N	SK-OV-3	B

16	9.25	Unknow	-	-	249.9650	248.9577	-	203.1, 180.9, 112.9	$[M-H]^-$	-	SK-OV-3	C
17	14.32	1-glyceryl-5-nitro-pyrimidin-2-one	-	$C_7H_9N_3O_5$	215.0546	214.0473	1.91	n.d	$[M-H]^-$	KPFXGQSQPSOBBF-UHFFFAOYSA-N	SK-OV-3	B
18	2.99	Benzylpenicilloic acid	Penicilloic acid	$C_{16}H_{20}N_2O_5S$	352.1083	351.1010	2.23	353.0, 307.1, 273.1, 229.1, 158.0, 137.1, 117.0	$[M-H]^-$	HCYWNSXLUZRKJX-RWMBFGLXSA-N	SK-OV-3	B
19	5.14	N-[[[acetamido(propyl)carbamoyl]-propionamido-amino]-azido-(ethylcarbamoylamino)methyl]acetamide	-	$C_{15}H_{28}N_{10}O_5$	428.2246	427.2176	2.28	427.2, 409.2, 397.2, 365.2, 353.2, 266.1, 208.1, 187.1, 166.1, 143.1, 127.0, 107.0, 94.9	$[M-H]^-$	-	SK-OV-3	B
20	13.97	1,3-Bis-(d-mannos-4-yloxy)-2-propylamine	-	$C_{15}H_{29}NO_{14}$	447.1556	446.1483	4.77	446.2, 341.1, 263.1, 179.0, 161.0, 143.0, 113.0, 104.0	$[M-H]^-$	POFVONUXNPPAQR-LGARRYCISA-N	SK-OV-3	B
21	2.45	2-[Hydroxy-bis(4-hydroxyphenyl)methyl]benzene sulfonic acid	-	$C_{19}H_{16}O_6S$	372.0654	353.0476	3.49	353.0, 289.1, 271.1, 243.1, 195.0, 180.0, 93.0	$[M-H-H_2O]^-$	QZYIKVKRLOQAOX-UHFFFAOYSA-N	SK-OV-3	B
22	0.64	Unknow	-	$C_7H_4N_4O_7P_2$	317.9550	316.9477	1.48	248.9, 180.9, 113.9, 112.9	$[M-H]^-$	-	SK-OV-3	C

23	8.58	Unknow	-	$C_6H_{14}O_6$	182.0764	181.07102	8.17	181.1, 163.1, 119.0, 112.9, 101.0	$[M-H]^-$	-	SK-OV-3	C
24	1.97	N-formyl-L-methionine	N-formyl amino acid	$C_6H_{11}NO_3S$	177.0457	176.03085	1.00	178.0, 134.1, 98.1, 89.0	$[M-H]^-$	PYUSHNKNPOHWEZ-YFKPBYRVSA-N	SK-OV-3	B
25	3.07	(1-ketothian-4-yl)-[4-(methylamino)-6-(1,2,4-triazol-1-yl)-s-triazin-2-yl]amine	-	$C_{11}H_{16}N_8OS$	308.1167	309.12040		309.1, 292.1, 263.1, 191.1, 164.0, 146.1, 136.1, 128.0, 113.0, 100.0, 91.0, 86.0	$[M-H]^+$	YIITYHDRMZBEQT-UHFFFAOYSA-N	SK-OV-3	B
26	8.67	Indoline	Indoles	C_8H_9N	119.0728	120.08000	5.71	118.1	$[M-H]^+$	LPAGFVYQRIESJQ-UHFFFAOYSA-N	SK-OV-3	B
27	1.92	L-leucine residue	L-α-amino acid residue	$C_6H_{11}NO$	113.0837	114.09110	3.39	114.1, 96.1	$[M-H]^+$	-	SK-OV-3	B
28	3.07	Unknow	-	$C_7H_{11}NO_2S$	173.0506	174.05079	4.11	128.1, 114.1, 94.1	$[M-H]^+$	-	SK-OV-3	C
29	3.07	2-(4,6-Diaminopyrimidin-2-yl)sulfanyl-N-(3-morpholin-4-yloxadiazol-3-ium-5-yl)acetamide	-	$C_{12}H_{16}N_8O_3S$	352.1071	353.11042	1.06	353.1, 335.1, 317.1, 309.1, 292.1, 263.1, 217.1, 202.0, 189.1, 174.0, 160.0, 146.1, 136.1, 128.0, 120.1,	$[M-H]^+$	-	SK-OV-3	B

								114.0, 100.0, 91.0, 87.0				
30	6.60	Carnitine	Trimethyl Ammonium Compounds	$C_7H_{15}NO_3$	161.1041	162.1114	6.27	163.1, 162.1 104.0, 103.1, 103.0, 102.1	$[M-H]^+$	PHIQHXFUZVPYII-ZCFIWIBFSA-N	SK-OV-3	B
31	3.06	Unknow	-	$C_6H_9NO_2S$	159.0352	160.0435	0.06	114.0	$[M-H]^+$	-	SK-OV-3	C
32	6.64	1-Methylnicotinamide	Nicotinic Acids	C_7H_8N2O	136.0622	137.0695	10.36	138.1, 137.1, 94.1, 92.0	$[M-H]^+$	LDHMAVIPBRSVRG-UHFFFAOYSA-O	SK-OV-3	B
33	5.97	Propionyl-carnitine	Trimethyl Ammonium Compounds	$C_6H_{15}N_{17}O_2$	217.1289	218.1362	11.17	219.1, 218.1, 160.1, 159.1, 144.1, 129.1, 99.0, 86.0, 85.0	$[M-H]^+$	UFAHZIUFPNSHSL-UHFFFAOYSA-N	SK-OV-3	B
34	8.57	N-Amidino-L-aspartic acid	Dicarboxylic acid	$C_5H_9N_3O_4$	175.0583	176.0656	3.51	130.1, 94.1	$[M-H]^+$	VVHOUVWJCQOYGG-REOHCLBHSA-N	SK-OV-3	B
35	4.81	Unknow	-	$C_4H_4N_2O_2$	112.0263	113.0336	8.21	n.d	$[M-H]^+$	-	SK-OV-3	C
36	8.67	Phenylalanine	Amino Acids	$C_9H_{11}NO_2$	165.0785	166.0857	0.91	131.0, 121.1, 120.1, 119.1, 118.1, 107.0, 104.0, 130.0, 102.0	$[M-H]^+$	COLNVLDHVKWLRT-QMMMGPOBSA-N	SK-OV-3	B
37	8.85	3-Indoleacrylic acid	Monocarboxylic acid	$C_{11}H_9NO_2$	187.0628	188.0701	2.31	146.1, 143.1, 142.1,	$[M-H]^+$	PLVPPLCLBIEYEA-	SK-OV-3	B

								119.1, 118.1, 115.0, 91.0		AATRIKPKSA-N		
38	12.34	Unknow	-	$C_6H_7NO_3$	141.0406	142.0478	13.91	n.d	$[M-H]^+$	-	SK-OV-3	D
39	5.72	Isovalerylcarnitine	Trimethyl Ammonium Compounds	$C_{12}H_{23}NO_4$	245.1598	246.1670	10.67	247.2, 246.2, 188.1, 187.1, 144.1, 129.1, 103.1, 86.0, 85.0	$[M-H]^+$	IGQBPDJNUXPEMT-UHFFFAOYSA-N	SK-OV-3	B
40	10.39	Unknow	-	C_8H_9NO	135.0678	136.0751	3.38	n.d	$[M-H]^+$	-	SK-OV-3	D
41	1.78	Unknow	-	$C_3H_9N_3O_3$	135.0655	136.0728	8.55	n.d	$[M-H]^+$	-	SK-OV-3	D
42	10.40	Phenylpyruvate	Phenylpyruvic Acids	$C_9H_8O_3$	164.0474	165.0550	6.92	123.0, 95.0	$[M-H]^+$	BTNMPGBKDVTSJY-UHFFFAOYSA-N	SK-OV-3	B
1’	13.56	Unknow	-	$C_8H_{18}N_2O_4S$	238.0976	237.0903	2.45	237.1, 207.1, 193.1, 106.9	$[M-H]^-$	-	OVCAR-3	C
2’	2.98	Unknow	-	$C_8H_{18}N_2O_4S$	280.0677	279.0605	2.31	279.1, 213.0, 128.0	$[M-H]^-$	-	OVCAR-3	C
3’	9.72	Unknow	-	$C_5H_3NO_3$	125.0135	124.0063	32.48	124.0, 106.9	$[M-H]^-$	-	OVCAR-3	C
4’	9.74	Unknow	-	$C_7H_5N_4O_7P$	287.9864	286.9792	10.82	124.0, 106.9	$[M-H]^-$	-	OVCAR-3	C
5’	11.70	Unknow	-	-	385.9439	384.9367	-	248.9, 180.9, 112.9	$[M-H]^-$	-	OVCAR-3	C
6’	2.96	N-(ketomethylene)carbamic acid 3-carbonisocyanatidoyloxypropyl ester	-	$C_7H_6N_2O_6$	214.0209	213.0137	9.05	166.9, 146.9, 128.0, 115.9	$[M-H]^-$	BINFXCOCDCKZHZ-UHFFFAOYSA-N	OVCAR-3	B

7’	2.91	3-phenyl-1-(thiadiazol-4-yl)prop-2-yn-1-one	-	$C_{11}H_6N_2OS$	214.0192	213.0120	3.80	213.0, 145.0, 128.0, 115.9, 96.9	$[M-H]^-$	KZKGDOCGAWKIIY-UHFFFAOYSA-N	OVCAR-3	B
8’	2.98	L-pyroglutamic acid (Glutamate)	L-alpha-amino acid	C_5H_7NO3	129.0425	128.0352	0.21	128.0	$[M-H]^-$ $[M-H]^+$	ODHCTXKNWHHXJC-VKHMYHEASA-N	OVCAR-3	B
9’	13.53	Unknow	-	-	498.1748	497.1675	-	497.2, 237.1, 193.1, 106.9	$[M-H]^-$	-	OVCAR-3	D
10’	13.83	Glycerophosphocholine	Glycerophosphates	$C_8H_{20}NO_6P$	257.1027	258.1100	0.28	258.1, 184.1 166.1, 125.0, 104.1, 86.1	$[M-H]^+$	SUHOQUVVVLNYQR-UHFFFAOYSA-N	OVCAR-3	B
11’	2.96	Unknow	-	$C_7H_7NO_4$	169.0343	152.0310	21.18	n.d	$[M-H-H_2O]^+$	-	OVCAR-3	
12’	14.11	Glutamine	Amino Acid	$C_5H_{10}N_2O_3$	146.0694	147.0766	0.66	130.0, 102.0, 84.0	$[M-H]^+$	ZDXPYRJPNDTMRX-VKHMYHEASA-N	OVCAR-3	B
13’	13.84	Unknow	-	$C_5H_{13}NO$	103.0999	104.1071	2.94	n.d	$[M-H]^+$	-	OVCAR-3	
14’	3.80	L-aspartic acid	Amino Acid	$C_4H_7NO_4$	133.0368	134.0440	5.48	n.d	$[M-H]^+$	CKLJMWTZIZZHCS-REOHCLBHSA-N	OVCAR-3	B
15’	2.96	-	-	-	146.9964	169.9861	-	n.d	$[M-Na]^+$	-	OVCAR-3	
16’	3.79	N-Acetyl-L-aspartic acid	Amino Acid Derivative	$C_6H_9NO_5$	175.0469	198.0357	8.07	134.0, 116.0, 99.0, 94.1, 88.0	$[M-Na]^+$	OTCCIMWXFLJLIA-BYPYZUCNSA-N	OVCAR-3	B
17’	6.07	Glutamic Acid	Non-Essential Amino Acid	$C_5H_9NO_4$	147.0523	148.0595	6.26	n.d	$[M-H]^+$	WHUUTDBJXJRKMK-VKHMYHEASA-N	OVCAR-3	B
18’	6.56	Methylthioadenosine	Deoxyadenosines	$C_{11}H_{15}N_5O_3S$	297.0866	298.0938	10.40	298.1, 145.0, 136.1,	$[M-H]^+$	WUUGFSXJNOTRMR-	OVCAR-3	B

								119.0, 97.0		IOSLPCCCSA-N		
19'	14.60	2-(trimethylammonio)ethyl hydrogen phosphate (Phosphorilcholine)	Choline	$C_{10}H_{28}N_2O_8P_2$	366.1310	367.13383	2.98	367.1, 198.1, 184.1, 125.0, 104.1, 86.1	$[M-H]^+$	YHHSONZFOIEMCP-UHFFFAOYSA-N	OVCAR-3	B
20'	12.32	Unknow	-	$C_6H_5N_3O$	135.0414	136.0414	13.28	n.d	$[M-H]^+$	-	OVCAR-3	D
21'	14.02	[1-[2-[2-(2-Diethoxyphosphorylethoxy)ethoxy]ethylamino]-1-oxopropan-2-yl]carbamic acid	-	$C_{14}H_{29}N_2O_8P$	384.1670	385.17432	0.94	239.1, 152.0, 147.1, 143.1, 130.0, 112.1, 99.1, 88.0, 84.0	$[M-H]^+$	ODRZJFHNOOWUPW-UHFFFAOYSA-N	OVCAR-3	B
22'	6.56	2-Hydroxymethylserine	Amino Acids, Neutral	$C_4H_9NO_4$	135.0580	136.0611	2.41	298.1, 145.0, 136.1, 119.0, 103.0, 97.0, 92.0	$[M-H]^+$	ZRPDXDBGEYHEBJ-UHFFFAOYSA-N	OVCAR-3	B

[a]Mean accurate mass error for negative and positive ESI acquisition modes, respectively.

n.d.: not detected; InChi-Key: IUPAC international chemical identifier according to PubChem; Level of identification (A-D): A-standard or NMR, B-MS/MS, C-MS^E, D-MS only.